APRIL 25, 2018
VOLUME 118
NUMBER 8

pubs.acs.org/CR

CHEMICAL REVIEWS

RNA: FROM SINGLE MOLECULES TO MEDICINE

ACS Publications
Most Trusted. Most Cited. Most Read.

www.acs.org

CHEMICAL REVIEWS

Review

Cite This: *Chem. Rev.* 2018, 118, 4120–4155

pubs.acs.org/CR

Life under the Microscope: Single-Molecule Fluorescence Highlights the RNA World

Sujay Ray,[†] Julia R. Widom,[†] and Nils G. Walter*

Single Molecule Analysis Group and Center for RNA Biomedicine, Department of Chemistry, University of Michigan, Ann Arbor, Michigan 48109, United States

ABSTRACT: The emergence of single-molecule (SM) fluorescence techniques has opened up a vast new toolbox for exploring the molecular basis of life. The ability to monitor individual biomolecules in real time enables complex, dynamic folding pathways to be interrogated without the averaging effect of ensemble measurements. In parallel, modern biology has been revolutionized by our emerging understanding of the many functions of RNA. In this comprehensive review, we survey SM fluorescence approaches and discuss how the application of these tools to RNA and RNA-containing macromolecular complexes in vitro has yielded significant insights into the underlying biology. Topics covered include the three-dimensional folding landscapes of a plethora of isolated RNA molecules, their assembly and interactions in RNA-protein complexes, and the relation of these properties to their biological functions. In all of these examples, the use of SM fluorescence methods has revealed critical information beyond the reach of ensemble averages.

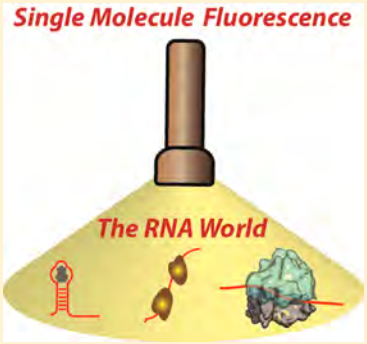

CONTENTS

1. INTRODUCTION

In 1989, Thomas R. Cech and Sidney Altman shared the Nobel Prize for their contributions to the discovery of catalytic properties of RNA.[1,2] Coincidentally, in the same year, W.E. Moerner and Lothar Kador first detected fluorescence from a single molecule (SM) at liquid helium temperature using frequency modulation spectroscopy.[3] Back in those days, no one would have dreamed that over the next couple of decades, these two fields would even be mentioned in the same sentence. Yet, significant advances in our understanding of RNA biology and SM detection technology have propelled these fields into an incredibly fruitful collaboration.

RNA, in one way or another, is involved in nearly every cellular process. The canonical function of RNA is to convert the information contained in a cell's DNA into functional proteins. In this process, known as the "central dogma", transcribed messenger RNAs (mRNAs) serve as an amplified read-out of the protein-coding genes. Two other RNAs are central to the protein production process: the ribosomal RNA

Special Issue: RNA: From Single Molecules to Medicine

Received: August 30, 2017
Published: January 24, 2018

DOI: 10.1021/acs.chemrev.7b00519
Chem. Rev. 2018, 118, 4120–4155

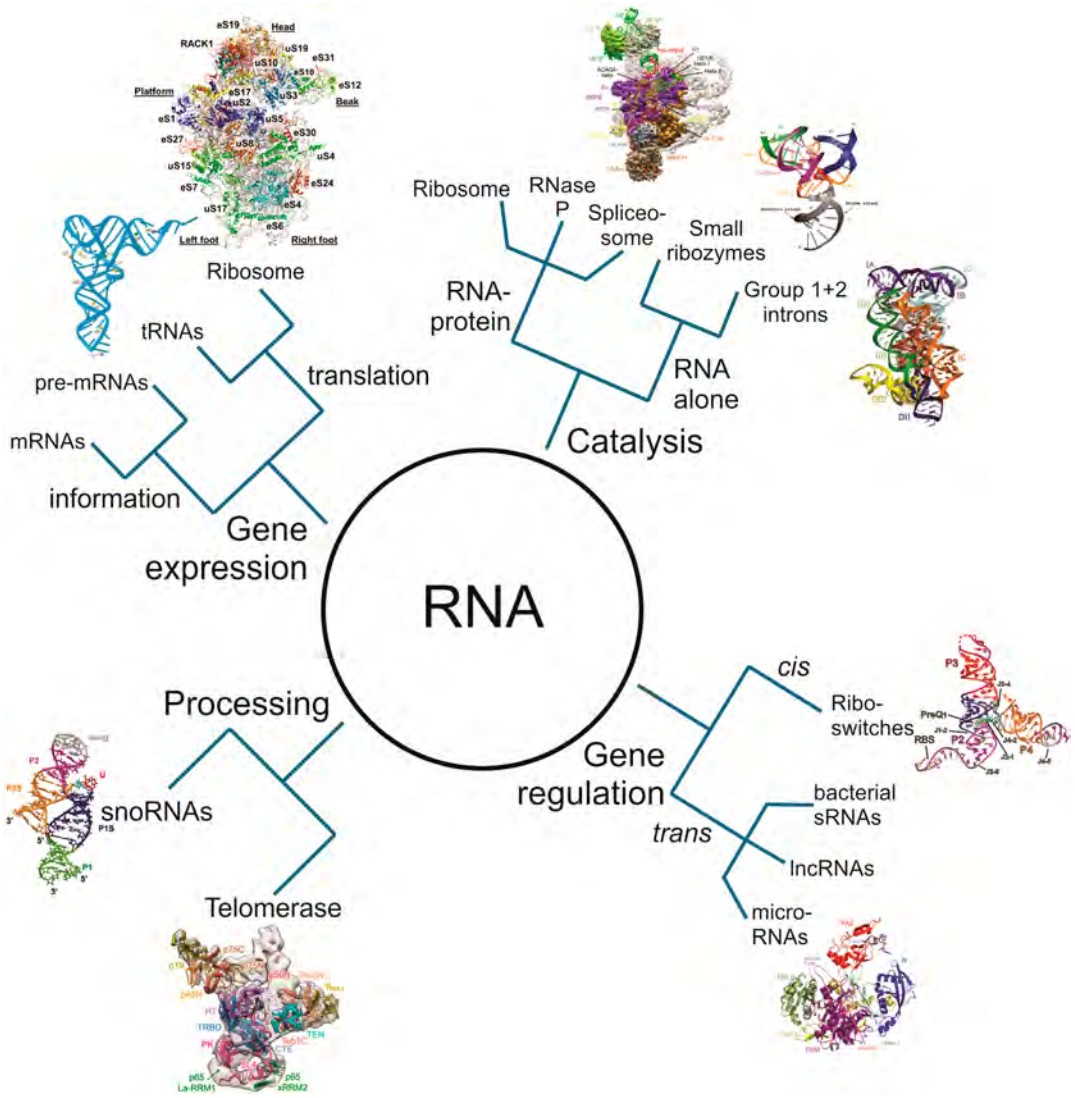

Figure 1. The many roles of RNA in biology. Reproduced with permission from ref 11. Copyright 2000 RNA Society. Reproduced with permission from ref 12. Copyright 2007 The National Academy of Sciences of the USA. Reproduced with permission from ref 13. Copyright 2008 American Association for the Advancement of Science. Reproduced with permission from ref 14. Copyright 2012 Elsevier Inc. Reproduced with permission from ref 15. Copyright 2015 American Association for the Advancement of Science. Reproduced with permission from ref 16. Copyright 2015 Macmillan Publishers Limited. Reproduced with permission from ref 17. Copyright 2017 Macmillan Publishers Limited. Reproduced with permission from ref 18. Copyright 2015 National Academy of Sciences. Reproduced with permission from ref 19. Copyright 2017 National Academy of Sciences.

(rRNA) that creates the enzymatic core of the protein synthesis machinery, and the transfer RNAs (tRNAs) that translate the genetic code into a series of amino acids. However, this conventional narrow view of RNA function has been revolutionized over the past several decades. The human genome project, which laid open the cellular genetic catalog, revealed the astounding fact that protein-coding genes account for only ∼1.2% of the human genome.[4−6] Subsequent studies found that although just 1.2% of the genome is transcribed to mRNA for protein production, at least 75% of the genome is transcribed as noncoding RNA (ncRNA).[7,8] Hundreds of thousands of distinct ncRNAs, with great structural and functional diversity, have been identified in cells.[9,10] These RNAs accomplish a multitude of biological functions including catalysis (for example, small ribozymes and as key components of the ribosome and spliceosome), the genetic material of some viruses, and regulation of gene expression (riboswitches, long ncRNAs, or lncRNAs, and microRNAs, to name a few) (Figure 1). The diversity and complex functional networks of these different RNAs led researchers to pursue RNA studies, initially applying traditional biochemical assays. However, these approaches are limited by the ensemble averaging and loss of spatiotemporal information caused by the concurrent observation of billions of molecules. The development of SM fluorescence techniques in the last couple of decades filled this void, providing valuable insights that have greatly advanced our understanding of the structure, dynamics, and function of RNA.

In this review, we first briefly summarize the development of RNA research over the last several decades. Next, we discuss the almost parallel development of SM fluorescence microscopy tools. We further review technical details of SM fluorescence microscopy that are relevant to RNA research, including common experimental guidelines. Finally, we high-

DOI: 10.1021/acs.chemrev.7b00519
Chem. Rev. 2018, 118, 4120−4155

light specific applications of SM fluorescence tools to investigate RNA structure, dynamics, and function in vitro. Throughout this section, we follow the growing complexity of in vitro systems that are being studied by SM fluorescence techniques, starting from simple isolated RNAs and RNA-protein complexes and culminating in complex RNA-protein macromolecular machines. These in vitro studies provide valuable insight into the function of the plethora of RNAs found in the cell. Our review is intended to compile the insights revealed by previous studies and to motivate and inspire the development of new assays and areas of investigation for future RNA research, driven by the revelations uniquely emerging from SM fluorescence techniques.

2. BIOLOGICAL AND TECHNICAL OVERVIEW

2.1. A Brief History of RNA Biology

By the early 1980's, researchers started to recognize that RNA is capable of far more than what it was originally credited for, in Francis Crick's central dogma of molecular biology.[20] It turned out not to be merely an intermittent carrier of biological information between DNA and proteins. Rather, RNA is a multifunctional biological molecule, capable of transferring biological information in a manner similar to DNA, but also proficient to catalyze biological reactions, as do proteins and enzymes. From the time of its initial discovery until today, RNA biochemistry has always intrigued researchers. Dr. James Darnell, in his book, *RNA: Life's Indispensable Molecule*, provides a comprehensive and captivating account of RNA research from the early 20th century to the present day, explaining key features of RNA research.[21] Many seminal RNA biochemistry discoveries arose before the 1980's, including transcription of DNA to RNA, pre-mRNA splicing, and the role of RNA in protein production. However, researchers still considered RNA to be an intermittent information carrier from DNA to protein.

In 1982, researchers in Thomas Cech's lab at the University of Colorado at Boulder first published on a self-cleaving RNA enzyme in *Tetrahymena*, starting a boom in RNA research.[1] Within the same time frame, researchers in Dr. Sidney Altman's lab at Yale University discovered another RNA-enzyme, ribonuclease P (RNase P), that is essential for activation of inactive tRNAs.[2] These two enzymes contradicted the basic assumptions about RNA that existed at the time, forever altering the course of modern RNA biology. RNA molecules that are adequate to catalyze biological reactions were named ribozymes (ribonucleic acid + enzyme).[1] Researchers started to appreciate the fact that the presence of what may seem like a small hydroxyl group at the 2' position of the ribose sugar in RNA makes it a uniquely different molecule than DNA. The flexibility of the typical single-stranded form of RNA enables it to fold in a variety of secondary and tertiary structures that endow it with the proteinlike ability to catalyze numerous biological reactions. Indeed, the enzymatic activity of RNA had been hidden in plain sight in a complex at the heart of the central dogma of molecular biology: the ribosome. Despite some protein components, more than 60% of this megadalton-sized protein production factory is made of RNA. Another essential RNA-catalyzed biological reaction is pre-messenger RNA (pre-mRNA) splicing in eukaryotes, in which nonprotein-coding regions of the pre-mRNA are removed to make protein-coding mRNA. The splicing machinery, the spliceosome, contains five small nuclear RNAs (snRNAs) that have been shown to comprise the active site that catalyzes the splicing reaction.[22] Many such "small" and "large" RNA structural motifs have been discovered ever since, starting from more ribozymes that catalyze their own cleavage and ligation reactions, to complex multiple RNA-protein assemblies such as the spliceosome and the ribosome. RNA biology evolved and advanced around discoveries such as these.

By the mid-1990's, the hot topics of RNA research included mostly ribozymes, translation, and pre-mRNA splicing. At this point, RNA biologists began to appreciate that the complex three-dimensional folding of RNA is crucial for its enzymatic activity. Approaches to obtain crystal structures of different ribozymes started to become available, providing structural insights into RNA catalysis.[23,24] Yet, while scientists had already appreciated that genes are commonly interrupted by introns that must be removed by pre-mRNA splicing,[25,26] the chemical reactions and structural rearrangements involved in splicing were only vaguely understood. Experiments began to reveal examples of alternative splicing where removal of different introns yields different proteins from the same DNA sequence.[26] Among many examples, RNA-related research at that time embraced the biochemical characterization of translation, tRNAs,[27,28] RNase P,[29−31] HIV RNA, and RNA editing.[32,33]

Looking back from 20 years later, it is clear that RNA research has been further revolutionized.[34] To put things in perspective, the total number of RNA-related research articles in the last 20 years has been more than quadrupled compared to the previous two decades. Nowadays it seems astonishing that from its discovery in the 1930's to around the mid-1980's, RNA was so underappreciated that the field evolved only very slowly. The discovery of ribozymes revitalized the field, yet only in the last couple of decades have we started to uncover the full functional repertoire of RNA. The list of things that were still unknown in the mid-1990's and are known now is compelling. Researchers have started to discover many types of riboswitches, regulatory RNA structures that bind to small ligand molecules and control transcription and/or translation in bacteria.[35−39] Using X-ray crystallography and cryo-electron microscopy, they solved crystal structures of complex RNA-protein structures such as the ribosome[40−47] and spliceosome.[17,48−54] Structures of the ribosome revealed the fact that the rRNA, and not the ribosomal proteins, catalyzes peptide bond formation during protein production.[55,56] We now understand that telomerase uses a built-in RNA template to add DNA sequences to the end of the chromosome to maintain genomic stability.[57] Scientists discovered RNA interference, in which small interfering RNAs (siRNAs) function in RNA-induced silencing and post-transcriptional gene expression regulation.[58,59] Discoveries of microRNAs (miRNAs) revealed how a single small RNA can interact with many partially paired sequences of diverse mRNAs to collectively impair their translation.[60−64] We are also starting to understand the roles of long noncoding RNAs (lncRNAs) in transcriptional gene expression regulation and a diverse set of other functionalities.[7,65−67] These advances have in part been aided by emergent new tools; for example, we can now perform high-throughput genome- and transcriptome-wide sequencing studies instead of characterizing only a few RNAs or RNA-protein complexes at a time, enabling a comprehensive characterization of transcription and translation mechanisms.[68,69] With the discovery of CRISPR-Cas9 and related systems, we have further identified how a bacterial immune

DOI: 10.1021/acs.chemrev.7b00519
Chem. Rev. 2018, 118, 4120−4155

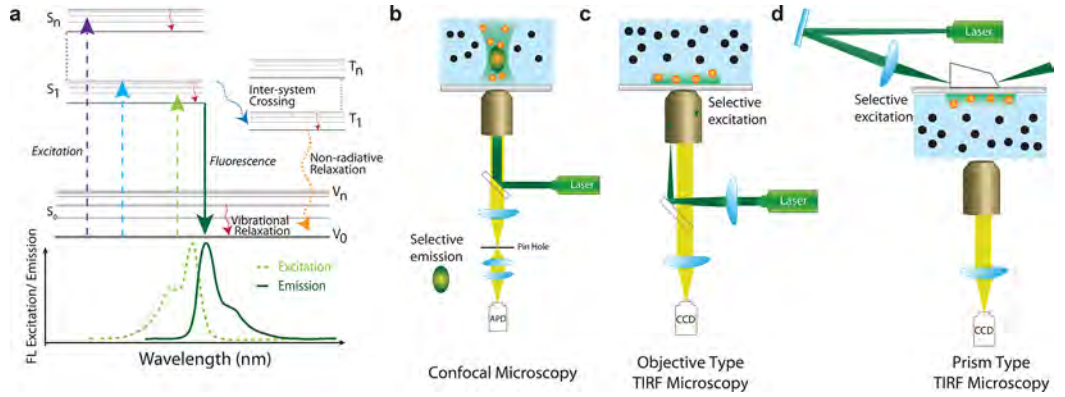

Figure 2. Photophysical properties of fluorescent molecules and different SM excitation and emission methods. (a) Jabłoński Diagram: A photophysical description of fluorescence. S_0, S_1–S_n, and T_1-T_n represent the singlet ground state, singlet excited states and triplet excited states, respectively. Schematic representations of excitation and emission pathway of different SM microscopes: (b) confocal, (c) objective type TIRF and (d) prism type TIRF.

system uses a RNA-guided protein to detect and destroy foreign viral DNA.[70−72] This insight from basic research has given us a very efficient tool to make genome editing practical by generating sequence-specific double-strand DNA breaks. Thus, RNA science has evolved rapidly and significantly over the years, leading to more than 30 scientists winning Nobel Prizes for experimental work on RNA-related research.[73]

2.2. A Brief History of Single Molecule Fluorescence Microscopy

Far from the emerging world of RNA biology, another field of research was also evolving at a rapid pace, that of single molecule fluorescence microscopy. Fluorescence had been known since the 16th century during the European Renaissance when people started to notice that some elements absorb light and emit a different color of light.[74] However, the name fluorescence was coined much later in 1852 by George Gabriel Stokes.[75] Although fluorescence had been used in the disparate fields of basic physics and chemistry as a detection technique, the observation of single fluorescent molecules did not come until 1989. Moerner and co-workers first detected fluorescence from a single dopant molecule of pentacene in a *p*-terphenyl host crystal at liquid helium temperature using frequency modulation coupled with ultrasonic modulation to reduce background signals.[3] In 1993 Betzig and co-workers first detected single molecules at room temperature,[76] an important step toward the application of SM detection under ambient conditions. The last piece of the puzzle was to use aqueous conditions, which are indispensable for biological measurements. Two years later, in 1995, this challenge was finally conquered with the use of total internal reflection fluorescence (TIRF) microscopy to study single myosin proteins.[77] These initial experiments paved the way for the application of SM fluorescence technologies to more complex biological problems. From the beginning of the twenty-first century, SM fluorescence and molecular biology have worked together ceaselessly, with the complexity of biological problems promoting the development of new SM methods, and those methods boosting studies of still more complex systems.

2.2.1. Fluorescence Microscopy. Fluorescence is a process in which a susceptible molecule (known as a "fluorophore" or simply "dye") becomes excited by absorbing energy from an external stimulus (typically visible- or ultraviolet wavelength light) and eventually emits lower frequency light while transitioning from an electronically excited state to the ground state. Figure 2a represents a classical Jabłoński diagram that is used to describe fluorescence in terms of electronic states.[78] Beginning in its ground state, the fluorophore absorbs photons that have the energy necessary to promote an electronic transition. In order to promote this transition, the incident light must be nearly resonant with the energy gap between the electronic states. Excitation is initially followed by relaxation to the lowest vibrational energy level of the first electronic excited state and then by relaxation back to the electronic ground state. If photons are emitted as a result of this second relaxation process, the process is called fluorescence. As both the absorbance and the emission are dependent on the energy gap between the ground and excited states of the particular molecule, each fluorophore has a distinct absorbance and emission spectrum (Figure 2a).

Use of fluorescence in biological sciences has grown remarkably over the last three decades. It forms the basis of dominant technologies used in many different fields including biophysics, biochemistry, biotechnology, neurobiology, immunology, DNA sequencing, medical diagnosis, and more. This widespread popularity stems from the inherent sensitivity and specificity of fluorescence detection. Fluorescence is readily distinguished from background scattering because the emission wavelength is red-shifted relative to the excitation wavelength.[79] This phenomenon is known as the "Stokes shift" and occurs due to vibrational and solvent relaxation in the excited state prior to emission. The varying emission and excitation spectra of different dyes allow multiplexing, in which multiple dyes can be monitored simultaneously. Furthermore, the emission can be localized to a high degree of accuracy and precision in order to pinpoint the location of the emitter based on a whole set of super-resolution fluorescence microscopy techniques.[80,81] For typical biological applications, small organic dye molecules or variants of naturally occurring fluorescent proteins are attached to the molecules of interest.[79] Detection of fluorescence from the dyes can, therefore, provide information about the existence and localization of multiple biomolecules. Quantum dots are also finding increasing use in SM fluorescence measurements, offering enhanced brightness, high quantum yield, narrow emission profile, large Stokes shifts, and excellent photostability. Due to their extended photostability, quantum dots have been particularly advantageous in single molecule particle tracking experiments.[82−84] However, their relatively large size (~6−60 nm hydrodynamic diameter) and tendency to adsorb

DOI: 10.1021/acs.chemrev.7b00519
Chem. Rev. 2018, 118, 4120−4155

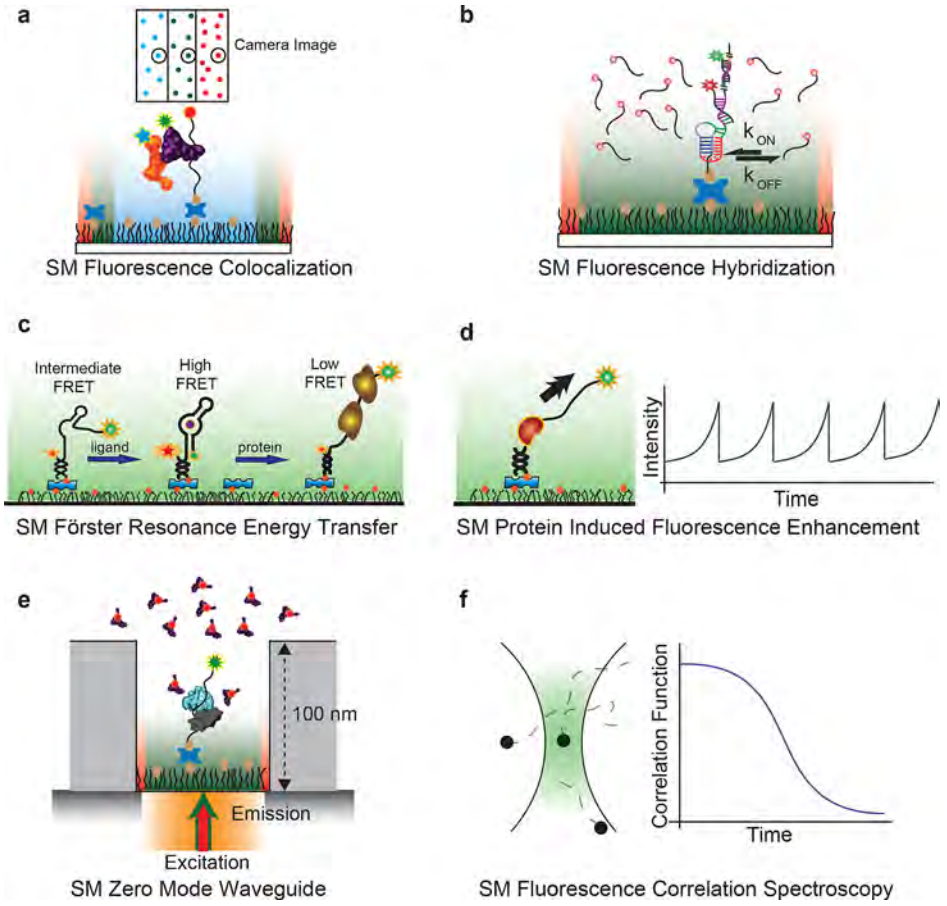

Figure 3. The different SM fluorescence techniques employed in RNA research. The schematics represent single molecule (a) fluorescence colocalization, (b) fluorescence hybridization, (c) Förster resonance energy transfer, (d) protein induced fluorescence enhancement, (e) zero mode waveguide, and (f) fluorescence correlation spectroscopy.

proteins into a corona are currently the main drawbacks to their use, particularly for distance-dependent measurements such as FRET.[85]

Over the years, fluorescence microscopy techniques have developed significantly. Conventional epifluorescence microscopes have been used regularly in biological experiments for decades. These fluorescence microscopes are typically equipped with a broad-spectrum excitation light source that is filtered to transmit a specific excitation wavelength. The emitted fluorescence is collected by an objective lens and sent to a photodetector (typically a photodiode or camera). An emission filter is placed before the detector to block any scattered excitation light. The simple design of the epifluorescence microscope led to its use in the study of a vast array of biological systems.[86,87] However, in the epifluorescence imaging scheme, the full sample space within the light path is excited at the same time. The resulting image includes fluorescence not only from the sample plane but also from all other planes above and below the sample. As a result, the actual image is blurred by a large contribution of unfocused fluorescence as background. This background fluorescence considerably lowers both the sensitivity and specificity inherent to fluorescence measurements.

Several imaging techniques have evolved to increase the quality of fluorescence images by reducing unwanted background fluorescence, and they generally fall under the categories of selective excitation and selective emission. To elaborate, in the strategy of selective emission, the whole volume of the sample is excited in a way analogous to epifluorescence, but the background is reduced by collecting the emission from only a very small focused volume. Examples of this type of microscopy include confocal microscopy (Figure 2b) and spinning disk confocal microscopy. An alternate strategy is a selective excitation, where only a small portion of the sample is illuminated, and as a result, the molecules that are outside the excitation volume do not contribute to the background. Examples of this type of microscopy include TIRF microscopy (Figure 2, panels c and d), selective plane illumination microscopy (SPIM), and two-photon excitation microscopy, to name a few. Here we will discuss two techniques that are widely used for SM imaging: confocal microscopy and TIRF microscopy (Figure 2, panels b–d).

In the confocal microscope, a large sample volume is first excited by a light source focused on the sample plane. The emitted fluorescence is then collected by an objective lens and focused onto a pinhole (Figure 2b). The pinhole (typically on the scale of a few microns in diameter) only allows light from the sample plane to pass through and eliminates light from the out of focus planes, decreasing the background from the unfocused planes. The size of the pinhole essentially determines the confocal volume that contributes to the fluorescence signal, which is recorded with a sensitive point detector like a photomultiplier tube (PMT) or an avalanche photodiode (APD).[88,89] Consequently, the sample has to be scanned to produce a two-dimensional (or three-dimensional) image. By contrast, TIRF microscopy is based on the theory of

DOI: 10.1021/acs.chemrev.7b00519
Chem. Rev. 2018, 118, 4120–4155

total internal reflection of light. When light travels from an optically dense to a less dense medium and the angle of incidence exceeds the critical angle between the two media, it undergoes total internal reflection (TIR) at the interface between the two media. Although most of the light is reflected, a small fraction of light, termed an evanescent wave, travels along the interface between the two media, where its amplitude decays exponentially with distance from the interface, creating a thin lamina along the surface (Figure 2, panels c and d). TIR provides inherently selective excitation of molecules near the surface, while molecules away from the surface (beyond the penetration depth of ∼100−200 nm, depending on the incident angle) are not excited by the evanescent wave and therefore do not contribute to background. As a wide-field technique, the entire illuminated surface can be imaged at once using a sensitive camera such as an electron multiplying charge-coupled device (EMCCD) or a scientific complementary metal-oxide-semiconductor (sCMOS). After first being invented to study cell movements,[90] total internal reflection fluorescence (TIRF) microscopy evolved as one of the leading techniques to reduce background in fluorescence-based imaging.[91−93]

There are certain key differences between these two techniques. TIRF microscopy allows simultaneous detection of hundreds of molecules using a sensitive camera. While simultaneous detection aids in obtaining robust statistics, it comes at the cost of compromised temporal sensitivity. Confocal microscopy is limited to detection of one molecule at a time, but the use of a photodiode rather than a camera enables temporal resolutions that are of 10 orders of magnitude faster than that of TIRF systems. Thus, these two techniques offer complementary strengths.

2.2.2. Single Molecule Fluorescence Techniques. Both confocal and TIRF microscopy provide the prerequisites for single molecule detection by increasing the contrast between the very weak desired signal and the background. Once this technical foundation had been laid, SM methods experienced a rise in popularity as a result of their capability to access critical molecular details compared to their predecessor biochemical techniques. Traditional biochemical methods typically interrogate the kinetic or thermodynamic behavior of billions of molecules together and yield measures of the average behavior of the system, leading them to be termed "bulk assays". Over the years bulk assays have been vastly informative and allowed researchers to learn a great deal about the overall behavior of biological systems. However, molecular details such as the partitioning between reaction pathways or the inherent heterogeneity in the system are quite often inaccessible due to ensemble averaging, yet represent important determinants of biology. In contrast, SM methods enable direct detection of molecular subpopulations, transiently visited states, rare molecular events, nonuniform kinetic behavior, and more. With careful design of the experiment, the potential of SM measurements for new discoveries is virtually limitless. In the following section, we discuss several foundational SM approaches that have been applied to RNA (Figure 3).

2.2.2.1. SM Fluorescence Localization. The focused emission from a single molecule appears in an image as a two-dimensional point-spread function whose width depends on the wavelength of the emitted light and the numerical aperture (N.A.) of the objective used to collect emitted photons. Two-dimensional image analysis techniques exploit the typically Gaussian shape of the point spread function to localize the fluorophore with a high degree of precision (on the order of a few nanometers), often referred to as "super-resolution" or "nanoscopy" as it breaks the classical diffraction limit of optical microscopy.[80,94,95] Moreover, different dye molecules have different emission wavelengths and thus are chromatically differentiable, allowing detection to be multiplexed with several distinct dye molecules attached to different biomolecules (Figure 3a). As many macromolecular machines contain multiple components, details about their composition, stoichiometry, assembly pathways, and compositional heterogeneity can be determined through simple colocalization measurements by labeling multiple components with different fluorophores.[96] While it does not measure interactions directly, colocalization between dyes suggests that the molecules are in close proximity and therefore may be interacting with one another and/or a common substrate or binding partner.

2.2.2.2. SM Fluorescence Hybridization. In SM fluorescence hybridization studies, dynamic binding and dissociation events are measured to understand the binding specificity and affinity of two biomolecules. In these assays, a biomolecule of interest is tethered to a surface, labeled with a fluorophore to mark its position on the slide. A binding partner labeled with a different dye interacts dynamically with the surface-immobilized molecule, and its binding and unbinding kinetics report valuable information about the interactions between those two molecules (Figure 3b). The colocalization of the two fluorophores helps to eliminate false positives generated from nonspecific binding of the probe to the slide. An example of such a technique is Single Molecule Kinetic Analysis of RNA Transient Structure (SiM-KARTS).[97] In this approach, a fluorescently labeled nucleic acid probe is used to probe changes in the structure of a long target RNA through repeated binding and dissociation events. Probes can be designed so that binding is so transient that it minimally affects the secondary or tertiary structures of the RNA target. Similar kinetic techniques have been used to study the binding kinetics of RNA-DNA, RNA-RNA, and RNA-protein complexes, or to detect and count single RNA biomarker molecules.[98]

2.2.2.3. SM Förster Resonance Energy Transfer (smFRET). Förster (or fluorescence) resonance energy transfer (FRET), which reports on the distance between two fluorophores over a range of 1−10 nm, is currently perhaps the most popular SM fluorescence technique (Figure 3c). FRET, named after Theodor Förster who explained the phenomenon theoretically,[99] occurs through a nonradiative long-range dipole−dipole interaction between a pair of fluorophores. In this process, a donor dye is initially excited by an external light source. When the acceptor dye is physically close to the donor, most of the relaxation energy of the donor electrons is transferred to the acceptor molecule. The transfer of energy from the donor to the acceptor molecule results in the donor returning to its electronic ground state, and the acceptor transitioning to an electronically excited state. Relaxation from this excited state results in fluorescence emission from the acceptor. The energy transfer efficiency is inversely proportional to the sixth power of the distance between donor and acceptor molecule and is given by $E_{\mathrm{FRET}} = 1/\left(1 + \left(\frac{R}{R_0}\right)^6\right)$, where R is the distance between the donor and the acceptor. R_0 is the characteristic distance of the FRET pair at which half of the donor energy is transferred to the acceptor. It is unique for different donor−acceptor pairs, typically in the range of 3−8 nm, and is a function of, among other factors, the spectral

DOI: 10.1021/acs.chemrev.7b00519
Chem. Rev. 2018, 118, 4120−4155

overlap of donor emission and acceptor excitation, and the relative orientation of their transition dipole moments. Experimentally, the FRET efficiency is estimated as the ratio of acceptor intensity to the total intensity of donor and acceptor, $E_{FRET} = I_A/(I_D + I_A)$. The representation of E_{FRET} as a normalized acceptor intensity provides crucial practical advantages by making it independent of the individual donor and acceptor intensities. Therefore, compared to other single molecule techniques, FRET-based studies have gained significantly larger tolerance of experimental variability such as inhomogeneity of the excitation laser beam, external vibrations, signal amplification characteristics, etc. Thus, FRET functions as an approximate molecular ruler over a length scale of a few nanometers, making it an ideal tool to study many biomolecular systems (Figure 3c). Single molecule detection technologies, both in TIRF mode and in confocal mode, can be used to measure FRET at the single molecule level. The use of small organic dye molecules with high quantum yields enables biomolecules of interest to be labeled with minimal perturbation. smFRET is widely used to study both intramolecular conformational dynamics of nucleic acids and proteins as well as intermolecular interaction between distinct species.[100,101] For the purposes of this review, we will only discuss its applications to RNA-related systems.

2.2.2.4. SM Protein-Induced Fluorescence Enhancement. It had been shown previously that the quantum yield of cyanine-based fluorescent dyes changes proportionally with the local viscosity of the dye molecule,[102,103] with increased viscosity decreasing the efficiency of a cis−trans isomerization process that yields dark states and can lead to photodamage. This property is quite useful in the SM imaging field: if a protein molecule binds very close to a fluorescent dye, that changes the local viscosity of the dye and results in an increase of fluorescence, an effect known as protein induced fluorescence enhancement (PIFE).[104,105] In these assays, the fluorescent dye is typically attached to RNA or DNA and binding of a protein close to the dye leads to an enhancement of fluorescence intensity (Figure 3d). For example, PIFE has been used frequently to study the movement of helicases on DNA/RNA tracks.[106] The increase in intensity due to PIFE is linearly proportional to the distance between the dye and the protein and is sensitive over a range of 0−4 nm.[106] Time-correlated single photon counting measurements have shown that the fluorescence lifetime of the dye is strongly correlated with the PIFE effect.[107] In comparison to smFRET, smPIFE requires only one dye molecule and binding or movement of a protein. PIFE is sensitive over shorter distances than FRET, making it a complementary tool to study close-range RNA-protein interactions.

2.2.2.5. SM Excitation with Zero Mode Wave Guides. One of the drawbacks of SM measurements is that in order to minimize background, the dye concentration in the solution is limited to between picomolar and at maximum tens of nanomolar concentrations. Many biological processes, however, require micromolar or higher concentrations of binding partners. This challenge can be tackled by reducing the conventional observation volume to attoliter volumes. Zero mode wave guides (ZMWs), consisting of holes of subwavelength dimension in a thin metal film, provide a way to study SMs at higher dye concentrations; upon light exposure, only the bottom of each hole will be illuminated by an evanescent field, whereas the metal film otherwise blocks the light and thus excitation of excess fluorophores (Figure 3e).[108,109] Recent measurements have demonstrated significant plasmonic enhancement of fluorescence and smFRET signals using particularly aluminum-based ZMWs,[110] whereas nanopores have been employed to improve the loading of ZMWs for DNA sequencing applications.[111]

2.2.2.6. SM Fluorescence Correlation Spectroscopy. Unlike the other fluorescence-based SM techniques, the parameter of interest for fluorescence correlation spectroscopy (FCS) is not the fluorescence intensity itself but its fluctuations over time.[112,113] Typically, FCS is used in a confocal configuration with a particularly small pinhole to reduce background and achieve SM fluorescence sensitivity from a particularly small volume element. Other than the random noise, signal fluctuations occur either due to diffusion through the open volume element or structural changes of the biomolecule associated with the fluorophore. FCS analyzes the resulting fluorescence intensity fluctuations by quantifying both the correlation of the fluctuation over time and deviation in amplitude from the mean intensity (Figure 3f). The amplitude fluctuation from the mean value provides thermodynamic information whereas the correlation over time provides kinetic information about the system. These parameters encode information about structural changes in the biomolecule, diffusion rates, aggregation, and stoichiometry of binding. Variations of the FCS technology exist that use multicolor detection such as in fluorescence cross-correlation spectroscopy (FCCS),[114,115] dual beam detection,[116] or fluorescence lifetime detection through time-correlated single photon counting (TCSPC),[117] which all have introduced additional dimensions to the original FCS technique.

2.2.3. General Experimental Guidelines. For SM fluorescence-based assays, the optical setup, sample preparation, data analysis, and interpretation are all critical components that often have to be optimized on a case-by-case basis. While each SM fluorescence technique thus differs in some of these aspects, certain underlying principles can be discerned.

2.2.3.1. Optical Setup. Typically, a laser line is used as the excitation source. Although technically it is possible to use a white lamp or a light-emitting photodiode and suitable filter sets as the excitation source, it is uncommon.[118−120] Depending on the application, multiple laser lines are often coupled together using dichroic mirrors for simultaneous or interleaved multicolor excitation. For confocal setups, the laser beam is then collimated to the back of a high numerical N.A. objective and focused onto the sample plane. A high N.A. objective is important for a tight focus on the sample plane. In contrast, for excitation in the TIRF mode, the laser beam is deflected at an angle greater than the critical angle either within a high N.A. objective (called "objective type TIRF" or oTIRF, Figure 2c) or by coupling the beam into a prism that guides it to a reflecting slide surface (called "prism type TIRF" or pTIRF, Figure 2d), with the name referring to the optic responsible for directing the light at the sample.[121] In both cases, an evanescent wave is generated in the sample chamber that only excites molecules very close to the surface.

The fluorescence is similarly collected by a high N.A. objective, which in confocal and oTIRF microscopes is the same objective used for excitation. High N.A. objectives are used again in this case to increase the range of angle over which the emitted light can be collected (for example, a water immersion objective with N.A. of 1.2 can collect light over a half angle of ∼64°). The collected beam is focused by a tube lens (typically within the microscope body) and passed through

DOI: 10.1021/acs.chemrev.7b00519
Chem. Rev. 2018, 118, 4120−4155

an emission filter to chromatically eliminate any scattered excitation light. The tube lens is selected such that the output beam is focused near the exit port of the microscope (180−200 mm focal length). For confocal imaging, a small (∼1 μm in diameter) pinhole is placed at the focal point of the tube lens to spacially reject emission from out-of-focus planes. In contrast, TIRF imaging collects all emitted light without any spatial filtering. The collected light is then either sent to a detector or further processed downstream. As TIRF generally enables detection of several hundreds of molecules simultaneously in a wide field of view, a charge-coupled device (CCD) camera is typically used to detect the single molecules. Although such a detection technique enables a substantial number of molecules to be monitored in parallel, it limits the data acquisition rate to currently about 1 kHz at best. Complementarily, a confocal setup only images light from the focus of the beam so that a more sensitive single pixel detector is sufficient for imaging. Typically APDs or PMTs are used for this purpose, allowing acquisition speeds up to tens of megahertz. In FCS, the sample signal itself fluctuates over time, whereas in laser scanning confocal microscopy, a meandering sample scanning pattern gradually images a larger field of molecules; alternatively, spinning disc confocal microscopy uses an expanded laser beam together with rapidly spinning discs carrying arrays of microlenses and pinholes to near-simultaneously sample a larger field of view.

Many applications require spectral discrimination of the emitted signal. For this purpose, the focused beam from the exit port of the microscope is collimated by an additional lens and then further processed using different methods including but not limited to dichroic mirrors, filters, polarizers, polarizing beam splitters, partial beam intensity splitting mirrors, and additional lenses. The processed beam is then focused onto the detector by a final set of lenses.

2.2.3.2. Sample Chamber Preparation. For single molecule detection, it is critical that the molecule of interest be at a low enough concentration that the fluorescence signal from one molecule does not influence the signal from another. For example, sample concentrations for solution-based methods such as confocal microscopy are limited to the picomolar range. This is to ensure that multiple molecules do not diffuse through the focus of the laser at the same time, which would provide an averaging effect. The freely diffusing molecules can be imaged very fast but only for a brief period of time, which is dependent on the diffusion coefficient of the observable molecule. However, many biochemical reactions occur on time scales of seconds. Surface immobilization of molecules allows information to be gathered from a particular molecule for extended time periods (hundreds of seconds, limited only by photodamage to the dye). In surface-tethered SM experiments, one of the most crucial elements is the surface itself, which needs to be free of fluorescent impurities and should be minimally absorptive to reduce nonspecific binding of biological molecules. As a general theme, the surface constituents should be neutral or negatively charged under aqueous conditions at neutral pH so that they are repellent to nucleic acids. Many different surface cleaning and passivation techniques have been developed, all with their respective advantages and drawbacks. One common passivation approach involves surface coating by bovine serum albumin (BSA),[122,123] or bovine casein.[124−126] These proteins are adsorbed to the surface before relevant biomolecules of interest are introduced to the system. Nevertheless, due to competitive nonspecific binding with the proteins of interest, these methods provide insufficient passivation for protein-focused SM experiments. A more widely used surface passivation technique employs polyethylene glycol-succinimidyl valerate (PEG-SVA).[127,128] This negatively charged polymer is very effective in preventing nonspecific adsorption of biomolecules; however, the process of passivation is time-consuming and the required reagents are expensive. Other relatively recent surface passivation techniques include dimethyl-dichlorosilane (DDS)-Tween-20,[129] poly-L-lysine-PEG copolymer (PLL−PEG), and heparin-based methods.[130] These new approaches provide similar or better surface quality compared to PEG-SVA-based passivation, in addition to lower cost and/or faster processing.

In analogy to solution-based SM experiments, fluorescently labeled biomolecules need to be specifically bound to the surface at a density sufficiently low to avoid overlapping of multiple molecules. To this end, a small percentage (1−10%) of surface passivating molecules is typically modified by biotin. Streptavidin, a tetrameric protein with very high affinity for biotin (dissociation constant $K_d = 10^{-15}$ M), is then introduced into the sample chamber.[131,132] This biotin−streptavidin linker has a rupture force of ∼1000 pN, making it one of the most stable noncovalent bonds.[133,134] The three additional binding sites of the surface-bound streptavidin are available to the biomolecule of interest, which is also modified with biotin. The binding specificity and stability of the biotin−streptavidin linkages makes it one of the most efficient and popular surface immobilization approaches. However, click chemistry linkers and other binding partners have been used in certain cases.[135,136] Click chemistry linking techniques are based on covalent bond formation and are therefore even stronger than biotin−streptavidin linkers. The removal of the streptavidin protein from the system permits the use of UV probes, which would otherwise be masked by the tryptophan fluorescence from the protein. However, one of the main limitations of these techniques is that, in most cases, the biological samples have to withstand rather "harsh" click chemistry reaction conditions. Development of mild reaction conditions could potentially make click chemistry based attachment techniques more popular. Vesicle encapsulation techniques have also been used, wherein the molecule of interest is isolated from the surface in a vesicle comprised of a mixture of biotinylated and nonbiotinylated lipids.[137,138] Other surface tethering techniques include antibody-mediated pulldown of tagged biomolecules. These types of pulldown assays allow specific isolation of the molecule of interest from a complex mixture.[139]

2.2.3.3. Sample Preparation. SM fluorescence measurements by definition require a fluorophore to exist somewhere within the complex of interest, and the choice of an appropriate fluorophore is the key to successful SM measurements. In ensemble fluorescence studies, the signal consists of fluorescence from billions of dye molecules together. As a result, the stability and brightness of individual dye molecules are not critical. However, for SM measurements, choice of the dye(s) is of paramount importance. An ideal dye for SM fluorescence should be photostable with minimal intensity fluctuations on the experimental time scale and should have high extinction coefficient and quantum yield. Native fluorophores such as tryptophan, tyrosine, and certain enzyme cofactors exist, but these have yet to be widely adopted for SM imaging because of their low brightness and limited experimental versatility.[140] For in vitro applications, small organic dyes are often favored over fluorescent proteins and quantum dots because their small size

DOI: 10.1021/acs.chemrev.7b00519
Chem. Rev. 2018, 118, 4120−4155

is likely to exert minimal perturbations to the system.[141] Furthermore, some fluorescence techniques demand additional criteria for dye selection. For example, the excitation and emission spectra of the dyes need to be well-separated in wavelength for multiple fluorophore SM assays, to avoid cross-excitation and detection. Most experiments, therefore, require that a small molecule fluorophore is artificially incorporated into the sample in some way. A number of methods have been employed for dye incorporation, with the ideal choice depending on the specific question being pursued. First, the complex of interest can be assembled on a relatively simple, fluorophore-labeled scaffold. Among many other examples, this approach has been used to study the spliceosome, with the pre-mRNA fluorophore-labeled at specific sites.[142−144] This was accomplished by ligating together two synthetic, fluorophore-labeled oligonucleotides to generate a minimal but efficiently spliced substrate.[145] Fluorophores can be site-specifically incorporated into long RNAs by ligation of short-labeled oligonucleotides to longer in vitro transcribed RNA or hybridization of short labeled oligonucleotides to extensions of the native RNA.[146,147] Proteins can be labeled by fluorophore-labeled antibodies against epitopes within the protein.[148] These approaches have the advantage that they do not require modification of the sequence of the substrate, although the fluorophores still have the potential to interfere with function.

In many cases, the sequence of the labeling target must be altered to allow incorporation of a fluorophore, a challenge that is nearly unavoidable when a protein is the desired labeling target. This challenge has been approached from a number of different angles. For proteins, these include labeling single-cysteine mutants of proteins with a dye-maleimide conjugate[143] and peptide tags that are covalently or noncovalently modified by enzymes.[149] More complex methods involve protein ligation mediated by inteins,[150] or incorporation of unnatural amino acids.[151] Several of these strategies have analogues that are used for surface-immobilization of complexes for TIRF microscopy, usually by attaching a biotin moiety rather than a fluorophore, which is then captured on a streptavidin-coated microscope slide, as described above. The most common approaches are biotinylation of a nucleic acid scaffold small enough for chemical synthesis, and capture of a sequence on the complex of interest with either a complementary oligonucleotide or an antibody, although any of the techniques described above could in principle be modified to incorporate a biotin rather than a fluorophore. In general, proteins are more challenging to label than RNA since each protein behaves differently and a labeling technique optimized for one may not work for another at all; by comparison, RNAs behave more consistently because of their more homogeneous chemical makeup with just four instead of 20 basic building blocks. Moreover, preparing long RNAs by solid-phase synthesis or in vitro transcription is relatively straightforward, and purification is facilitated by the fact that, unlike most proteins, RNAs can often be denatured and refolded without loss of biological function.

2.2.3.4. Data Processing. Data processing methods can vary widely across different types of SM fluorescence experiments. For experiments that image many molecules simultaneously, initial processing involves using local intensity differences to identify the locations of emitters. The intensity of each emitter is then tracked as a function of observation time to generate SM intensity traces. A gross level of initial screening is done to identify probable single molecules amid a background of fluorescent impurities and aggregated molecules, typically followed by manual curation to identify bona fide single molecules based on signal intensity, noise, and number of photobleaching steps. Background subtraction is also frequently done manually for each molecule by subtracting the signal intensity after photobleaching. Finally, data from many individual molecules are compiled together to generate histograms of observables such as FRET efficiency. Some attempts are being made at streamlining this analysis pipeline by making communal software available.[152,153]

The traces of individual molecules frequently exhibit fluctuations, which can provide valuable information on the dynamics of the system of interest. One of the most common techniques used to analyze dynamic data is hidden Markov modeling (HMM), which uses a multistate model to "idealize" noisy traces into a series of transitions between discrete states.[152] The challenge of defining the number of states present in a data set in order to avoid overfitting can be addressed by using the bayesian information criterion (BIC).[154] The number of states leading to the lowest value of the BIC after idealization can be selected as the most parsimonious model that describes the data. In experiments with multiple observables, such as the donor and acceptor intensities in smFRET experiments or the different components of polarization-resolved emission, correlations between the observables can often be expected. This fact can be exploited to build a global model that is more robust than the model that would be obtained for any given observable alone. For example, in studies on the spliceosome, HMM modeling was performed individually on donor and acceptor intensities and FRET efficiency, and only transitions that were found in all of these data sets were selected for further analysis.[142] A "change-point" analysis that is similar in concept has been applied to high-time-resolution polarization-sensitive measurements, in which a likelihood function is scanned over up to 16 different polarization channels, determining the most likely position of a transition over the entire data set.[155,156] Further analysis of single molecule time traces using techniques borrowed from other fields, such as bioinformatic clustering analysis[144] or neural spike train analysis,[97] can help further classify the behavior of larger numbers of individual molecules to identify statistically significant trends.

While single molecule fluorescence methods have contributed greatly to the understanding of RNA and other biological macromolecules, like all techniques, they come with certain shortcomings. Fluorophore labeling and surface immobilization require expensive materials and can potentially interfere with the properties of the biomolecules of interest. SM methods are most powerful in conjunction with appropriate bulk methods, which allow weaker signals to be accessed under less invasive conditions but lose access to dynamics and subpopulations that can be observed in SM experiments.

In addition to the SM fluorescence studies discussed here, SM force measurements have also been employed to study many aspects of RNA. Different force-based SM techniques, such as atomic force microscopy and optical and magnetic tweezers have provided significant insight into the thermodynamics and kinetics of RNA folding.[157−165] In addition to the observation of these dynamic molecules, force-based single molecule methods also provide manipulation capabilities in which force can be applied to the molecules in order to drive them along specific reaction coordinates. Furthermore, force and fluorescence have also been measured jointly as a coupled

DOI: 10.1021/acs.chemrev.7b00519
Chem. Rev. 2018, 118, 4120−4155

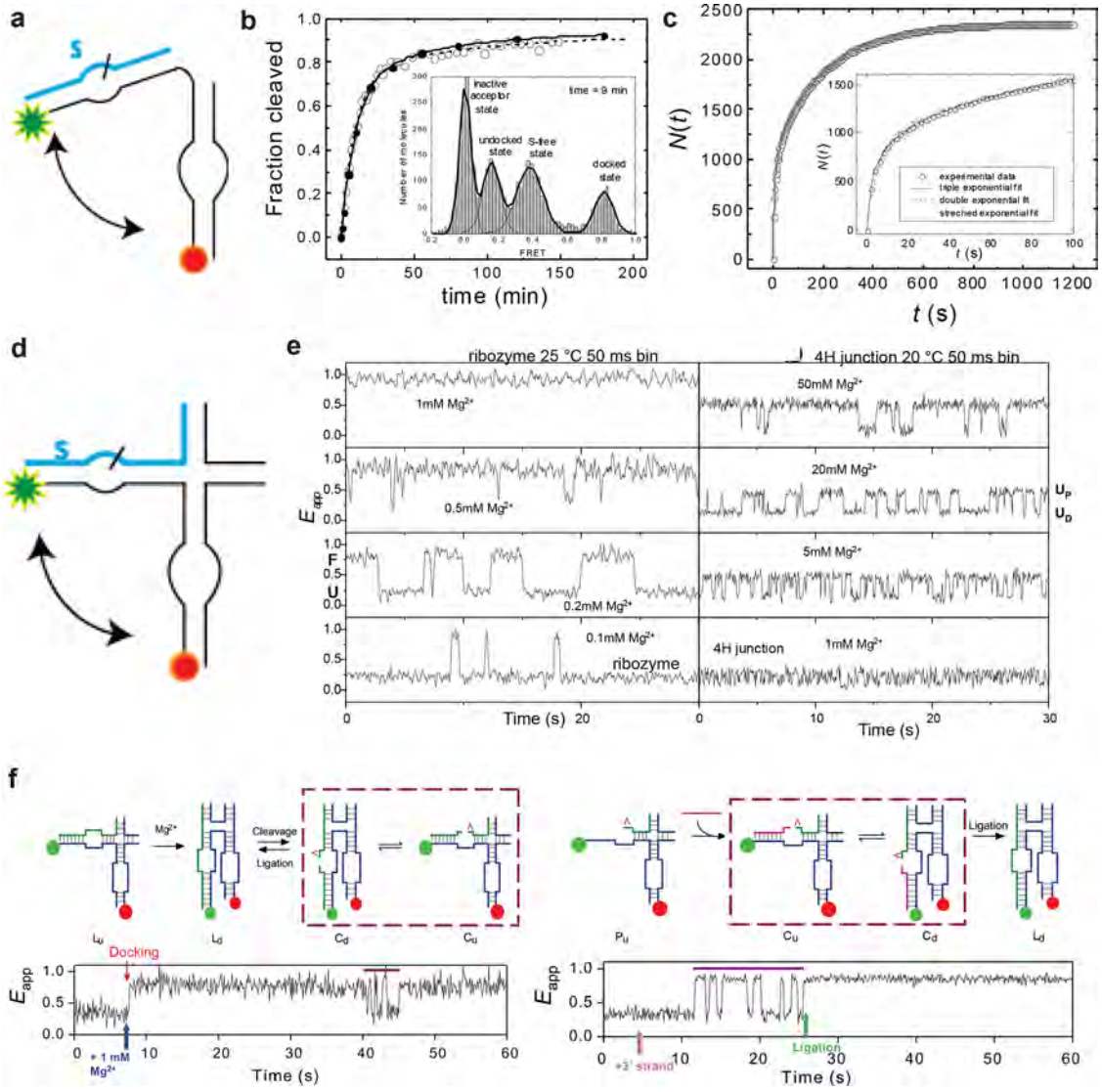

Figure 4. smFRET studies of the hairpin ribozyme. (a) Schematic of the hairpin ribozyme with only two internal loops. (b) Single-molecule and bulk solution measurements of enzymatic activities. The FRET efficiency histogram showed three distinct ribozyme populations: undocked (E_{FRET} = 0.15), docked (E_{FRET} = 0.81), and substrate-free ribozymes (E_{FRET} = 0.38). The S-free fraction is plotted against time, indicating heterogeneous reaction kinetics. (c) The undocking kinetics suggests four docked states of distinct stabilities. The inset represents other representative exponential functions that fit the data poorly. Panels (b) and (c) are reproduced with permission from ref 173. Copyright 2002 American Association for the Advancement of Science. (d) Schematic of the hairpin ribozyme with two internal loops and a four-way junction. (e) Structural transitions in single hairpin ribozyme molecules and loop-free 4H junctions at different Mg^{2+} concentration. Reproduced with permission from ref 174. Copyright 2003 The National Academy of Sciences of the USA. (f) smFRET study to assign cleaved and ligated states of hairpin ribozyme. The schematics of the assay to identify the ligated (left top panel) and cleaved (right top panel) form of the ribozyme. A sample SM time trace (left bottom panel) shows that upon addition of 1 mM Mg^{2+} (blue arrow) the ribozyme docks (high FRET) and remains docked until it exhibits a brief period of rapid undocking and docking signifying a cleavage event (purple bar). A sample time trace (right bottom panel), showing rapid docking-undocking (indicated by the purple bar) before a transition to the stably docked state. Reproduced with permission from ref 175. Copyright 2004 Nature Publishing Group.

technique.[166−170] Given the breadth of force-based single molecule studies on RNA, an entirely separate review is warranted to do proper justice to such studies and the multitude of additional biological information they provide.

3. SINGLE-MOLECULE FLUORESCENCE STUDIES OF ISOLATED RNA STRUCTURES

Technology development has always driven innovation in the field of molecular biology, and the development of SM technology is no exception. It was merely a matter of time before this emerging technological advancement would be used to study a rapidly emerging biological interest, RNA, and its structural dynamics. In fact, one of the earliest applications of SM detection to biology studied ligand-induced conformational dynamics of a single RNA molecule.[171] In this work, Ha et al. studied a three-helix junction RNA molecule and showed that in the presence of magnesium (Mg^{2+}) ions and upon binding of ribosomal small subunit protein S15, the RNA molecule transitions between an open and closed conformation. This advance established that SM fluorescence can be used to study conformational dynamics of RNA molecules. Furthermore, detection of highly heterogeneous distributions of RNA

DOI: 10.1021/acs.chemrev.7b00519
Chem. Rev. 2018, 118, 4120−4155

conformations at intermediate ion concentrations suggested differences in folding between different RNA molecules,[171] an observation possible only through SM experiments.

3.1. Ribozymes

Since the discovery of RNAs with enzymatic activity in the early 1980's, researchers have sought to understand the chemical pathways and structural rearrangements necessary for RNA-based catalysis. Development of SM methods provided a unique opportunity to study ribozyme molecules dynamically in real time. Early experiments on this front were performed using smFRET on the *Tetrahymena* ribozyme,[172] hairpin ribozyme,[173−176] and *Bacillus subtilis* RNase P ribozyme,[177] yielding significant fundamental insights into these RNAs.

The most studied in this set is the hairpin ribozyme, which is found in RNA satellites of certain plant viruses and provides a particularly instructive example. The native hairpin ribozyme comprises two major structural elements, a four-way RNA junction and two internal loops. Zhuang et al. studied the minimal active hairpin ribozyme with only two helices and their internal loops (Figure 4a), employing smFRET to investigate the structural dynamics.[173]

Dynamic traces, as well as FRET efficiency histograms, revealed three distinct populations: undocked (low FRET ∼ 0.15), docked (high FRET ∼ 0.81), and substrate-free ribozymes (intermediate FRET ∼ 0.38). The time-dependent population of the substrate-free state showed that almost all of the substrate is cleaved within 60 min (Figure 4b). SM traces also revealed that the cleavage reaction can occur only from the docked conformation. Although the docking process showed (largely) single-exponential kinetics, the undocking kinetics are more complex with as many as four different docked conformations (Figure 4c). Surprisingly, the ribozyme has a strong memory of the docked conformation, and individual molecules transition from one undocking behavior to another very rarely, a static heterogeneity subsequently found in other RNAs.[178,179] The authors hypothesized that the different docked states of the hairpin ribozyme may be representative of distinct hydrogen bonding or Mg^{2+} binding configurations between the loop regions or potentially mass-neutral chemical modifications.[180,181] Overall, their data showed that dynamics between the docked and undocked states are essential to establishing the catalytic center for the cleavage reaction.

In a separate smFRET study, Tan et al. showed that the conformational interplay between the hairpin ribozyme's loop motifs and its native four-way junction leads to at least two intermediate folding states.[174] In this study, they used a hairpin ribozyme encompassing its full four-way junction (Figure 4d). They first studied the effect of Mg^{2+} on the dynamics of this ribozyme. Mg^{2+} is known to stabilize the docked conformation, and SM fluorescence studies accordingly showed increasing high-FRET population with increasing Mg^{2+} concentration. To decouple the effect of the two internal loops from the junction dynamics, the loop regions were mutated to generate perfect sequence complementarity. Surprisingly, the junction itself shows dynamic behavior with two distinct FRET states. These two states are different from the docked and undocked states observed in their wild-type and are inherent to the junction dynamics (Figure 4e). The low-FRET state was labeled a distal undocked state, whereas the high-FRET state was assigned as a proximal undocked state, and these two states significantly interconvert at physiological Mg^{2+} concentration. Furthermore, the authors showed that the ribozyme inherits the dynamics of this four-way junction and exploits the resulting frequent encounters between the two loops to facilitate stable docking. Using a confocal microscope to achieve a 10 μs time resolution, the authors were also able to show that the proximal state is an obligatory intermediate between the docked and undocked conformation of the four-way junction ribozyme. That is, the proximal state brings the loop elements into close proximity, enabling accelerated folding and cleavage compared to the distal state.[174] A subsequent study by the authors revealed a direct effect of cleavage and ligation on the dynamics of the hairpin ribozyme.[175] They confirmed an overall bias toward ligation in the cleavage-ligation dynamics. Once the substrate is cleaved, the ribozyme undergoes more than 2 orders of magnitude faster docking and undocking. This docking-undocking process is kinetically so distinct that it allowed differentiation between the cleaved and ligated substrate. When the ribozyme is in the undocked state, the cleaved substrate can be released, whereas when it is in the docked conformation, the products can be ligated together or be (re)cleaved. Figure 4f shows two examples wherein a single ribozyme showed distinct kinetic behavior in the cleaved and ligated forms. This added quantitative information about the kinetics of formation of the stable docked active site, rapid undocking after cleavage, and a strong bias toward ligation allowed the authors to rationalize the existence of a stable circular template for the synthesis of the satellite RNA (+) strand during its double rolling circle replication. In an alternative approach, Liu et al. utilized Mg^{2+} pulse-chase experiments to differentiate each reaction intermediate of the two-way junction hairpin ribozyme by a distinct kinetic fingerprint at the SM level.[182] This method allowed them to unambiguously determine the rate constant of each reaction step and fully characterize the reaction pathway while using the cleavable substrate. The authors found the overall cleavage reaction to be rate-limited by the docking/undocking kinetics and internal cleavage/ligation equilibrium.[182] Thus, SM fluorescence studies on the hairpin ribozyme have revealed that complex structural rearrangements and dynamics of the loop and four-way junction elements can help quantitatively explain the cleavage and ligation reactions catalyzed by this RNA enzyme.

Aside from the extensive studies of the hairpin ribozyme, smFRET studies have revealed how distal tertiary structure interactions can help preorganize the catalytic core of the hammerhead ribozyme for functional activity;[183] how functional leakage and slow allostery may represent a general limitation to the performance of designed ligand-dependent ribozymes;[184] how folding of larger RNA enzymes such as the Varkud satellite (VS) ribozyme or the new twister ribozyme[185] is often organized hierarchically;[186] and how molecular crowders can enhance ribozyme folding.[187,188] Taken together, these examples highlight the role that ribozymes have played in inspiring the RNA field to embrace new technologies that reveal fundamental paradigms of RNA folding.

3.2. Riboswitches

Riboswitches are structured RNA motifs that regulate gene expression in response to physiological signals. Embedded in up to four percent of all bacterial mRNAs (including those of numerous pathogens), these regulatory elements change conformation upon ligand binding, modulating gene expression through mechanisms such as premature transcription termination (these are termed "transcriptional riboswitches") or repression of translation initiation (termed "translational

DOI: 10.1021/acs.chemrev.7b00519
Chem. Rev. 2018, 118, 4120−4155

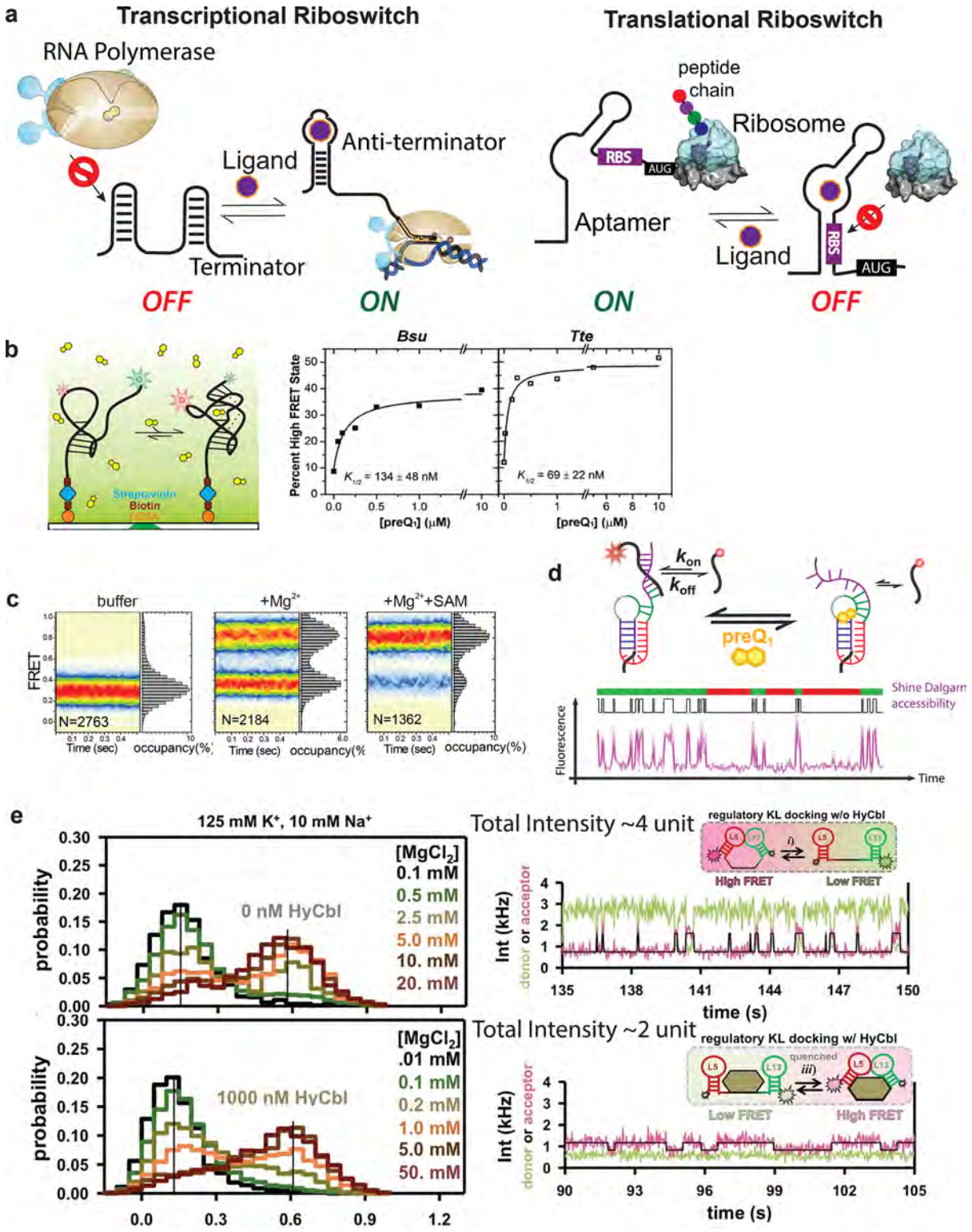

Figure 5. SM studies of various riboswitches. (a) Generalized mechanisms for riboswitch-mediated transcriptional and translational gene expression regulation. (b) Schematic of smFRET construct for study of the $preQ_1$ riboswitch (left). Percentage docked as a function of ligand concentration (right). Reproduced with permission from ref 190. Copyright 2013 Oxford University Press. (c) Dynamics of pseudoknot formation of the SAM-II riboswitch: FRET trace heat maps and histograms showing the mean FRET values of each state observed for the SAM-II riboswitch in the absence of Mg^{2+} and SAM ligand (left), 2 mM Mg^{2+} only (center), and 2 mM of Mg^{2+} and 10 μM SAM ligand (right). Reproduced with permission from ref 189. Copyright 2011 Nature Research. (d) Repeated binding and dissociation of the anti-SD probe labeled with Cy5 is monitored through colocalization with the mRNA. A representative SM trace shows bursts (green bars) and nonburst periods (red bars) identified through spike train analysis. Reproduced with permission from ref 97. Copyright 2016 Nature Publishing Group. (e) Representative SM traces showing KL docking kinetics in the absence (left) and presence (right) of hydroxocobalamin (HyCbl). Ligand binding significantly diminishes the fluorescence intensity providing an independent signature of ligand binding. HyCbl binding significantly decreases the undocking time. Reproduced with permission from ref 191. Copyright 2014 American Chemical Society.

DOI: 10.1021/acs.chemrev.7b00519
Chem. Rev. 2018, 118, 4120−4155

riboswitches") (Figure 5a). Their ligands, which include metabolites, vitamins, metal ions, nucleotides, amino acids, and more, bind to the so-called aptamer domain to act as physiological signals that modify the folding dynamics of a downstream expression platform of the riboswitch, therefore changing the expression of associated genes. Thus, any quantitative description of riboswitch action must involve a detailed understanding of its folding dynamics. Single molecule approaches are well-suited to observe individual folding trajectories independent of population averaging. That is likely why, within a few years of the first comprehensive identification of riboswitches in 2002, scientists started to use single molecule techniques to study their kinetic behavior.

Suddala et al. investigated two riboswitch aptamers that are structurally similar RNA pseudoknots but have different folding mechanisms (Figure 5b).[190] They focused on the preQ$_1$ (7-aminomethyl-7-deazaguanine) riboswitch family that includes some of the smallest metabolite-sensing RNAs found in nature. The two riboswitches they used also employ distinct mechanisms of gene expression regulation. The *Bacillus subtilis* (*Bsu*)-preQ$_1$ riboswitch regulates transcription termination; in contrast, the preQ$_1$ riboswitch from *Thermoanaerobacter tengcongensis* (*Tte*) controls translation initiation by partial sequestration of Shine-Dalgarno sequence. A combination of smFRET and Gō model-based computational simulations showed that, at near physiological Mg^{2+} concentration and pH and in the absence of ligand, both aptamers adopt similar prefolded state ensembles. They differ, however, in their ligand-mediated folding mechanisms. The preQ$_1$ ligand binds early to a partially unfolded conformation of the *Tte* aptamer and induces folding into the bound structure, consistent with an induced-fit model. In contrast, the *Bsu* aptamer has to first fold into a prefolded structure where late binding of preQ$_1$ signifies conformational selection from an existing ensemble of solution conformations. The translational *S*-adenosylmethionine type II (SAM-II) riboswitch shows similar ligand-dependent folding dynamics. Experimental data from Haller et al. support a model where Mg^{2+} helps the pseudoknot structure fold transiently becoming fully conformationally constrained only upon ligand binding, through a conformational selection mechanism (Figure 5c).[189]

A follow-up study on the preQ$_1$ riboswitch showed that the presence of Mg^{2+} finely tunes the folding pathway of the *Bsu* preQ$_1$ aptamer.[192] In the absence of Mg^{2+}, ligand binding promotes pseudoknot docking through specific stacking interactions and thus favors induced-fit where ligand binding precedes slow folding. The addition of as low as 10 μM Mg^{2+} shifts ligand binding toward the conformational selection mechanism by stabilizing a partially folded conformation sufficiently so that it can occur prior to ligand binding. This study demonstrated that combining kinetic and transition-state analyses of smFRET traces creates a powerful toolset to dissect the exquisite interdependence of ligand- and Mg^{2+} mediated folding of the RNA, where parallel induced-fit (binding first) and conformational selection (folding first) pathways partition riboswitch molecules on their journey across a complex folding free-energy pathway.

In a separate study, Rinaldi et al. showed directly that, for the full-length translational riboswitch-regulated *Tte* mRNA, ligand binding results in occlusion of the Shine-Dalgarno (SD) sequence.[97] The authors developed a SiM-KARTS assay to investigate the ligand-dependent RNA secondary structure and accessibility of the SD sequence of individual molecules, using a fluorescently labeled RNA oligonucleotide with same sequence as the anti-SD sequence of *Tte* ribosome, serving as a proxy for the full ribosome. Binding of the anti-SD probe led to intensity spikes, and the intermittent dark periods represented the unbound state. Spike train analysis revealed that individual mRNA molecules alternate between two conformational states, one characterized by "bursts" of probe binding associated with increased SD sequence accessibility expected for the undocked pseudoknot, the other leading to "nonbursts" due to limited SD sequence accessibility upon pseudoknot docking (Figure 5e). As expected, the lifetime of the probe-unbound state of the mRNA increases in the presence of ligand, shortening the bursts and prolonging the time between them. The authors hypothesized that even modest ligand-dependent sequestration of the SD sequence could have significant effects on this "bursty" gene expression pattern, as the untranslated RNAs may be targeted for degradation.[97]

In a study of a class II preQ$_1$ riboswitch, which carries an additional stem−loop structure within its 3′-terminal region immediately upstream of the Shine−Dalgarno sequence, Souliere et al. showed that the added structural feature increases the dynamic range of the riboswitch by decreasing its propensity toward spontaneous folding and increasing its responsiveness to ligand binding.[193]

Further studies on various riboswitches have revealed critical kinetic information related to their folding and gene expression regulation. smFRET studies on a lysine-dependent translational riboswitch measured the opening and closing rates of its aptamer domain and predicted an apparent dissociation equilibrium constant for lysine. The K_D obtained by this method fell more in line with the concentration range expected for thermodynamic control of gene expression than the constant observed in previous reports.[194] Another large riboswitch aptamer that senses thiamine pyrophosphate (TPP) is preorganized into a 'Y'-shaped structure in the presence of Mg^{2+} ion.[195] Yet, a high population with open forearms and residual dynamics in the bound state is detected by smFRET. Upon ligand recognition and binding, the riboswitch becomes further compacted, suggesting a mixed folding mechanism of conformational selection followed by induced fit. Such plasticity may facilitate entry and exit of the TPP ligand.[195]

In a cyclic diguanylate (c-di-GMP)-dependent riboswitch, the ligand-free RNA exists in four distinct populations that differ in dynamics between the undocked and docked conformations.[196] In the presence of c-di-GMP and Mg^{2+}, the docked state becomes stabilized. Furthermore, analysis of mutants demonstrated that tertiary interactions distal to the ligand binding site help preorganize the RNA for accelerated ligand recognition and binding.[196]

Holmstrom et al. used similar smFRET assays to dissect the dynamics of a hydroxocobalamin (HyCbl) binding riboswitch. Coincidentally, HyCbl is a quencher for the Cy3 fluorophore, allowing the authors to monitor the kinetics of ligand binding independent of conformational changes. These two sets of orthogonal observables allowed them to study conformational dynamics in both the ligand-bound and unbound forms. Figure 5f shows representative fluorescence time traces, where the intensity of the trace decreases significantly upon HyCbl binding, revealing that the undocking rate constant associated with the disruption of a long-range kissing loop interaction is substantially decreased when the ligand is bound to the RNA,

DOI: 10.1021/acs.chemrev.7b00519
Chem. Rev. 2018, 118, 4120−4155

which in turn results in preferential stabilization of the docked conformation.[191]

3.3. Other RNA Structural Motifs

As exemplified in the previous sections, SM fluorescence techniques are ideally suited for studying dynamic structural rearrangements of RNA. Naturally, many other RNA motifs with dynamic secondary and tertiary structures have been analyzed using SM tools. In this section, we survey some of these applications, further underscoring the unique insights provided.

Hohng et al. used smFRET to study a generic four-way junction, a very common structural motif in RNA,[197] already encountered in the preceding discussion of the hairpin ribozyme. The study explored the modularity of RNA structures, providing a technological building block to study more complex RNAs by SM fluorescence methods. The donor and acceptor fluorophores were terminally attached to two helical arms of the junction. The junction folds by pairwise coaxial stacking of helical arms, resulting in two possible 2-fold symmetrical conformations so that the continuous strands fold in either parallel or antiparallel form. Similarly, the crossover stands adopt two possible stacking conformers. smFRET data revealed interconversion between parallel and antiparallel conformations with a bias toward antiparallel conformation in moderate salt conditions. In contrast, at high ionic strength, both Mg^{2+} and Na^{+} can stabilize the stacked conformation, leading to dynamic interconversion of the two conformations with incomplete stacking. The polymorphic and dynamic character of the four-way RNA junction provides a source of structural diversity.

Another prevalent structural motif important for complex RNA tertiary or quaternary structure formation is called a kissing complex (KC, sometimes referred to as kissing loops). KCs can be formed either inter- or intramolecularly when the unpaired nucleotides of two hairpin loops engage in Watson–Crick base pairs. The kinetics and thermodynamics of KC formation and subsequent strand-displacement reactions were studied by Salim et al. using smFRET.[198] For this study, the authors immobilized a donor fluorophore-labeled hairpin on the surface while the partner hairpin, labeled with an acceptor fluorophore, interacts with it to form a KC. Resulting smFRET trajectories showed transition between 0.5 and 0 FRET efficiency, representing KC formation and dissociation, respectively (Figure 6a). These complexes display an unusual level of stability relative to simple duplexes of the same sequence and can undergo multiple binding-dissociation events before they irreversibly transition to the extended duplex form via a strand-displacement mechanism. FRET efficiency histograms showed at least three different populations representative of these three states (Figure 6b).

Werner et al. structurally and photophysically characterized a fluorophore binding RNA aptamer at the SM level using FCS.[199] The RNA aptamer SRB2m has a high affinity for the disulfonated triphenylmethane dye sulforhodamine B and for patent blue V (PBV). Results suggested that sulforhodamine B binds to SRB2m with high specificity, predominantly forming a dimer in solution. Interestingly, interactions of PBV with SRB2m result in an improved signal-to-noise ratio due to enhanced molecular brightness once bound, as well as leading to dissociation of the SRB2m dimers into monomers. Such fluorophore-binding RNA aptamers provide a tool for potentially visualizing single RNA molecules in crowded cellular environments.[200]

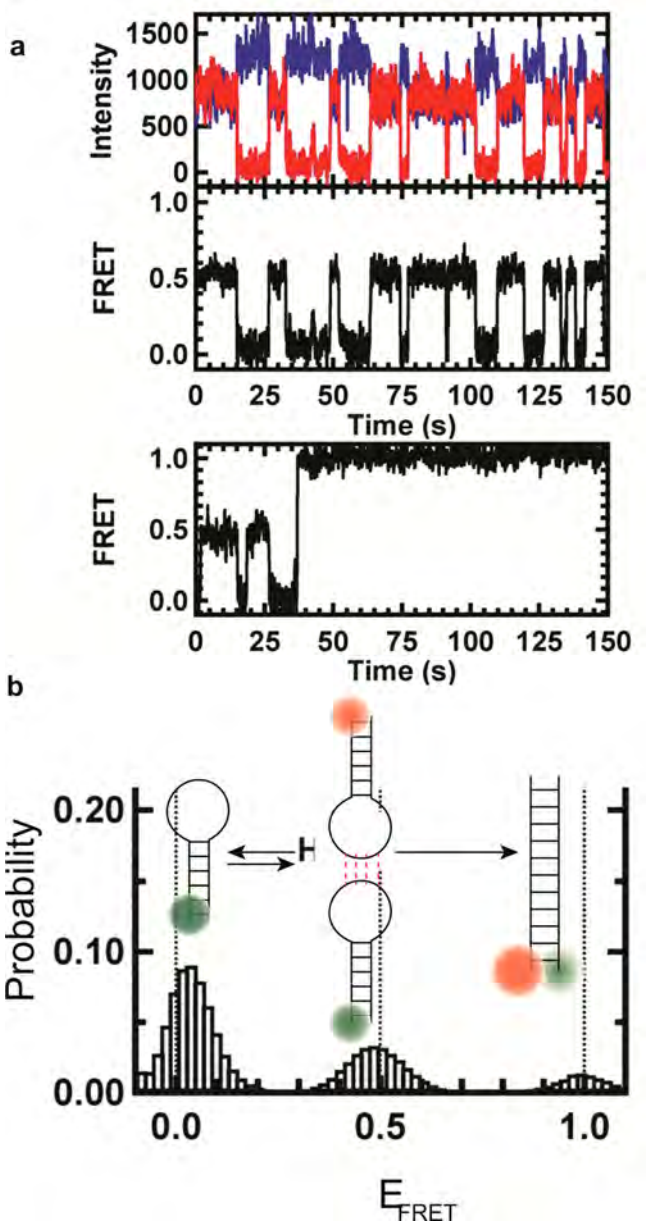

Figure 6. smFRET studies of an RNA kissing-loop interaction. (a) Typical single-molecule time traces with donor (blue) and acceptor (red). The corresponding FRET trajectory shows states with FRET efficiencies of 0.0 and 0.5, representative of single hairpin and assembled kissing complexes, respectively. The bottom panel shows a FRET trace in which after several kissing interactions extended duplex formation is observed in real time. (b) FRET efficiency histogram shows 0.0, 0.5, and 1.0 FRET states representative of single hairpin, kissing complex formation, and extended duplex formation. Each schematic represents the corresponding states. After formation of the duplex, the molecules are trapped in that form under experimental conditions. Reproduced with permission from ref 198. Copyright 2012 Biophysical Society.

Holmstrom et al. used SM imaging techniques to study telomeric RNA consisting of the template sequence for DNA synthesis and a functionally critical pseudoknot motif, which can also exist as a less stable hairpin.[201] Employing temperature-controlled smFRET and urea-based denaturing assays, the

DOI: 10.1021/acs.chemrev.7b00519
Chem. Rev. 2018, 118, 4120–4155

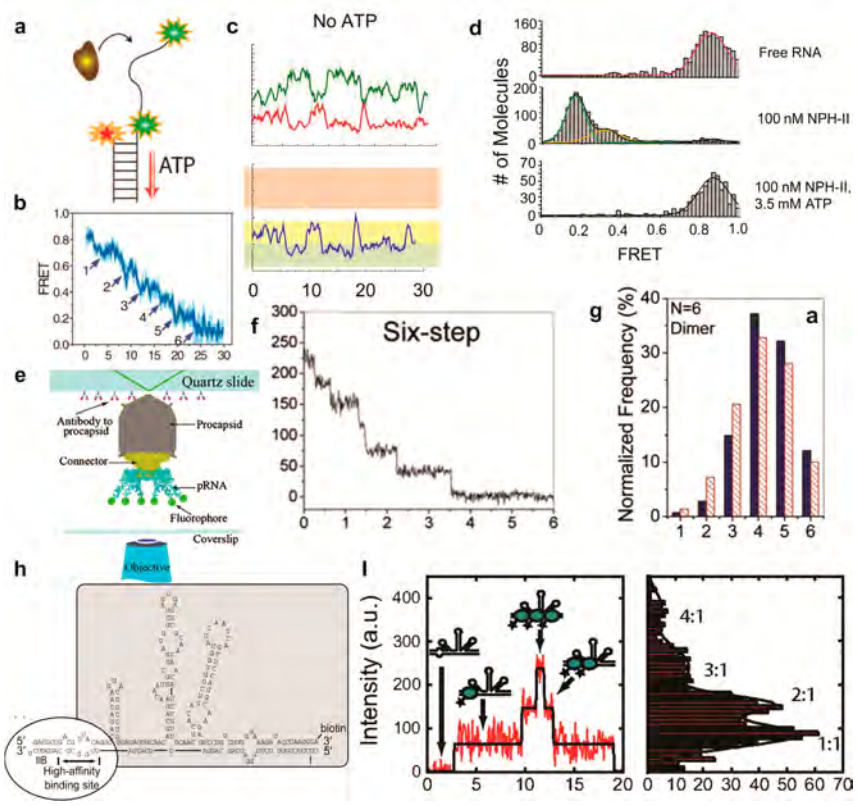

Figure 7. Various examples of SM studies of protein-RNA interactions. (a) Schematic of partial duplex DNA/RNA construct for smFRET-based duplex unwinding studies of RNA helicases. The 3′ single strand overhang serves as a motif for protein binding. The acceptor is attached at the single strand-double strand junction, and the donor is attached either at the junction (Myong et.al.) or at the 3′ end (Fairman-Williams et.al.). (b) NS3 unwinds duplex DNA in 3-bp steps. Six unfolding steps are identified for 18 bp duplex. Reproduced with permission from ref 202. Copyright 2007 American Association for the Advancement of Science (c) Representative smFRET time trace showing two structurally different conformations upon NPH-II binding to RNA. (d) smFRET histograms of NPH-II binding to RNA. Lines indicate Gaussian fits of each FRET population. NPH-II binding to RNA partial duplex shows at least two distinct conformations (FRET 0.33 and 0.15) compared to the protein unbound RNA (FRET 0.85). Upon addition of ATP, the duplex is unfolded and the donor strand is released. Panels (c) and (d) are reproduced with permission from ref 204. Copyright 2012 Elsevier Ltd. (e) Experimental design for quantized photobleaching of fluorescent pRNA in procapsid/pRNA complexes. Each pRNA is labeled with a dye at its 5′ end. (f) Photobleaching analysis of procapsid-pRNA complex. Fluorescence intensity plots over time showing six steps in photobleaching. (g) Fitting a statistical model to the empirical photobleaching step histogram supports binding of three dimers as opposed to six monomers. Panels (e), (f), and (g) are reproduced with permission from ref 205. Copyright 2007 European Molecular Biology Organization. (h) Sequence and secondary structure of the RRE construct. (i) Representative fluorescence intensity trajectory for a single complex of Rev and RRE. The fluorescence intensity histogram shown on the right is fit with 4 Gaussian peaks (black lines), corresponding to discrete Rev: RRE stoichiometry. Panels (h) and (i) are reproduced with permission from ref 206. Copyright 2009 National Academy of Sciences.

authors studied the folding thermodynamics and kinetics of the hairpin−pseudoknot structural equilibrium. High-speed solution-based SM assays revealed that a two-nucleotide mutation disrupts the complementarity and destabilizes the folding of the pseudoknot by substantially (by ∼400-fold) reducing the folding rate constant while only nominally increasing the unfolding rate constant (by ∼5-fold). SM fluorescence studies such as these on isolated RNA motifs continue to lay the foundation for investigations of larger RNAs and RNA-protein complexes.

4. SINGLE MOLECULE FLUORESCENCE STUDIES OF RNA-PROTEIN ASSEMBLIES

Building on the technical and biological foundation laid by the studies described above, recent work has focused on the expansion of SM techniques to ever more complex biological systems. In parallel, established techniques have been extended to yield data with ever greater quantity, quality, and information content. Similar to the experiments on simpler systems, SM fluorescence experiments on large RNA-protein assemblies require the fundamental components of fluorophore labeling, excitation, detection, background minimization, and, in many but not all approaches, immobilization. While these requirements produce technical challenges that must be overcome in order to study such systems, they also provide lenses through which experiments can be designed to report on specific questions of interest. Examples of these adaptations will be highlighted throughout the following discussion. Macromolecular machines based on RNA-protein assemblies are characterized by binding and dissociation of different factors, extensive conformational heterogeneity, and dispersed conformational fluctuations even within a single complex. They, therefore, exhibit precisely the kind of behavior that is ideally dissected through SM studies.

4.1. Two-Component RNA-Protein Interactions

The interplay between RNA and proteins is central to almost every vital process in the cell. Diverse RNA binding proteins (RBPs) can recognize single-stranded RNA, double-stranded RNA, three-dimensional structural features of folded RNAs, or

DOI: 10.1021/acs.chemrev.7b00519
Chem. Rev. 2018, 118, 4120−4155

they may bind RNA nonspecifically.[88] In this section, we discuss studies involving isolated, single-component RBPs.

One of the pioneering studies on RNA helicases was performed by Myong, Ha, and co-workers on NS3 helicase, which is essential for replication of the hepatitis C virus.[105,202,203] Using smFRET they showed that NS3 unwinds a DNA duplex in discrete 3-base pair (bp) steps. The authors designed their substrates with duplexes of either 18 or 9 bp followed by 20 nucleotides (nt) of a single-stranded 3′ overhang. The donor and acceptor dyes were placed on the two opposite strands of the duplex at the double-to-single strand junction (Figure 7a). Consequently, the dyes move further apart as the duplex is unwound and the longer single strands are generated, resulting in progressively lower FRET efficiency. NS3 loads onto the overhang region and hydrolyzes ATP to unwind the duplex. smFRET traces revealed this as a multistep process where the number of steps can be correlated with the total number of available base pairs. For an 18-bp duplex, about six steps were observed, whereas a 9-nt duplex requires only 3 steps; hence, the authors proposed an unwinding mechanism wherein the helicase unwinds RNA in steps of 3 bp (Figure 7b). Furthermore, dwell time analysis showed at least three hidden steps before each unwinding step, suggesting a spring-loaded mechanism whereby three ATP hydrolysis steps accumulate tension and eventually results in the burst of a 3-bp unwinding. Upon encountering a barrier, NS3 slips back very rapidly and repeats the unwinding process for multiple rounds. Utilizing an RNA substrate with a 19-bp duplex and a 24-nt 3′ overhang, Fairman-Williams and Jankowsky showed that similar viral RNA helicases of the NS3/NPH-II group unwind RNA duplexes by processive, directional translocation on one of the duplex strands.[204] Instead of placing both dyes at the junction, they placed the acceptor at the junction and the donor at the end of the 3′ overhang (Figure 7a). As a result, NPH-II binding to the overhang alters the FRET efficiency relative to that of the free RNA. The smFRET data and transition state analyses show that the NPHII-RNA complex adopts at least two distinct conformations (Figure 7, panels c and d). These are transiently formed, cannot be detected in bulk assays, and can be attributed to various stages of ATP binding and hydrolysis. Using nonhydrolyzable ATP analogs, the authors showed that, while ATP hydrolysis is not required for the binding of the protein, ATP binding is essential for stable binding. Upon ATP hydrolysis, NPH-II unwinds the duplex and the donor strand dissociates.

In another study, Linden et al. performed confocal-based smFRET experiments on *Thermus thermophilus* DEAD box helicase Hera.[207] They labeled each side of the interdomain cleft in the helicase core with donor and acceptor and observed changes in FRET efficiency upon binding to RNA. Structured RNA induces a switch to the closed conformation of the helicase core and stimulates the intrinsic ATPase activity of Hera, leading to ATP-dependent hairpin unwinding. Similar unwinding activity was observed in RNA helicases from other bacteria. For example, the same group investigated the interdomain dynamics in *Bacillus subtilis* DEAD box helicase YxiN using a similar experimental scheme. They found that YxiN maintains an open conformation in the presence of ADP and RNA, which turns into a compact structure upon binding to ATP and RNA.[208]

Ait-Bara et al. have summarized different solution-based RNA-protein interaction studies using smFRET and provided a detailed experimental scheme.[209] In particular, they described in detail the requirements for smFRET-based assays to monitor conformational changes of RNA-protein interactions in solution with a focus on how the folding of an antiterminator hairpin is influenced by the binding of the antitermination protein. In a different solution-based study, Schuttpelz et al. used glycine-rich RNA-binding protein AtGRP7 from *Arabidopsis thaliana*, which binds to its own RNA transcript to control gene expression at the transcriptional level. Using solution-based FCS, they were able to show that AtGRP7 binds to single-stranded DNA and RNA with similar affinity. Upon binding to AtGRP7, the mRNA loses considerable conformational flexibility. These results suggest that AtGRP7 binding shapes the RNA into an extended form to facilitate post-transcriptional modifications.[210]

Shu et al. used an SM fluorescence photobleaching technique to count how many packaging RNA (pRNA) molecules constitute the bacteriophage phi29 DNA-packaging motor.[205] To this end, each pRNA molecule was labeled with a single Cy3 fluorophore and purified before attachment to the procapsid (Figure 7e). Although individual molecules cannot be resolved in a 20 nm capsid, quantized photobleaching steps from the colocalized pRNA molecules were counted to identify a stoichiometry of pRNA within the motor (Figure 7, panels f and g). Such stepwise photobleaching counting approaches have found broad application in measuring the stoichiometry of RNA assemblies and RNA-protein complexes (RNPs) in vitro and in the cell.[211−214]

Oligomerization of the protein Rev on the Rev Response Element (RRE) regulates the nuclear export of genomic human immunodeficiency (HIV)-1 RNA and partially spliced viral mRNAs encoding for structural proteins. Pond et al. studied RRE binding to Rev protein using SM localization assays.[206] A single-cysteine mutant of the Rev protein was specifically labeled with Alexa Fluor 555 to study the binding kinetics of Rev to RRE RNA. Typical fluorescence traces revealed distinct fluorescence intensity states, where each state reflects individual binding and dissociation events of Rev. The number of fluorescent intensity states not only yielded the stoichiometry of Rev binding but also, more importantly, reported that binding events are dependent on the presence of an internal loop of the RRE, indicating an ordered rather than stochastic assembly process (Figure 7, panels h and i). Dwell-time analyses during individual Rev-RRE assembly events revealed that each Rev monomer binds rapidly to the RRE, with faster bimolecular rate constants than observed in bulk. Taken together, these studies are providing the technological foundation needed for accessing still more complex, multi-component, macromolecular machines such as the ones discussed below.

4.2. RNA Interference

RNA interference (RNAi) refers to a gene regulation mechanism in which ∼22 nucleotides long microRNA (miRNA) duplexes are loaded into the multiprotein RNA-induced silencing complex (RISC), where they help identify and target specific mRNAs for translational repression and eventual cellular degradation based on partial complementarity with the miRNA guide strand. RISC also possesses intrinsic endonuclease activity, which is activated in the presence of small interfering RNAs (siRNAs) that are fully complementary to their targets.[215] Since its discovery in 1998, the RNAi pathway has shown itself to be a natural conduit for biomarker

DOI: 10.1021/acs.chemrev.7b00519
Chem. Rev. 2018, 118, 4120−4155

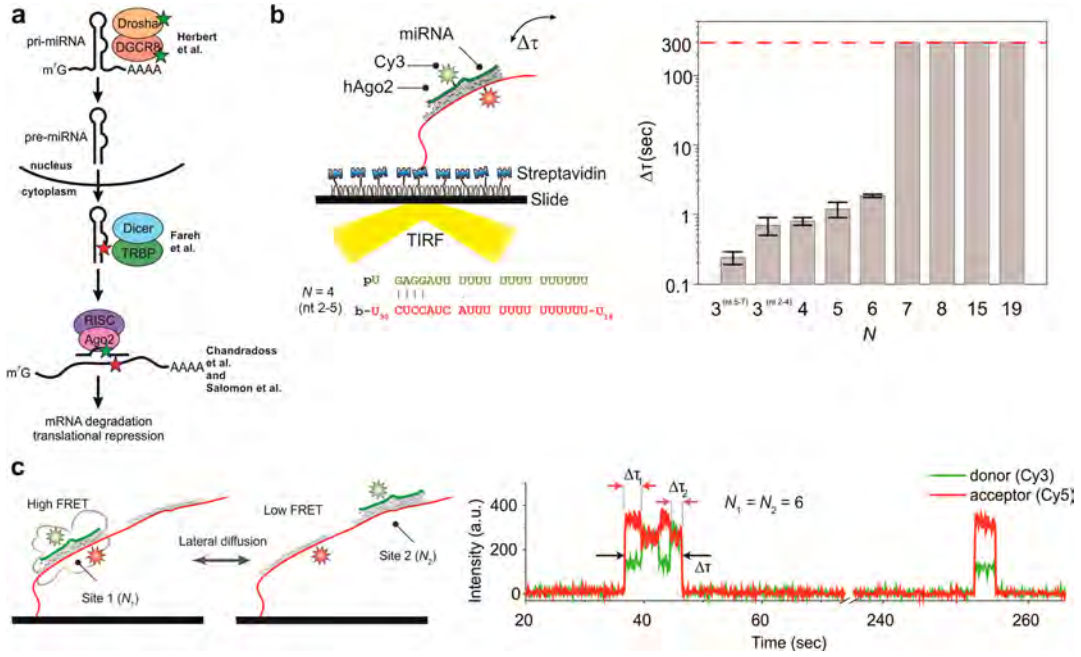

Figure 8. Recognition of RNA interference targets by Ago2. (a) The miRNA biogenesis pathway. Colored stars indicate the labeling sites used for various studies discussed in the text. (b) Binding of Ago2 loaded with fluorophore-labeled miRNA to a labeled, immobilized RNA target (left). The bound time $\Delta\tau$ was determined as a function of the number of miRNA-target base pairs. It increases greatly when a 7-nucleotide seed sequence at the 5′ end of the miRNA is fully paired (right). (c) 1D Diffusion of Ago2 was studied using an immobilized RNA target with two adjacent binding sites (left). A high-FRET state is observed when Ago2 is bound at "Site 1", and a mid-FRET state is observed when it is bound at "Site 2" (right). Ago2 was found to fluctuate between the two binding sites without dissociating, implicating sliding as a mechanism for target location. Reproduced with permission from ref 219. Copyright 2015 Elsevier Inc.

identification and drug development, as well as a powerful research tool for modulating the expression of specific genes. As a result, there has been widespread interest in the mechanisms of miRNA biogenesis and target recognition by RISC, leading to the application of SM fluorescence tools to study individual steps in the RNAi pathway.

The miRNA biogenesis pathway includes both nuclear and cytoplasmic events, with initial transcripts, termed primary microRNAs (pri-miRNAs), being trimmed into stem-loop structures by the Drosha- and DGCR8-containing microprocesser complex (MC) in the nucleus (Figure 8a). The pre-microRNAs (pre-miRNAs) generated by this process are then transported into the cytoplasm and cleaved into linear duplexes by a complex of Dicer and TRBP.[216] The nuclear step of this process was investigated by Nguyen et al.[217] and Herbert et al.,[218] who combined biochemical methods with SM photobleaching analysis to elucidate the stoichiometry of the MC, which had been the subject of conflicting evidence and extensive debate. Nguyen et al. immobilized a pri-miRNA substrate and observed the association of the GFP-labeled RNA binding domain of DGCR8 and mCherry-labeled Drosha. They found that GFP and mCherry frequently bound simultaneously, indicating that the MC might be preassociated in the absence of RNA, and found by photobleaching analysis that the most common stoichiometry was 2:1 DGCR8:Drosha.[217] Consistent with these results, Herbert et al. found the same stoichiometry despite several differences between the studies. In particular, Herbert et al. covalently labeled CLIP- and SNAP-tagged Drosha and DGCR8, respectively, with fluorophores, and then immobilized immunoprecipitated MC in the absence of RNA through antibodies bound to a Myc tag on Drosha. In addition, they used full-length DGCR8 instead of only the RNA-binding domain and small-molecule fluorophores instead of fluorescent proteins.[218] Together, these studies provided strong evidence for MC being preassembled as a heterotrimer in the absence of pri-miRNA and maintaining that stoichiometry once bound.

Fareh et al. studied pre-miRNA processing by Dicer, the next step in miRNA biogenesis.[220] They isolated FLAG-tagged, biotinylated Dicer via immunoprecipitation and studied the binding of fluorophore-labeled pre-let-7a-1 miRNA in the absence and presence of TRBP. The authors found through biochemical experiments that addition of TRBP makes Dicer resistant to high concentrations of RNA competing with its pre-microRNA substrate. Likewise, they found that addition of TRBP greatly enhances binding of prelet-7a-1 to immobilized Dicer in a background of competing tRNA. It was found that pre-miRNA-Dicer-TRBP complexes exhibit both long and short binding lifetimes that were assigned to two distinct binding modes of the pre-miRNA to Dicer. When a noncanonical pre-miRNA variant was used, TRBP was found to decrease the total number of binding events as well as the fraction of long binding events, suggesting that it aids in the rapid rejection of noncanonical substrates.[220]

Key steps of RNAi following miRNA biogenesis were investigated by Chandradoss et al., who performed smFRET measurements using immobilized, fluorophore-labeled RNA target and labeled miRNA-loaded Argonaute-2 (Ago2), a key protein component of the RISC complex (Figure 8, panels b and c).[219] Complementing earlier biochemical experiments,[221] they found that complementarity between the target and a "seed sequence" of at least 7 nucleotides at the 5′ end of the miRNA was required for stable Ago2 binding, while complementarity in the remaining sequence was not necessary (Figure 8b). By studying targets with two adjacent miRNA

DOI: 10.1021/acs.chemrev.7b00519
Chem. Rev. 2018, 118, 4120−4155

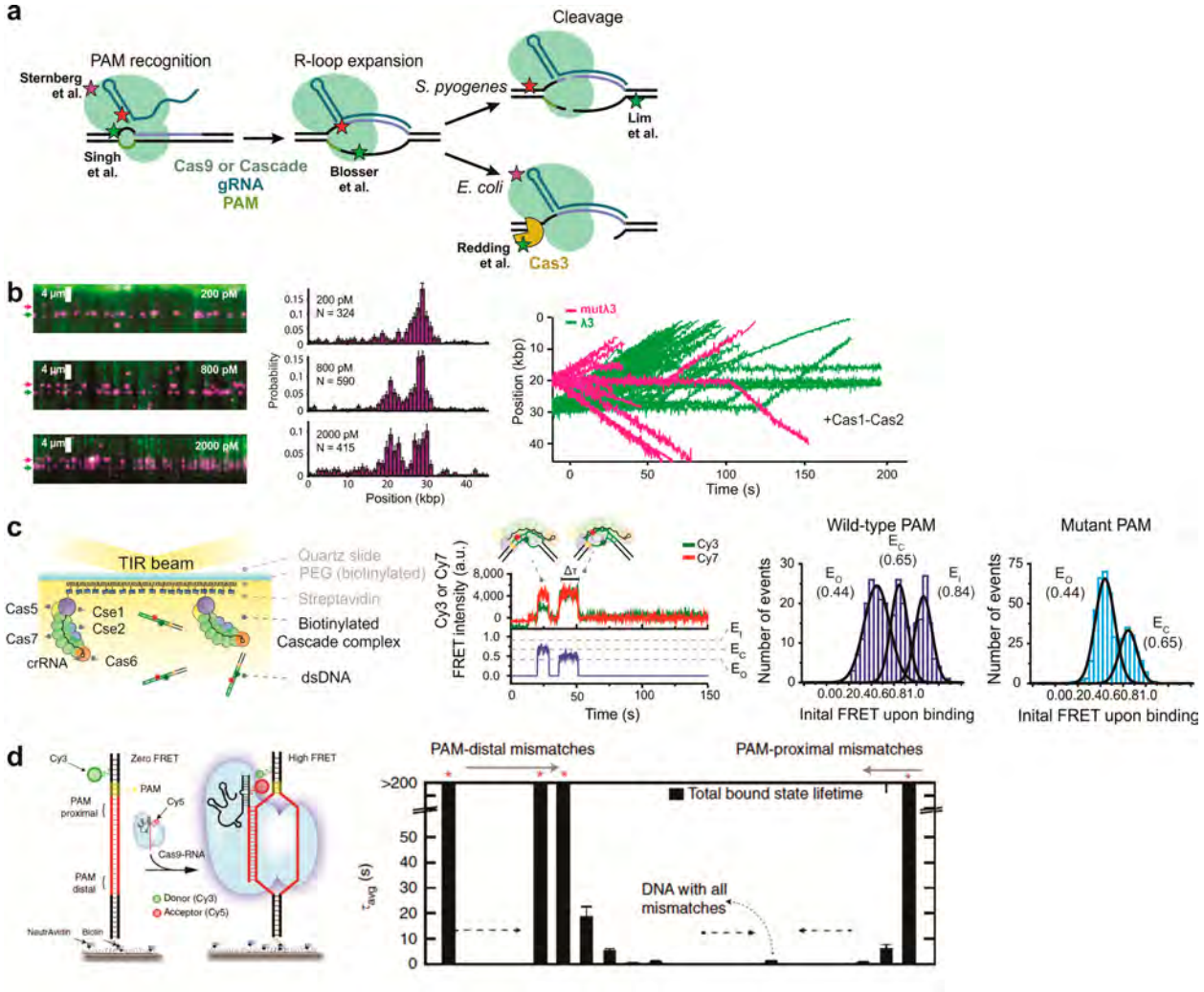

Figure 9. Study of CRISPR systems from *E. coli* and *S. pyogenes*. (a) Pathway of target recognition, binding and DNA degradation by guide RNA-Cas protein complexes. Colored stars indicate the labeling sites used for various studies discussed in the text. (b) Binding of quantum dot-labeled *E. coli* Cascade complex (purple) to a DNA curtain (green) at varying Cascade concentrations. A target sequence with a wild-type PAM at position ~29 kbp is populated at low Cascade concentrations, and a second target with a mutant PAM at position ~21 kbp additionally becomes populated at higher concentrations (left). Translocation of Cas3 is unidirectional at targets with WT PAM sequences (green) and bidirectional at targets with mutant PAM sequences (pink) (right). Reproduced with permission from ref 224. Copyright 2015 Elsevier Inc. (c) Conformational changes in a doubly labeled DNA target upon binding to immobilized Cascade. Three different DNA conformations are observed upon initial binding to a target with a WT PAM, whereas only two are observed upon binding to a mutant PAM sequence. Reproduced with permission from ref 225. Copyright 2015 Elsevier Inc. (d) Detection of binding of *S. pyogenes* Cas9 to fluorophore-labeled DNA targets. Several mismatches between the guide RNA and target are tolerated distal to the PAM, whereas the target region proximal to the PAM is highly sensitive to mismatches. Reproduced with permission from ref 226. Copyright 2016 Nature Research.

binding sites, they found that Ago2 utilizes limited 1-dimensional (1D) diffusion along the target to facilitate its search for sequence complementarity. They concluded that the widespread "subseed" sequences that contain only 2–4 nucleotides of complementarity likely play a role in maintaining stable Ago2 binding to a target and facilitate the 1D search for the seed sequence (Figure 8c).

This work was complemented by a study by Salomon et al., who compared the target-binding kinetics of naked miRNAs to Ago2-loaded miRNAs.[130] They discovered that the presence of Ago2 increases the rate of target sequence binding to nearly diffusion-limited levels. This is likely the result of Ago2 increasing the rate of duplex nucleation, which is the rate-limiting step in the binding of naked oligonucleotides. This effect is dependent on complementarity between the target and the miRNA seed sequence. In fact, complementarity at certain nonseed positions actually destabilizes Ago2 binding, a result that can inform the algorithms that are used to predict miRNA targets. The release of cleavage products was also accelerated relative to what would be expected for naked RNA duplexes.

In summary, SM experiments have provided significant insight into the stoichiometry and binding specificity of various complexes in the miRNA biogenesis pathway, as well as the mechanism of target recognition by Ago2.

4.3. CRISPR-Cas: A Genome-Editing Machine and Much More

The discovery of facile RNA-programmed DNA binding and cleavage by the bacterial immune system CRISPR (short for "clustered regularly interspersed short palindromic repeats") set off a genome-editing revolution that immediately impacted basic research and quickly expanded to impact medicine and

DOI: 10.1021/acs.chemrev.7b00519
Chem. Rev. 2018, 118, 4120–4155

social policy.[222] Optimizing the genome editing potential of the various CRISPR systems that have been discovered requires a mechanistic understanding of their diverse properties and activities, leading to questions that SM fluorescence methods are well-poised to answer.

While there is considerable diversity between the CRISPR systems of different bacteria, the fundamental units comprise at least one CRISPR-associated (Cas) protein and an RNA that, through base complementarity, targets a specific DNA sequence for degradation (Figure 9a). One of the first SM studies of CRISPR investigated what has become the most widely used system, that of *Streptococcus pyogenes* (*Spy*), which contains one protein (Cas9) and two RNAs, crRNA and tracrRNA, which can be fused and then are called guide RNA (gRNA).[72] Sternberg et al. utilized a DNA curtain technique, in which a phalanx of λ-DNA molecules is stretched by laminar flow and binding of fluorophore-labeled proteins to individual duplexes is detected. For this study, FLAG-tagged Cas9 was labeled with anti-FLAG-coated quantum dots.[223] It was found that while gRNA:Cas9 bound to the DNA with high affinity and specificity, it typically first underwent a series of nonspecific, nonproductive binding events. The locations of these events were found to be correlated with the density of protospacer adjacent motif (PAM) sequences that are short (typically 3-bp) recognition sites of the protein itself. The authors also found no evidence of 1D diffusion that might aid in target identification, and *apo* Cas9 lacking gRNA was found to bind and dissociate from the DNA nonspecifically.[223]

Next, Redding et al. expanded on this work by using DNA curtains to investigate the CRISPR system from *E. coli*, in which the analogue of Cas9 is the 5-protein Cascade complex (Figure 9b).[224] In contrast to *Spy* Cas9, about 25% of Cascade complexes exhibited signs of 1D diffusion, although these were not investigated further. Seeking to understand the mechanism by which the CRISPR system adapts to protective mutations in the PAM sequences of foreign DNA, the authors investigated Cascade binding to a target bearing wild-type and mutated PAM sequences. While recognition of the target sequence was much faster in the presence of a PAM, both wild-type and mutant PAMs yielded long-lived bound complexes. The functions of the Cascade-associated proteins Cas1, Cas2, and Cas3 were also investigated. It was found that in the presence of an intact PAM, Cas3 is recruited to the target by the Cascade complex, where it interacts with and nicks the DNA of the R-loop. It then translocates along and degrades the nontarget strand, generating a single-stranded DNA gap of up to 300 nt. This is an important step in the PAM-dependent degradation of foreign DNA. The proteins Cas1 and Cas2 recruit Cas3 to mutated PAM sites, triggering bidirectional translocation of Cas3 (Figure 9b). These findings provided insight into the priming activity of Cascade, which is triggered by mutations in the PAM or target sequence and facilitates the acquisition of new protospacers.

The *E. coli* Cascade complex was investigated further by Blosser et al., who used smFRET to monitor the distance between fluorophore labels that were placed on the DNA target strands in the region that is melted by Cascade (Figure 9c).[225] Two distinct conformations were observed in the Cascade-bound complex, with a third, transient FRET state often observed upon initial binding. The researchers hypothesized that the conformation accessed from the transient state was characteristic of the "interference" mode of Cascade, in which foreign DNA is cleaved. The other was predominant in the presence of targets harboring a PAM mutation, suggesting that it is associated with the priming activity discussed above.

Singh et al. used smFRET to observe binding and dissociation of Cas9:gRNA complexes from their targets, employing fluorophore-labeled guideRNA and labeled, immobilized target DNA (Figure 9d).[226] They found that the negative effects of gRNA-target mismatches proximal to the PAM resulted from interference with target binding. In contrast, up to 11 mismatches are tolerated at the PAM-distal end of the target before binding is negatively impacted. In the presence of many mismatches, intermediate FRET states were observed and assigned to a nonproductive sampling of the target by Cas9:gRNA.

Lim et al. used smFRET to investigate the effects of the assembly pathway on the efficiency of target cleavage by Cas9.[227] They used an immobilized DNA target that was fluorophore-labeled on both ends to visualize target cleavage. Due to the well-established fact that Cas9 remains tightly bound to its target after cleavage, they had to wash the slide surface with 7 M urea to remove Cas9 and the cleaved target fragment from the slide. They found that preincubation of Cas9 alone or Cas9 and crRNA at 37 °C leads to a conformational change in Cas9 that disrupts its cleavage activity. Addition of tracrRNA slowly restores cleavage activity over tens of minutes. This suggested that DNA and tracrRNA protect Cas9 from heating-induced conformational changes that impair its nuclease activity. The authors also observed reversible transitions between two conformations of the Cas9:gRNA:DNA complex that they identified as an open conformation in which the target:RNA duplex is not fully formed and a zipped conformation in which it is formed fully.[227]

The SM studies of CRISPR systems discussed above have revealed that initial target recognition is facilitated by the PAM sequence, followed by zippering, which replaces the DNA duplex with the gRNA:DNA hybrid. The different activities of the *E. coli* Cascade complex are associated with different conformations of the DNA upon binding. The two nucleotides adjacent to the PAM are critical for target recognition by *Spy* Cas9, while mismatches are tolerated distal to the PAM. Together, these results reveal properties of the CRISPR machinery that are relevant to both its biological functions and emerging technologies that make use of it.

4.4. RNA Transcription

SM methods have also provided extensive insight into numerous aspects of transcription (Figure 10a), with fluorescence-based methods so far being applied primarily to the study of initiation. It was long assumed that facilitated diffusion (FD) would be required for efficient promoter search and binding by RNA polymerase (RNAP), with typical models proposing that nonspecific binding to DNA reduces the dimensionality of the promoter search. However, SM colocalization and tracking experiments showed that, at least under in vitro conditions, promoter search by *E. coli* RNAP is dominated by 3D diffusion, with no evidence of a significant role for FD.[228,229]

The mechanism of bacterial transcription initiation after promoter binding has also received significant attention. Three models were proposed for the mechanism by which initiating RNAP repeatedly synthesizes abortive transcripts.[233] In the "transient excursion" model, RNAP translocates along the DNA in a manner similar to processive elongation before returning to the promoter and releasing the abortive transcript. In the

DOI: 10.1021/acs.chemrev.7b00519
Chem. Rev. 2018, 118, 4120−4155

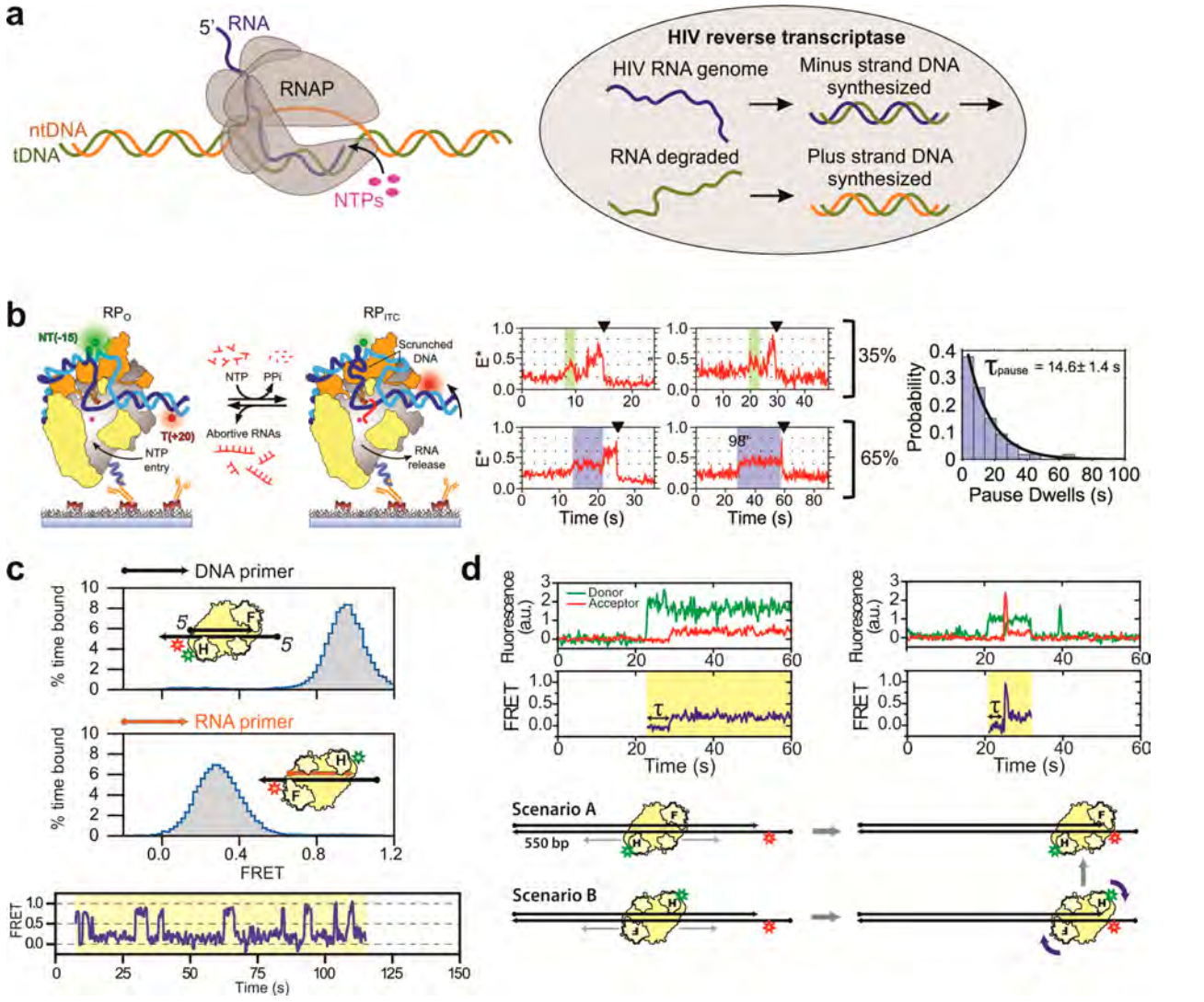

Figure 10. Molecular mechanisms of *E. coli* RNA polymerase and HIV reverse transcriptase. (a) (Left) Schematic of a bacterial transcription complex containing RNA polymerase, template (tDNA) and nontemplate (ntDNAs), and nascent RNA. (Right) Events in the life cycle of HIV that are catalyzed by HIV RTase. (b) DNA dynamics during early transcription were studied by placing fluorophores upstream and downstream of the transcription bubble. As NTPs were added, "scrunching" of the DNA yielded increasingly high FRET states. A long pause often precedes addition of the seventh NTP (right). Reproduced with permission from ref 230. Copyright 2016 Elsevier Inc. (c) Multiple binding modes of HIV RTase. RTase binds in opposite orientations on duplex DNA and RNA/DNA hybrids, resulting in high- and low-FRET states, respectively (top). On PPTs, it can spontaneously transition between these two orientations (bottom). Reproduced with permission from ref 231. Copyright 2008 Nature Publishing Group. (d) RTase can slide to the end of a target after binding, indicated by an increase in FRET efficiency shortly after binding (upper left). If RTase arrives at the end of the primer in a polymerization-incompetent, it can flip orientations, leading to the observation of a transient high-FRET state prior to flipping (upper right). Reproduced with permission from ref 232. Copyright 2008 American Association for the Advancement of Science.

"inchworming" model, in contrast, a flexible segment within RNAP enables the leading edge to translocate forward while the trailing edge remains bound to the promoter −35 element. Finally, in the "scrunching" model, RNAP remains fully bound to the promoter and reels the DNA through it while synthesizing abortive transcripts. Kapanidis et al. investigated these mechanisms by placing fluorophores at variable positions within the DNA and RNAP and obtaining equilibrium smFRET histograms.[233] They excluded the transient excursion model by showing that the trailing edge of RNAP does not move away from the upstream DNA during initial transcription and excluded the inchworming model by showing that RNAP itself does not expand during initial transcription. This process of elimination, along with the result that DNA upstream and downstream of the RNA/DNA hybrid come closer together during initial transcription, verified the scrunching model. As discussed below, this conclusion has since been supported by a number of other studies.

There has also been a recent interest in the mechanism of transcription start site (TSS) selection. In bacteria, this site was found through bioinformatic approaches to range from 7 to 8 base-pairs downstream of the -10 promoter element. This variation was shown to be the result of the DNA scrunching mechanism discussed above.[234] In an independent study, the effects of scrunching on initial transcription were investigated by smFRET (Figure 10b),[230] with a thorough kinetic analysis focusing on pausing in the vicinity of the TSS. Donor and acceptor fluorophores were both placed on the DNA template,

DOI: 10.1021/acs.chemrev.7b00519
Chem. Rev. 2018, 118, 4120−4155

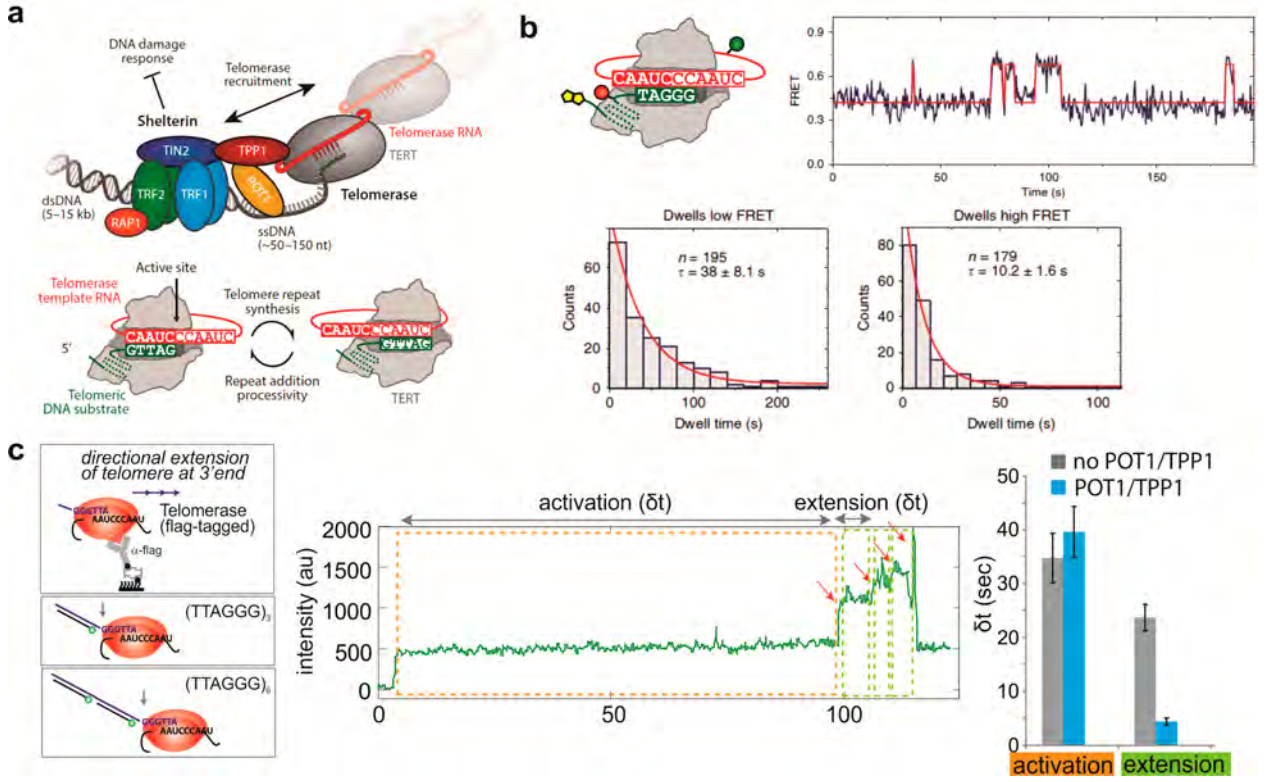

Figure 11. SM studies of the telomerase RNP holoenzyme. (a) Telomeres are protected from DNA damage by the Shelterin protein complex and are extended by the RNA-templated telomerase reverse transcriptase (top). The same six-nucleotide template portion of telomerase RNA is reused to synthesize multiple telomeric repeats (bottom). Adapted with permission from ref 238. Copyright 2017 by Annual Reviews. (b) After synthesis of a repeat, the DNA substrate fluctuates between different alignment registers with TR. The newly formed RNA/DNA hybrid is eventually trapped in the active site for further extension. When the fluorophores are placed on TR and the DNA substrate, this results in fluctuations between low- and high-FRET states. Reproduced with permission from ref 146. Copyright 2014 Nature Research. (c) Telomere extension detected by binding of fluorescent probes to telomeric repeats. After addition of dNTPs, an activation period is followed by an extension period in which multiple repeats are rapidly added (middle). The protein cofactors POT1 and TPP1 decrease the time required for extension without impacting the time required for activation. POT1 and TPP1 were also found to enhance repeat addition processivity (right). Reproduced with permission from ref 239. Copyright 2015 Macmillan Publishers Limited.

with the donor within the promoter and the acceptor downstream of the TSS. As also seen by Kapanidis et al.,[233] increases in FRET efficiency accompanied early transcription, as the downstream DNA was scrunched toward RNAP with each nucleotide addition cycle. It was found that RNAP enters a paused state after synthesis of a 6-mer nascent RNA, with slow extension to a 7-mer frequently followed by backtracking or transcript release.[230] Region 3.2 of sigma factor was found to limit RNA extension to a length of ≤6 nucleotides and to stabilize complexes containing nascent RNAs of this length. This work identified the transcription from a 6- to 7-nucleotide nascent RNA as a critical checkpoint in initial transcription.

4.5. Reverse Transcription

Outside of the most fundamental processes of DNA replication and transcription lie the related processes of RNA-templated RNA and DNA synthesis. They are particularly important for viruses with RNA genomes. Positive-sense RNA viruses can be translated directly by the host cell's protein synthesis machinery, but negative-sense viruses rely on RNA-dependent RNA synthesis to generate protein-coding RNA. Retroviruses typically rely on RNA-dependent DNA polymerases, also known as reverse transcriptases (RTases), to convert their RNA genomes into DNA for integration into the host genome.[235] Human immunodeficiency virus (HIV) reverse transcriptase is particularly interesting in that it possesses RTase activity, RNase H activity by which it degrades the RNA strand of the resulting RNA/DNA hybrid, and single-stranded DNA-dependent DNA polymerase activity by which it generates a dsDNA copy of its genome (Figure 10a).

Various aspects of the mechanism by which HIV RTase discriminates between these activities have been illuminated by smFRET.[231,232] Abbondanzieri et al. found that when a DNA primer was annealed to a DNA template, RTase bound in a conformation poised for DNA synthesis, with the RNase H domain positioned near the 5′ end of the primer and its polymerase domain near the 3′ end.[231] When an RNA primer was annealed to a DNA template, the enzyme bound with opposite orientation (Figure 10c). The "polypurine tract" (PPT) is a region of the HIV genome that is critical for plus-strand DNA synthesis, a process that engages multiple activities of RTase, particularly leading to cleavage of the RNA strand at the 3′ end of the PPT and initiation of DNA synthesis from this position. It was found that when RTase binds to substrates mimicking the PPT:DNA hybrid, it spontaneously transitions between the two orientations, exploring conformations that support both of the enzymatic activities required at that binding site.

Liu et al. discovered that RTase can slide on substrates containing an RNA primer bound to DNA.[232] HIV RTase exhibits low processivity, requiring it to repeatedly find the 3′

DOI: 10.1021/acs.chemrev.7b00519
Chem. Rev. 2018, 118, 4120−4155

end of the DNA primer after dissociation. The authors found that RTase binds to a DNA duplex in random locations and with random orientation, without any particular specificity for the 3′ end of a primer. Sliding and sometimes flipping are therefore required for the enzyme to arrive at the 3′ end of the primer in a polymerization-competent orientation (Figure 10d).

4.6. Telomerase: Specialized Reverse Transcriptase

Telomeres are the single-stranded 3′ overhangs of DNA at the ends of chromosomes that gained fame upon the discovery that the shortening of telomeres is a hallmark of aging. They consist of a canonical repeat sequence, capped by a G-rich sequence that folds into a G-quadruplex. To counter the shortening of telomeres that occurs with each cycle of RNA primer-dependent DNA replication and cell division, an RNP enzyme called telomerase catalyzes the RNA-templated synthesis of new telomeric repeats (Figure 11a). Telomerase RNA structure outside the template region is also critical for enzyme function, as several human genetic disorders are characterized by mutations in these regions. Furthermore, telomere maintenance is particularly important for the rapidly dividing cells that characterize human cancers.[236] SM fluorescence studies have been able to illuminate numerous aspects of telomerase structure and function.

Initial studies investigated the stoichiometry of the active complex formed between human telomerase reverse transcriptase protein (hTERT), human telomerase RNA (hTR), and the DNA substrate. Alves et al. used an SM fluorescence technique called two-color coincidence detection (TCCD) in which the absolute intensity in a given fluorescence channel is used to estimate how many fluorophores are contributing to it.[237] By locating the fluorophores on hTR, hTERT, and the DNA, it was found that the hTERT:hTR:DNA complex binds in an absolute stoichiometry of 1:1:1. While evidence exists for the existence of higher-order oligomers of telomerase, this study showed that at concentrations found in cells, monomers are predominant and the few 2:1 hTR:hTERT complexes observed are less stable than their functional monomeric counterparts.

The question of TERT stoichiometry was revisited several times. Wu et al. compared the stoichiometry resulting from different methods of assembly and affinity purification of telomerase.[240] They found through colocalization and stepwise photobleaching of labeled telomerase monomers that the enzyme exists as a mixture of (primarily) monomers and dimers. They found that the maximum population of multimers was obtained when TERT was overexpressed in mammalian cells (as opposed to reconstituted in rabbit reticulocyte lysate) and affinity-purified using a FLAG tag on the protein (as opposed to oligonucleotide hybridization with TR), suggesting that multimers may partly be artifacts. By monitoring dissociation of TERT after the extension has been completed, it was found that most of the extension activity is carried out by monomeric TERT. This was supported by investigation of mutants, where it was found that deletion of the proline/arginine/glycine-rich linker (PAL) and domain had little effect on catalysis but significantly suppressed dimer formation.

Parks et al. used smFRET to study the repeat addition processivity (RAP) that hTERT exhibits when it adds sequential telomeric repeat sequences.[146] Fluorophore labels were placed on the DNA and/or hTR, and complexes were immobilized through a biotin on the DNA. Analysis of photobleaching revealed that similar to the study discussed above, telomerase exists as a monomer under their experimental conditions. Complexes that had completed the synthesis of a single repeat sequence were found to exhibit dynamics as a result of sampling of hTR alignment registers by the 3′ end of the DNA substrate (Figure 11b). In contrast to previous assumptions, the authors found that denaturation of the RNA:DNA hybrid and reannealing into the new register were not the rate-limiting steps. Instead, they proposed a conformational arrangement that repositions the newly formed RNA:DNA hybrid into the hTERT active site to be rate-determining.

The template region of TR is flanked by a template boundary element (TBE) and a template recognition element (TRE). Berman et al. combined biochemical telomere extension assays with smFRET to monitor conformational changes in these elements.[241] They found that, as nucleotides are added within a repeat, the TRE gets compressed, placing a fluorophore label within it closer to a label on the DNA primer. The TBE, in contrast, gets extended upon nucleotide addition. The authors propose that this compressed TRE/extended TBE conformation stores mechanical energy that drives translocation. This supports an "accordion model" of telomerase translocation that is reminiscent of the "scrunching" in early transcription described above.

Parks et al. tracked the conformational rearrangements of TR during catalysis by performing smFRET on telomerase reconstituted with a set of TR variants containing 10 different pairs of labeling locations.[242] A homology model was constructed with constraints derived from smFRET, NMR, and chemical probing. Optimization of the structure to fit these constraints resulted in the prediction of one structure for stalled hTERT and two different structures for active hTERT. The active and stalled structures are related through a significant rotation of the hTR pseudoknot, although the pseudoknot itself remains intact. Covalent connection between the pseudoknot and the RNA template region is required for telomere repeat addition, while the pseudoknot was found to reside on the surface of the enzyme, together supporting a critical but indirect role for pseudoknot rearrangements in catalysis.

A technique for studying the enzymatic activity of single telomerase molecules was developed by Hwang et al.[239] Extension of DNA primers by telomerase was detected as an increase in signal from a labeled oligonucleotide that stably binds to two adjacent telomeric repeats (Figure 11c). This approach can be compromised by photobleaching or blinking of already-bound probes, so the authors performed a complementary analysis in which they counted photobleaching steps after a 30 min extension time. Addition of the shelterin complex proteins POT1 and TPP1 increased the average number of repeats added before dissociation as well as the rate of repeat addition, while the activation time before the first repeat addition was unchanged. Detecting PIFE and FRET with labeled telomere DNA revealed that POT1-TPP1 slides along the single-stranded DNA region of the telomere. The authors proposed that POT1-TPP1 accelerates translocation of telomerase to the next elongation register by sliding behind it.[239]

The studies on telomerase discussed here revealed that the functional telomerase complex contains a 1:1:1 stoichiometry of hTERT:hTR:DNA. The rate-limiting step during repeat addition is a rearrangement that positions the realigned RNA:DNA hybrid in the active site of hTERT. It was also

DOI: 10.1021/acs.chemrev.7b00519
Chem. Rev. 2018, 118, 4120−4155

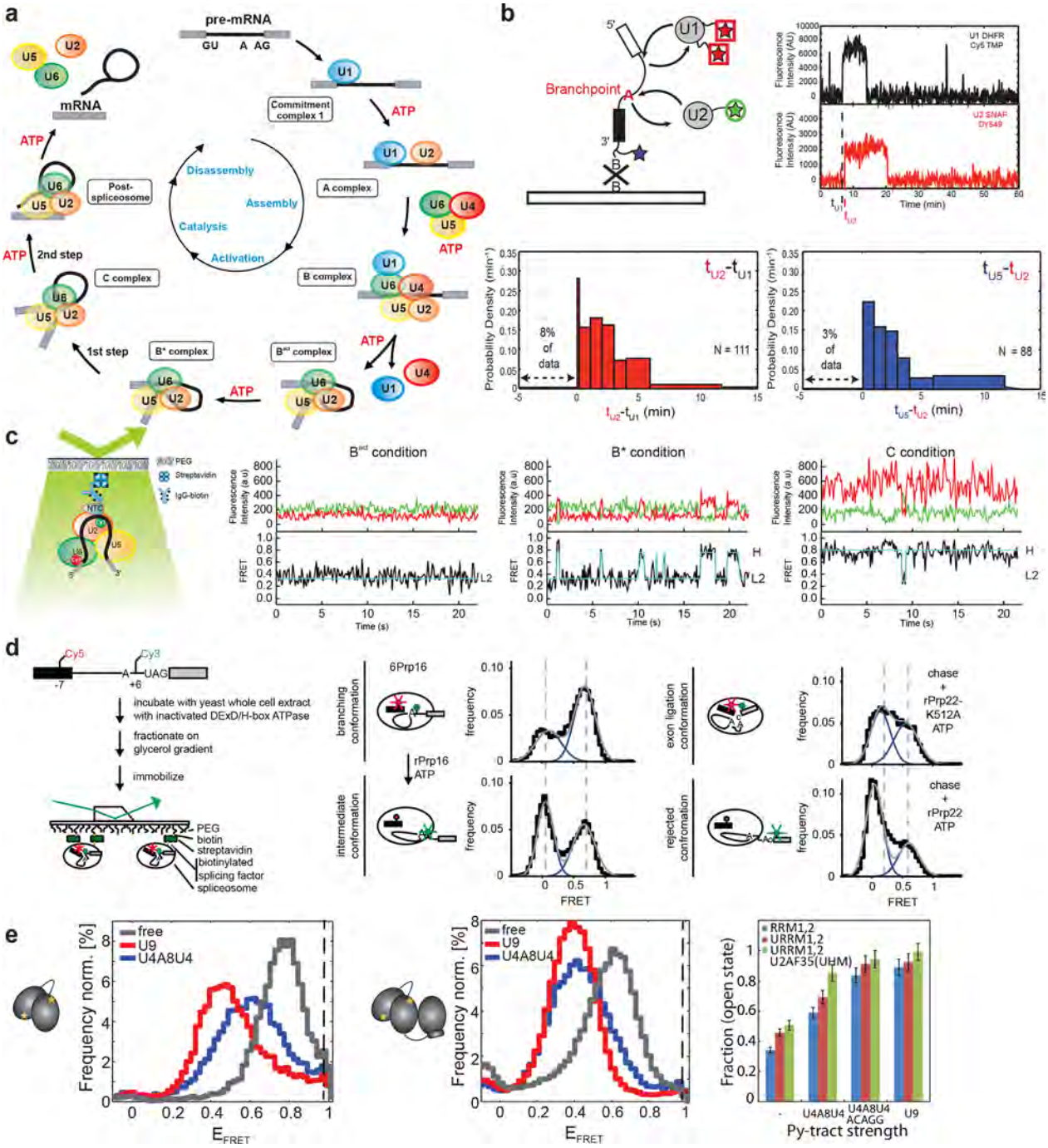

Figure 12. Assembly, catalytic activation, and regulation of the spliceosome. (a) The splicing cycle, indicating binding and dissociation of the snRNPs and steps in which ATP hydrolysis is required to promote conformational rearrangements. (b) Spliceosome assembly was studied by monitoring the binding and dissociation of fluorophore-labeled snRNPs. Binding is reversible (upper right) but has a largely enforced order of U1, followed by U2, U5 (likely as part of the tri-snRNP), and the NTC (bottom). Reproduced with permission from ref 149. Copyright 2011 American Association for the Advancement of Science. (c) Study of the B^{act}-to-B*-to-C complex transition by single-molecule pull-down FRET with the BP and 5′SS labeled. FRET traces show the static mid-FRET state that characterizes the B^{act} complex, fluctuations between mid-FRET and high-FRET states that characterize the branching-competent B* complex, and relatively stable high-FRET state that characterizes the postbranching C complex. Reproduced with permission from ref 143. Copyright 2013 Nature Research. (d) Pre-mRNA conformations in stalled spliceosomes were studied following purification via glycerol gradient centrifugation (left). The helicase Prp16 can separate the branchpoint and 5′SS after branching. When the BP and 5′SS are labeled, this results in a shift of population to lower E_{FRET} upon addition of Prp16 (middle). The helicase Prp22 can separate the 5′SS and 3′SS before exon ligation. When the 5′SS and 3′SS are labeled, this results in a shift of population to lower E_{FRET} upon addition of Prp22 (right). Both of these rearrangements represent proofreading mechanisms by which suboptimal substrates can be rejected. Reproduced with permission from ref 244. Copyright 2016 Elsevier Inc. (e) U2AF65 exists largely in a high-FRET "closed" conformation in the absence of RNA (gray) and transitions to a mid-FRET "open" state upon binding to RNAs with strong Py-tracts (red). Weak Py-tracts cause an intermediate shift (blue) (left). Addition of U2AF35 enables U2AF65 to adopt the open state even in the presence of weak Py-tracts (middle). Reproduced with permission from ref 245. Copyright 2016 National Academy of Sciences.

DOI: 10.1021/acs.chemrev.7b00519
Chem. Rev. 2018, 118, 4120−4155

found that additional telomere-bound proteins increase the processivity and DNA synthesis rate of telomerase. These studies provide insight into fundamental mechanisms of telomere maintenance that underlie their relevance to cancer and aging.

4.7. pre-mRNA Splicing

Many (and in humans almost all) eukaryotic transcripts are initially interspersed with nonprotein-coding sequences thousands of bases in length ("introns"). In order for the proper protein to be made from such RNAs, these must be removed and the coding regions ligated together with high accuracy, a process known as "splicing" (Figure 12a). In higher eukaryotes, alternative splicing is the major source of a highly diversified, tissue-specific proteome.[243]

Splicing is catalyzed by the spliceosome,[246] which consists of five small nuclear ribonucleoprotein particles (snRNPs, called U1, U2, U4, U5, and U6) and a host of auxiliary proteins. This complex catalyzes two sequential, site-specific transesterification reactions with high precision. In the first reaction, the 2′ hydroxyl (OH) group of the branchpoint (BP) adenosine attacks the phosphate backbone at the 5′ splice site (5′SS), converting the pre-mRNA substrate into a free 5′ exon and an intron lariat-exon intermediate. In the second reaction, the liberated 3′ OH group at the 5′SS attacks the phosphate at the 3′ splice site (3′SS) to generate a ligated mRNA product and a lariat intron byproduct.[246] The spliceosome must remove introns from the pre-mRNA with single-nucleotide accuracy in order to avoid frameshift mutations in the resulting protein. It is no surprise, therefore, that defects in splicing have been implicated in a multitude of human genetic diseases, caused either by cis-acting mutations that disrupt splicing signals in a particular pre-mRNA or by trans-acting mutations that disrupt the activity or regulation of the splicing machinery.[247]

4.7.1. Intact Spliceosomes. It has long been appreciated that the spliceosome is a highly dynamic machine, assembling anew on each pre-mRNA substrate, enabling precise and flexible control over the products.[248−252] The composition and structure of the spliceosome changes with each step in the splicing cycle, and what were previously considered to be defined intermediates have been found to rapidly and reversibly interconvert between different conformations. These are characteristics that SM techniques are uniquely poised to interrogate.

The potential of SM fluorescence as a tool to study splicing was first demonstrated by Crawford et al.[253] They found that a glucose-free oxygen-scavenging system was critical for maintaining dye stability while studying splicing in yeast whole cell extract (WCE) because glucose leads to depletion of ATP by endogenous hexokinase. They compared two of the labeling approaches described above, finding that hybridization of a short-labeled oligonucleotide to the intron allowed splicing to be observed but was plagued by spontaneous dissociation of the labeled probe. Covalent labeling eliminated this problem, although it required additional ligation steps to prepare the labeled pre-mRNA substrate. Hoskins et al. expanded on this work, using labeled SNAP and DHFR tags on proteins in the U1, U2, and U5 snRNPs to monitor spliceosome assembly (Figure 12b).[149] Two fluorophores were placed on each complex in order to differentiate reversible binding and dissociation from stable binding followed by photobleaching. It was found that the U1 snRNP rapidly binds to pre-mRNA in a 5′SS-dependent fashion, while U2, U5 (likely as part of the U4/U6.U5 tri-snRNP), and the 19 complex (NTC) follow in an ATP-independent fashion. This work also demonstrated that, while there is preferred order for binding of the snRNPs, every major component has the potential to bind reversibly. Their results also support the hypothesis that at each stage of spliceosome assembly, a subset of pre-mRNA molecules are shuttled onto a nonproductive pathway, perhaps as a proofreading mechanism.

Shcherbakova et al. later confirmed that, while binding of U1 prior to U2 is the predominant assembly pathway, the reverse occurred to varying extents on a number of different pre-mRNA substrates.[254] Complexes that assembled via U1-first and U2-first pathways were found to mature into active spliceosomes with comparable efficiency. This study demonstrated that the reversibility of early spliceosome assembly leads to flexibility in the association pathway. Additional SM evidence has shown that certain later steps of the splicing cycle, in particular the dissociation of the U4 snRNP, are not reversible. The irreversibility of U4 dissociation may be the result of the extensive rearrangements of intra- and intermolecular U6 base-pairing that sequester the sequences bound by U4 in the tri-snRNP.[255]

The reversibility of various steps of splicing was also demonstrated in the first smFRET studies of the spliceosome, when Abelson et al. observed splicing from the perspective of the pre-mRNA by placing fluorophore labels within the two exons.[142] The authors first screened a pool of yeast pre-mRNAs in search of a short and efficiently spliced intron, settling on a version of the gene *UBC4* with shortened exons. This RNA was smFRET labeled at the 5′SS and 3′SS and immobilized through a biotinylated capture oligonucleotide, and limiting ATP and mutations at the branchpoint and 3′SS were used to stall splicing at specific points in the splicing cycle. The resulting data suggested that the spliceosome, like the ribosome,[256] operates close to equilibrium, with ATP hydrolysis by helicase splicing factors enabling proofreading of splice site and branch site selection.

Subsequent work combined colocalization and smFRET to study relative positioning of the 5′SS and BP during spliceosome assembly.[257] Splicing was stalled at specific points by limited ATP and inactivation of the U2 and U6 snRNAs, and SNAP-tagged components of the snRNPs and the protein-only NTC were used to visualize spliceosome assembly. The authors found that the 5′SS and BP were in close proximity in the buffer but transitioned to a distal conformation upon arrival of the U1 snRNP. A distal conformation was maintained throughout spliceosome assembly, with a transition to a proximal conformation being observed only after binding of the NTC initiated the first transesterification reaction. Notably, additional evidence for this conformational change has emerged from recent cryo-EM structures of splicing intermediates. Specifically, a structure of the yeast B^{act} complex revealed that while the U2/U6 catalytic center of the spliceosome is formed in this complex, electron density corresponding to protein separates the 5′SS from the catalytic center.[258]

Krishnan et al. zeroed in on the first chemical reaction of splicing in their study of 5′SS and BP positioning, using heat-inactivation of the factor Prp2 to stall splicing at the pre-step 1 B^{act} complex stage.[143] Additional specificity was obtained by using an antibody against a TAP-tagged factor in the NTC (Cef1) for immobilization, as the NTC does not bind to the spliceosome until the B^{act} stage (Figure 12c).[259] In this work, it was found that, in the B^{act} complex, the BP and 5′SS are distal,

DOI: 10.1021/acs.chemrev.7b00519
Chem. Rev. 2018, 118, 4120−4155

and that the pre-mRNA does not exhibit extensive conformational fluctuations. Addition of Prp2, its cofactor Spp2, and ATP yielded a dynamic B* complex in which transitions were observed between the low-FRET state that characterized the B^{act} complex and a high-FRET state. Further addition of Cwc25 yielded a population of complexes that remained stably in the high-FRET state, which was confirmed by additional experiments to result from C complexes that have completed the first chemical reaction of splicing. On the basis of these results, the authors concluded that spliceosome activation proceeds via a Brownian ratchet mechanism, in which ATP hydrolysis by Prp2 unlocks reversible fluctuations in the conformation of the pre-mRNA (and likely other components of the spliceosome), with Cwc25 acting as a pawl that facilitates the first step of splicing by trapping the conformation in which the BP and 5′SS are in close proximity.[143,260]

Further specificity was achieved in later studies by utilizing glycerol gradient ultracentrifugation to purify stalled spliceosomes after blocking splicing with approaches such as limited ATP, immunodepletion of splicing factors, and dominant negative mutations in splicing factors (Figure 12d).[244] Through biochemical experiments and smFRET, it was found that the RNA helicase Prp16 can separate the 5′SS and BP both before and after branching, enabling both the "sampling" of potential branch sites and postbranching proofreading. The helicase Prp22 was found to affect the positioning of the 5′SS and 3′SS prior to exon ligation in a similar manner. Both helicases are therefore involved in the repositioning of the pre-mRNA to facilitate selection of optimal BP and 3′SS nucleotides, and the same "winching" mechanism of their translocation along an RNA can lead to distinct outcomes depending on the relative speeds of splicing chemistry and helicase action.[244]

4.7.2. Isolating Spliceosome Sub-Components. In parallel with these experiments on assembled splicing intermediates, researchers have been investigating isolated components of the spliceosome in great detail. For example, the U2 snRNA can adopt two distinct conformations, termed stem IIa and stem IIc. It has been shown that stem IIa promotes spliceosome assembly, and that stabilization of stem IIc promotes splicing of mutant branch site and 3′SS sequences.[261] Rodgers et al. used smFRET to study toggling between these two conformations, finding that in the absence of Mg^{2+} or protein, U2 primarily adopts the stem IIc conformation. Addition of Mg^{2+} and/or the protein Cus2p favored formation of stem IIa, suggesting that they may help to regulate stem IIa/IIc dynamics within the spliceosome.[262]

The U6 snRNA forms an extended duplex with the U4 snRNA in the U4/U6.U5 tri-snRNP but base-pairs with U2 in the catalytically activated spliceosome. In another study, Rodgers et al. therefore investigated the conformational dynamics of the U4/U6 duplex in isolation, observing conformational dynamics that they assigned to the formation and dissociation of the "telestem", an intramolecular structure within the U6 snRNA.[263] It was found that telestem formation facilitates unwinding of the U4/U6 duplex, a critical prerequisite to the assembly of the catalytic core of the spliceosome. Mutations to the telestem interfere with tri-snRNP assembly and confer growth defects. Hardin et al. further used smFRET to study the U4/U6 duplex at varying stages of U4/U6 di-snRNP assembly.[264] The construct used in this work lacked the telestem, explaining their observation of a distinct lack of conformational dynamics in the naked U4/U6 duplex. Recombinant proteins Snu13, Prp31, and Prp3/4 were added sequentially to the U4/U6 duplex, and the RNA conformation was monitored by smFRET between the 5′ stem-loop of U4 and the 3′ end of U6. Prp31 and Prp3/4 were found to have opposing effects on U4/U6 structure, while Snu13 had little effect. Overall, proteins and divalent ions were found to have only minor effects on U4/U6 conformation.

Moving one step further in the splicing cycle, Guo et al. investigated the conformational dynamics of the yeast U2/U6 snRNA complex, which is proposed to be responsible for catalysis of splicing.[265] Genetic and NMR evidence had suggested that U2/U6 can adopt three-helix and four-helix structures under different conditions. Recent work utilizing chemical probing of RNA secondary structure provided additional evidence that these structures form in the spliceosome.[266] Switching between the three- and four-helix conformations changes the accessibility of the "AGC triad", known to base-pair with U2 in the catalytically active state. Guo et al. placed fluorophores on U6 and used smFRET to investigate this system, finding that the three-helix structure was favored at very high concentrations of Mg^{2+} and that an obligate intermediate was formed during transitions between the two. They hypothesized that, in vivo, under relatively constant Mg^{2+} concentrations, proteins may instead fulfill the requirement for modulating the four-helix/three-helix equilibrium. Karunatilaka and Rueda dove further into U2/U6 dynamics in their study of the effects of post-transcriptional modifications.[267] Using a similar labeling strategy as Guo et al. to study human U2/U6, they observed a similar three-state system in which a three-helix structure was favored at high Mg^{2+} concentrations. They found that the post-transcriptional modifications pseudouridine and 2′-*O*-methylguanosine destabilize the three-helix conformation by about 0.5 kcal/mol. As this effect was small, they concluded that post-transcriptional modifications likely play a role in protein recognition, rather than directly modulating RNA structure. Still, it is important to keep in mind that structural features of isolated RNAs in vitro do not necessarily manifest within the larger, more constraining context found in vivo.[268]

Interactions between the pre-mRNA and protein components of the spliceosome have also been probed in the absence of other factors. Two recent reports combined structural and SM fluorescence studies to investigate recognition of 3′SS signals by the U2 auxiliary factor (U2AF), which exists as a heterodimer containing large (U2AF65) and small (U2AF35) subunits.[245,269] Voith von Voithenberg et al. performed NMR spectroscopy on a minimal U2AF heterodimer, finding that domains that are highly mobile in the isolated protein become rigid in the presence of polypyrimidine tract (Py-tract) RNA.[245] By combining SM fluorescence intensity and lifetime measurements, the authors showed that a doubly labeled U2AF65 monomer interconverts between "open" (mid-FRET) and "closed" (high-FRET) conformations on a submillisecond time scale. Addition of a pre-mRNA with a strong polypyrimidine tract (Py-tract) such as U9 shifted population to the open conformation, as did the addition of U2AF35 monomer. This shift occurred to a lesser extent with weak Py-tracts such as U4A8U4 (Figure 12e). These results suggest that U2AF35 may help U2AF65 overcome its low affinity for weak Py-tracts, an interpretation consistent with observations that U2AF35 is required for splicing of weak 3′ splice sites. While the details of their data differed, Agrawal et al. similarly observed using smFRET that Py-tract binding stabilizes an "open" conformation of U2AF65.[269]

DOI: 10.1021/acs.chemrev.7b00519
Chem. Rev. 2018, 118, 4120−4155

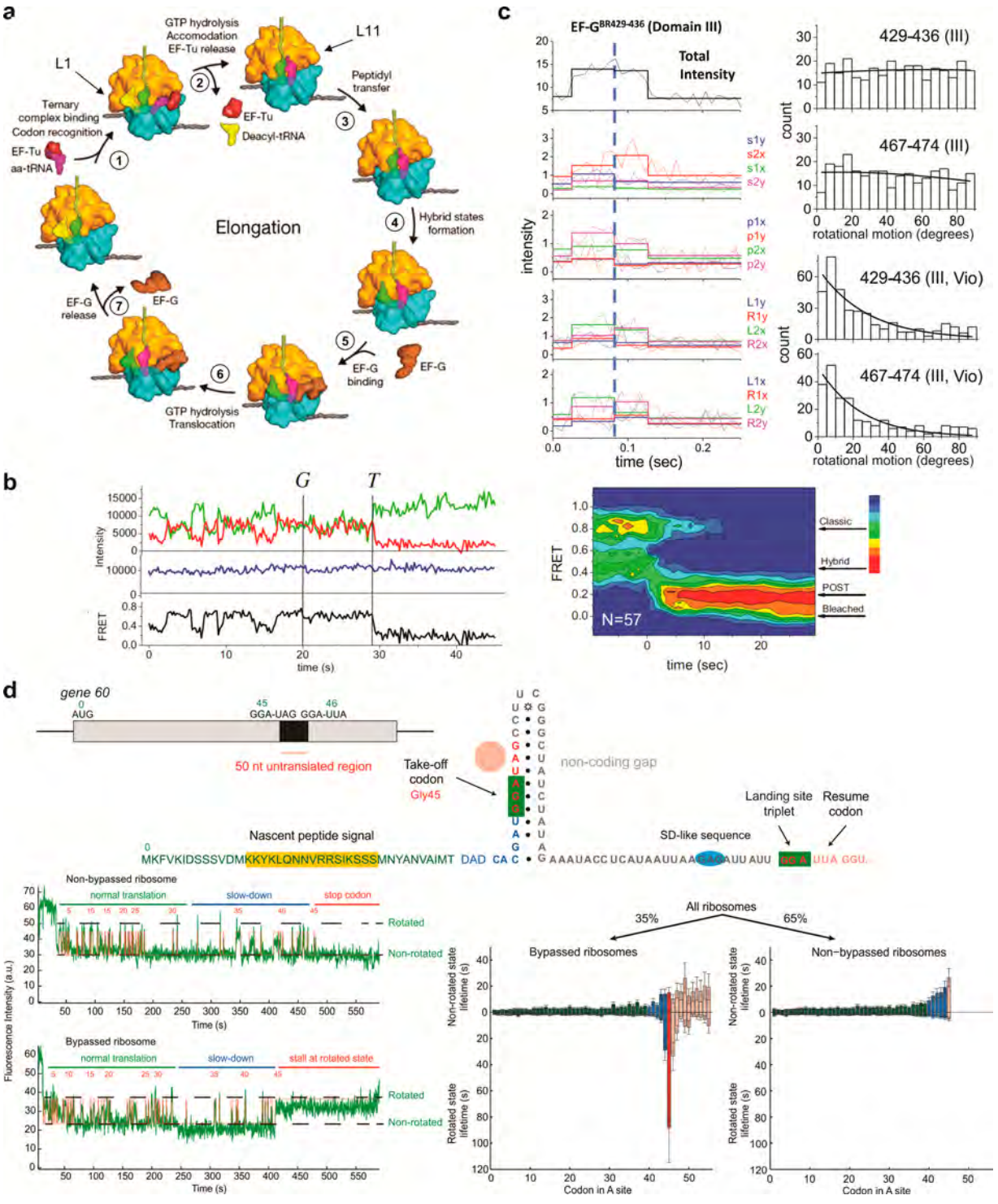

Figure 13. Protein and RNA dynamics during mRNA translation. (a) The elongation cycle of the bacterial ribosome. (b) Study of ribosome translocation by monitoring FRET between multiple tRNAs and between tRNAs and the ribosome. In the absence of EF-G, the ribosome fluctuates between conformations in which the tRNAs are in classical (high-FRET) and hybrid (mid-FRET) states. Addition of EF-G (at the time marked "*G*" in the traces) suppresses these fluctuations and leads to a rapid transition to a low-FRET post-translocation state. Panels (a) and (b) are reproduced with permission from ref 278. Copyright 2011 Elsevier Inc. (c) Study of rotational motions in EF-G by polarization-resolved single-molecule microscopy. (Left) Rapid increases in overall fluorescence intensity indicate EF-G binding events, while changes in the relative intensities of 16 polarization-resolved signals indicate rotations of the labeled domain of EF-G. (Right) Histograms binning the angles of rotations observed during EF-G binding events. Two different fluorophore positions (residues 429−436 and 467−474 of domain III) indicate that domain III exhibits large reorientations. These reorientations are suppressed in the presence of Viomycin. Reproduced with permission from ref 279. Copyright 2016 National Academy of Sciences. (d) Translational bypassing on T4 gene 60 mRNA. Translating ribosomes fluctuate between rotated and nonrotated states. Upon reaching the "takeoff" codon, ribosomes that bypass exhibit a long-lived rotated state. Reproduced with permission from ref 280. Copyright 2015 Elsevier Inc.

DOI: 10.1021/acs.chemrev.7b00519
Chem. Rev. 2018, 118, 4120−4155

As a remarkably complex machine containing many protein and RNA species, many questions about the spliceosome remain that will undoubtedly be addressed through future SM studies. For example, the experiments performed on intact spliceosomes have been largely limited to observing conformational dynamics within the pre-mRNA, leaving unanswered questions about positioning and dynamics of the snRNA and protein components of the spliceosome. The recent explosion in cryo-electron microscopy structures of different splicing intermediates[17,49,52,259,270,271] is likely to inspire numerous hypotheses that can be tested using SM methods, as well as will provide guidance in practical matters such as choosing labeling sites so as not to interfere with function. The field of splicing is therefore ripe for continued investigation through SM approaches.

4.8. mRNA Translation

One of the most fascinating, profound, and complex RNA-enzymes resides at the heart of the central dogma of molecular biology: the ribosome. It is the ribonucleoprotein (RNP) machine that catalyzes protein synthesis in all organisms. Ribosomal RNA comprises nearly two-thirds of the entire ribosome, which is organized into a large and a small subunit. The 0.9 MegaDalton (MDa) *E. coli* ribosomal small subunit (also known as the 30S subunit) contains a 1.5-kilobase RNA and about 20 different proteins. The 30S subunit functions as a decoding platform by binding to the mRNA and the proper set of aminoacyl−tRNAs (tRNAs).[272,273] Complementing this regulatory activity, the large subunit is about 1.5 MDa in size, contains a large and a small rRNA and about 34 proteins, and houses the peptidyltransferase center that catalyzes peptide bond formation between the amino acids in a growing polypeptide chain. The ribosome carries three binding sites for tRNA molecules: the A site binds to the aminoacyl-tRNA containing the next amino acid to be incorporated, the P site accommodates the peptidyl-tRNA that partakes in peptidyl transfer, and the E site contains the newly deacylated tRNA before it exits the ribosome. During the translation process, the small subunit first recognizes and binds to specific sequences on the mRNA (termed Shine-Dalgarno or SD sequences), guided by three initiation factors (IF1−3) that facilitate translation initiation. It is thought that IF1 first binds to the A site and prevents tRNA binding during initiation. IF2 then recruits the formyl-methionine initiator tRNA (fMet-tRNA^{fMet}) to the P site.[274] After the initiation phase, the IFs dissociate and the 50S large subunit joins the complex, enabling protein synthesis to begin (Figure 13a). Each aminoacyl-tRNA carries the amino acid corresponding to a three-nucleotide codon on the mRNA. Two proteins, elongation factor Tu (EF-Tu) and elongation factor G (EF-G), facilitate the elongation process. EF-Tu recruits the aminoacyl-tRNA to the A-site and EF-G promotes translocation of the ribosome from one codon to the next. At the end of the elongation cycle, a stop codon is reached, which is recognized by a protein release factor binding to the A site that promotes the deacylation of the peptidyl-tRNA, and finally, the ribosomal subunits dissociate and the peptide chain is released.[275,276] Although the eukaryotic ribosomal subunits are larger in size with more RNA and protein components, the basic translation process is evolutionarily conserved from its bacterial counterpart.[277]

Bacterial translation has been a topic of interest to researchers for decades, and many antibiotics function by interfering with various steps of translation.[281,282] Several interfere with the process of tRNA selection, which was the subject of an early SM study on the ribosome.[283] It was known that tRNA selection occurs in two steps, separated in time by GTP hydrolysis by EF-Tu. Blanchard et al. investigated this process by tracking smFRET between fluorescently labeled tRNA^{fMet} and tRNA^{Phe}.[283] In this work, three intermediates were observed on the tRNA selection pathway, beginning with a low-FRET state observed during the initial codon-anticodon interaction. A mid-FRET state results from a conformational rearrangement of EF-Tu and the ribosome upon productive codon recognition. This conformational change contributes to tRNA selection fidelity, as it is dependent on the proper codon-anticodon base pairing. GTP hydrolysis by EF-Tu leads to another arrangement that favors release of the tRNA, yielding a high-FRET state. This conformational change provides another opportunity for proofreading, where the stability of the interactions between the tRNA and the ribosome (as opposed to just between the codon and anticodon) is assessed within a distinct structural context.

Later studies investigated tRNA "hybrid states" that form after the ribosome loosens its grip on the A-site tRNA but before its translocation to the P site.[284,285] Kim et al. observed two distinct hybrid states that exist in equilibrium with the classical A site and P site states. The nature of the hybrid states were probed by changing the aminoacylation status of the tRNAs, deleting ribosomal protein L1, and making mutations to the ribosome. These studies supported the hypothesis that the so-called hybrid 1 state contains an A/P hybrid peptidyl-tRNA and a P/E hybrid deacylated tRNA in their experiments. This state is presumed to be an intermediate on the translocation pathway. Hybrid state 2 was characterized by A/A-P/E tRNA configurations.

This work was followed by Fei et al.'s investigation of relative motion between the ribosome itself and elongator tRNAs.[286] This study was inspired by a series of cryo-EM structures that showed direct interactions between the L1 stalk of the 50S subunit and the elbow of the newly deacylated tRNA in the hybrid P/E configuration.[287] By placing smFRET fluorophores site-specifically on ribosomal protein L1 and on tRNA^{Phe}, they were able to monitor the coupling of conformational fluctuations of the L1 stalk and tRNA. A pretranslocation complex was found to exhibit fluctuations between two conformational states. In contrast, the L1 stalk was found to be static relative to the E/E site tRNA in a post-translocation complex.[287]

Chen et al. expanded on this work by investigating ribosome translocation using smFRET between fluorophore-labeled ribosomal protein L11 and A- and P-site labeled tRNAs.[278] They found that pretranslocation ribosomes exhibited conformational fluctuations on an ∼2 s time scale, with dynamics observable between the tRNA and L11, as well as between the two tRNAs (Figure 13b). Binding of EF-G halted these fluctuations and promoted translocation through a transient hybrid intermediate. The authors concluded that fluctuations of L11 and the A-site and P-site tRNAs are coupled and that these conformations are suppressed by binding of the protein factors near the A-site.[278]

Chen et al. further investigated EF-G using polarization-resolved SM fluorescence microscopy.[279] The researchers immobilized the ribosome in a manner that restricted its rotational mobility and labeled EF-G with a bifunctional dye to likewise minimize the rotational mobility of the dye. They measured 16 polarized fluorescence intensities (PFIs) and used

DOI: 10.1021/acs.chemrev.7b00519
Chem. Rev. 2018, 118, 4120−4155

the change-point analysis discussed earlier to identify rotation events during EF-G binding (Figure 13c). The authors observed large reorientations of domain III of EF-G that were blocked by the antibiotics viomycin and spectinomycin, which inhibit translocation downstream of GTP hydrolysis by EF-G; however, smaller motions of domain III and the other domains persisted. The authors proposed a model in which EF-G exerts an initial power stroke that unlocks fluctuations in the ribosome, with further motion in EF-G acting as a pawl that traps the ribosome in a post-translocated state.[279]

Armed with this knowledge about the canonical translation pathway, researchers have branched out to study specific examples of noncanonical translation. On some mRNAs, the ribosome is programmed to frameshift backward by one nucleotide onto an overlapping reading frame. Chen and co-workers studied −1 frameshifting in the *E. coli* dnaX mRNA, finding that, at the frameshifting site, the ribosome entered a long pause in the rotated state.[288] The population of ribosomes that did not experience frameshifting did not exhibit this pause. The authors proposed that this paused state is stabilized by interactions between two RNA elements: a hairpin to the 3′ side of the ribosome and an internal SD sequence to its 5′ side.[288]

In a subsequent study, the same authors investigated the translation of bacteriophage T4 gene 60 mRNA, which involves the programmed bypassing of 50 nucleotides.[280] Similar to what was observed at the frameshifting site on *dnaX*, they found that at the Gly45 "takeoff" codon, a subset of ribosomes exhibits a long pause in the rotated state, during which bypassing occurs (Figure 13d). Ribosomes that terminate translation rather than bypass do not exhibit this pause. This rotated pause requires a hairpin containing a UUCG tetraloop to the 3′ side of the takeoff codon, and an additional hairpin to the 5′ side. The authors suggested that refolding of these hairpins provides the impetus for forwarding motion across the bypassed section, with the ribosome then scanning for the proper landing codon aided by a SD-like sequence.[280]

SM fluorescence studies of translation have recently also branched into the eukaryotic ribosome. Petrov et al. studied translation initiation by the yeast ribosome on the internal ribosome entry site (IRES) of the cricket paralysis virus (CrPV) RNA, measuring colocalization between labeled mRNA and 40S and 60S subunits.[289] While the predominant assembly pathway involves initial binding of the 40S subunit followed by recruitment of the 60S subunit, simultaneous subunit recruitment was observed in up to 30% of traces at low Mg^{2+}. Both pathways facilitated binding of a fluorophore-labeled tRNA, suggesting that both produce functional elongation complexes. The 80S ribosome was found to fluctuate between the 0 and +1 frames before tRNA binding commits it to one of the two frames. While cap-dependent initiation follows a series of reversible steps, binding of the ribosome to the IRES was found to be essentially irreversible, demonstrating the extent to which viruses can subjugate the cellular translation machinery.[289]

Taken together, the SM studies described above show that translation is a highly dynamic process exhibiting strong coupling between tRNA binding and dissociation, GTP hydrolysis by elongation factors, and inherent ribosome dynamics. mRNA sequence and structure can further modulate this process, in some cases leading to noncanonical events such as translational bypassing. The ribosome continues to be an exemplary case study illustrating the power of SM methods to dissect the properties of extremely complex macromolecular machines.

5. PROSPECTS FOR FUTURE SM RNA RESEARCH

In this review, we have embarked to chronicle the almost parallel emergence of a vastly expanded universe of RNA molecules of profound and pervasive biological function and of fluorescence microscopy tools that enable the study of single RNA molecules under (near-) physiological conditions. As is typical in science, the interfaces of disciplines as well as of biology and technology provide a rich landscape for both basic discovery and practical utility. Consequently, we are only at the beginning of what promises to remain the fertile playground of single molecule RNA biosciences for years to come. This review aimed to illustrate some of the recent work that has been paving the way.

Future advances in SM tools stand to further facilitate the analysis of the plethora of emerging RNA structures, dynamics, and functions. As surveyed in this article, more observables and a better understanding of the full capabilities of single molecule fluorescence tools are already enabling the tackling of more and more complex molecular RNP machines; future developments will heighten throughput and increasingly make the transfer of these techniques into the cell possible.[200,213,290] Science generally advances through technological bursts; the leaps and bounds over the past two decades in our knowledge of the cellular RNA repertoire through the advent of next-generation sequencing technologies will likely synergize with ongoing advances in SM microscopy to render our current snapshot the beginning of an exponential growth in single molecule RNA bioscience.

AUTHOR INFORMATION

Corresponding Author

*E-mail: nwalter@umich.edu. Tel. (734) 615-2060.

ORCID

Sujay Ray: 0000-0003-1076-0436

Nils G. Walter: 0000-0002-7301-1275

Author Contributions

†S.R. and J.R.W. contributed equally to this work.

Notes

The authors declare no competing financial interest.

Biographies

Sujay Ray was born in 1986 in Asansol, India. He received his bachelor's degree from University of Calcutta in 2007, followed by a master's degree from Indian Institute of Technology, Kharagpur, in Physics. He earned his Ph.D. from Kent State University, in Kent, Ohio, in 2014 while working on a DNA secondary structure, known as G-Quadruplex and its interaction with various proteins, under the supervision of Dr. Hamza Balci. He worked as a postdoctoral fellow for one year in Dr. Qiong Yang's lab before joining Dr. Nils Walter's lab at the University of Michigan, Ann Arbor. He is broadly interested in developing novel single molecule techniques to study and manipulate individual biomolecules and complex biological machinery. Apart from assembling, maintaining a high-resolution prism-TIRF type single molecule microscope, he is working towards unraveling the role of noncoding RNAs in translation initiation.

Julia R. Widom received her B.A. in chemistry from Northwestern University in 2009. In 2013, she completed her Ph.D. in physical

DOI: 10.1021/acs.chemrev.7b00519
Chem. Rev. 2018, 118, 4120−4155

chemistry in the laboratory of Andrew H. Marcus at the University of Oregon, where she used fluorescence-detected two-dimensional electronic spectroscopy to study the structures and excited state dynamics of biomolecules. She is now a postdoctoral fellow in the laboratory of Nils Walter at the University of Michigan, where she is supported by an NIH K99 Pathway to Independence Award. In her current research, she combines single-molecule fluorescence and biochemical techniques to study the molecular mechanisms of RNA transcription and splicing.

Nils G. Walter was born in 1966 in Frankfurt am Main, Germany. He received his "Vordiplom" (B.S.) and "Diploma" (Masters) from the Technical University of Darmstadt after performing research with Hans-Günther Gassen on the physiochemical characterization of a protein dehyrogenase enzyme. He earned his Dr. Ing. while studying molecular in vitro evolution of DNA and RNA using fluorescence techniques with Nobel laureate Manfred Eigen at the Max-Planck-Institute for Biophysical Chemistry, Göttingen. For his postdoctoral studies, he turned to RNA enzymes under the guidance of John M. Burke at the University of Vermont in Burlington, Vermont. He is currently the Francis S. Collins Collegiate Professor of Chemistry, Biophysics, and Biological Chemistry in the College of Literature, Science and the Arts of the University of Michigan in Ann Arbor, Michigan. His research interests focus on noncoding RNA through the lens of single molecule fluorescence techniques. He founded and currently directs the Single Molecule Analysis in Real-Time (SMART) Center, as well as cofounded and currently codirects the Center for RNA Biomedicine at Michigan.

ACKNOWLEDGMENTS

This work was supported by NIH R01 Grants GM062357, GM118524, and GM122803 to N.G.W. and NIH K99 Pathway to Independence Award GM120457 to J.R.W.

REFERENCES

(1) Kruger, K.; Grabowski, P. J.; Zaug, A. J.; Sands, J.; Gottschling, D. E.; Cech, T. R. Self-Splicing RNA: Autoexcision and Autocyclization of the Ribosomal RNA Intervening Sequence of Tetrahymena. *Cell* **1982**, *31*, 147−157.
(2) Guerrier-Takada, C.; Gardiner, K.; Marsh, T.; Pace, N.; Altman, S. The RNA Moiety of Ribonuclease P Is the Catalytic Subunit of the Enzyme. *Cell* **1983**, *35*, 849−857.
(3) Moerner, W. E.; Kador, L. Optical Detection and Spectroscopy of Single Molecules in a Solid. *Phys. Rev. Lett.* **1989**, *62*, 2535−2538.
(4) Birney, E.; Stamatoyannopoulos, J. A.; Dutta, A.; Guigo, R.; Gingeras, T. R.; Margulies, E. H.; Weng, Z. P.; Snyder, M.; Dermitzakis, E. T.; Stamatoyannopoulos, J. A.; et al. Identification and Analysis of Functional Elements in 1% of the Human Genome by the Encode Pilot Project. *Nature* **2007**, *447*, 799−816.
(5) Carninci, P.; Kasukawa, T.; Katayama, S.; Gough, J.; Frith, M. C.; Maeda, N.; Oyama, R.; Ravasi, T.; Lenhard, B.; Wells, C.; et al. The Transcriptional Landscape of the Mammalian Genome. *Science* **2005**, *309*, 1559−1563.
(6) Harrow, J.; Frankish, A.; Gonzalez, J. M.; Tapanari, E.; Diekhans, M.; Kokocinski, F.; Aken, B. L.; Barrell, D.; Zadissa, A.; Searle, S..et al. Gencode: The Reference Human Genome Annotation for the Encode Project. *Genome Res.* 2012, *22*, 1760−1774.
(7) Guttman, M.; Amit, I.; Garber, M.; French, C.; Lin, M. F.; Feldser, D.; Huarte, M.; Zuk, O.; Carey, B. W.; Cassady, J. P.; et al. Chromatin Signature Reveals over a Thousand Highly Conserved Large Non-Coding RNAs in Mammals. *Nature* **2009**, *458*, 223−227.
(8) Djebali, S.; Davis, C. A.; Merkel, A.; Dobin, A.; Lassmann, T.; Mortazavi, A.; Tanzer, A.; Lagarde, J.; Lin, W.; Schlesinger, F.; et al. Landscape of Transcription in Human Cells. *Nature* **2012**, *489*, 101−108.
(9) Belinky, F.; Bahir, I.; Stelzer, G.; Zimmerman, S.; Rosen, N.; Nativ, N.; Dalah, I.; Iny Stein, T.; Rappaport, N.; Mituyama, T.; et al. Non-Redundant Compendium of Human Ncrna Genes in Genecards. *Bioinformatics* **2013**, *29*, 255−261.
(10) Tuck, A. C.; Tollervey, D. RNA in Pieces. *Trends Genet.* **2011**, *27*, 422−432.
(11) Shi, H.; Moore, P. B. The Crystal Structure of Yeast Phenylalanine Trna at 1.93 a Resolution: A Classic Structure Revisited. *RNA* **2000**, *6*, 1091−1105.
(12) Wu, H.; Feigon, J. H/Aca Small Nucleolar RNA Pseudouridylation Pockets Bind Substrate RNA to Form Three-Way Junctions That Position the Target U for Modification. *Proc. Natl. Acad. Sci. U. S. A.* **2007**, *104*, 6655−6660.
(13) Toor, N.; Keating, K. S.; Taylor, S. D.; Pyle, A. M. Crystal Structure of a Self-Spliced Group Ii Intron. *Science* **2008**, *320*, 77−82.
(14) Elkayam, E.; Kuhn, C.-D.; Tocilj, A.; Haase, A. D.; Greene, E. M.; Hannon, G. J.; Joshua-Tor, L. The Structure of Human Argonaute-2 in Complex with Mir-20a. *Cell* **2012**, *150*, 100−110.
(15) Jiang, J.; Chan, H.; Cash, D. D.; Miracco, E. J.; Ogorzalek Loo, R. R.; Upton, H. E.; Cascio, D.; O'Brien Johnson, R.; Collins, K.; Loo, J. A.; et al. Structure of *Tetrahymena* Telomerase Reveals Previously Unknown Subunits, Functions, and Interactions. *Science* **2015**, *350*, aab4070.
(16) Khatter, H.; Myasnikov, A. G.; Natchiar, S. K.; Klaholz, B. P. Structure of the Human 80s Ribosome. *Nature* **2015**, *520*, 640−645.
(17) Bertram, K.; Agafonov, D. E.; Liu, W. T.; Dybkov, O.; Will, C. L.; Hartmuth, K.; Urlaub, H.; Kastner, B.; Stark, H.; Luhrmann, R. Cryo-Em Structure of a Human Spliceosome Activated for Step 2 of Splicing. *Nature* **2017**, *542*, 318−323.
(18) Liberman, J. A.; Suddala, K. C.; Aytenfisu, A.; Chan, D.; Belashov, I. A.; Salim, M.; Mathews, D. H.; Spitale, R. C.; Walter, N. G.; Wedekind, J. E. Structural Analysis of a Class Iii Preq1 Riboswitch Reveals an Aptamer Distant from a Ribosome-Binding Site Regulated by Fast Dynamics. *Proc. Natl. Acad. Sci. U. S. A.* **2015**, *112*, E3485−E3494.
(19) Nguyen, L. A.; Wang, J.; Steitz, T. A. Crystal Structure of Pistol, a Class of Self-Cleaving Ribozyme. *Proc. Natl. Acad. Sci. U. S. A.* **2017**, *114*, 1021−1026.
(20) Crick, F. H. On Protein Synthesis. *The Symposia of the Society for Experimental Biology* **1958**, *12*, 138−163.
(21) Darnell, J. RNA: Life's Indispensable Molecule; *Cold Spring Harbor Laboratory Press*: New York, 2011.
(22) Fica, S. M.; Tuttle, N.; Novak, T.; Li, N.-S.; Lu, J.; Koodathingal, P.; Dai, Q.; Staley, J. P.; Piccirilli, J. A. RNA Catalyses Nuclear Pre-Mrna Splicing. *Nature* **2013**, *503*, 229−234.
(23) Golden, B. L.; Gooding, A. R.; Podell, E. R.; Cech, T. R. A Preorganized Active Site in the Crystal Structure of the Tetrahymena Ribozyme. *Science* **1998**, *282*, 259−264.
(24) Pley, H. W.; Flaherty, K. M.; McKay, D. B. Three-Dimensional Structure of a Hammerhead Ribozyme. *Nature* **1994**, *372*, 68−74.
(25) Chow, L. C.; Gelinas, R. E.; Broker, T. R.; Roberts, R. J. An Amazing Sequence Arrangement at the 5′ Ends of Adenovirus 2 Messenger RNA. *Cell* **1977**, *12*, 1−8.
(26) Berget, S. M.; Moore, C.; Sharp, P. A. Spliced Segments at the 5′ Terminus of Adenovirus 2 Late Mrna. *Rev. Med. Virol.* 1977, *10*, 356−362; discussion 355−356.
(27) Jahn, M.; Rogers, M. J.; Soll, D. Anticodon and Acceptor Stem Nucleotides in Trna(Gln) Are Major Recognition Elements for E. Coli Glutaminyl-Trna Synthetase. *Nature* **1991**, *352*, 258−260.
(28) Sharp, S. J.; Schaack, J.; Cooley, L.; Burke, D. J.; Soil, D. Structure and Transcription of Eukaryotic Trna Genes. *CRC Reviews in Biochemistry* **1985**, *19*, 107−144.
(29) Guerrier-Takada, C.; Gardiner, K.; Marsh, T.; Pace, N.; Altman, S. The RNA Moiety of Ribonuclease P Is the Catalytic Subunit of the Enzyme. *Cell* **1983**, *35*, 849−857.
(30) Marquez, S. M.; Chen, J. L.; Evans, D.; Pace, N. R. Structure and Function of Eukaryotic Ribonuclease P RNA. Mol. *Mol. Cell* **2006**, *24*, 445−456.

DOI: 10.1021/acs.chemrev.7b00519
Chem. Rev. 2018, 118, 4120−4155

(31) Evans, D.; Marquez, S. M.; Pace, N. R. RNAse P: Interface of the RNA and Protein Worlds. *Trends Biochem. Sci.* **2006**, *31*, 333−341.
(32) Arts, G. J.; Benne, R. Mechanism and Evolution of RNA Editing in Kinetoplastida. *Biochim. Biophys. Acta, Gene Struct. Expression* **1996**, *1307*, 39−54.
(33) Benne, R. RNA Editing in Trypanosomes. *Eur. J. Biochem.* **1994**, *221*, 9−23.
(34) Walter, N. G. Going Viral: Riding the RNA Wave to Discovery. *RNA* **2015**, *21*, 756−757.
(35) Nou, X.; Kadner, R. J. Adenosylcobalamin Inhibits Ribosome Binding to Btub RNA. *Proc. Natl. Acad. Sci. U. S. A.* **2000**, *97*, 7190−7195.
(36) Grundy, F. J.; Henkin, T. M. The S Box Regulon: A New Global Transcription Termination Control System for Methionine and Cysteine Biosynthesis Genes in Gram-Positive Bacteria. *Mol. Microbiol.* **1998**, *30*, 737−749.
(37) Winkler, W. C.; Cohen-Chalamish, S.; Breaker, R. R. An Mrna Structure That Controls Gene Expression by Binding Fmn. *Proc. Natl. Acad. Sci. U. S. A.* **2002**, *99*, 15908−15913.
(38) Winkler, W.; Nahvi, A.; Breaker, R. R. Thiamine Derivatives Bind Messenger RNAs Directly to Regulate Bacterial Gene Expression. *Nature* **2002**, *419*, 952−956.
(39) McCown, P. J.; Corbino, K. A.; Stav, S.; Sherlock, M. E.; Breaker, R. R. Riboswitch Diversity and Distribution. *RNA* **2017**, *23*, 995−1011.
(40) Santos, N.; Zhu, J.; Donohue, J. P.; Korostelev, A. A.; Noller, H. F. Crystal Structure of the 70s Ribosome Bound with the Q253p Mutant Form of Release Factor Rf2. *Structure* **2013**, *21*, 1258−1263.
(41) Jenner, L.; Melnikov, S.; Garreau de Loubresse, N.; Ben-Shem, A.; Iskakova, M.; Urzhumtsev, A.; Meskauskas, A.; Dinman, J.; Yusupova, G.; Yusupov, M. Crystal Structure of the 80s Yeast Ribosome. *Curr. Opin. Struct. Biol.* **2012**, *22*, 759−767.
(42) Feng, S.; Chen, Y.; Gao, Y. G. Crystal Structure of 70s Ribosome with Both Cognate Trnas in the E and P Sites Representing an Authentic Elongation Complex. *PLoS One* **2013**, *8*, e58829.
(43) Yusupov, M. M.; Yusupova, G. Z.; Baucom, A.; Lieberman, K.; Earnest, T. N.; Cate, J. H.; Noller, H. F. Crystal Structure of the Ribosome at 5.5 a Resolution. *Science* **2001**, *292*, 883−896.
(44) Takasu, A.; Watanabe, K.; Kawai, G. Analysis of Relative Positions of Ribonucleotide Bases in a Crystal Structure of Ribosome. *Nucleosides, Nucleotides Nucleic Acids* **2002**, *21*, 449−462.
(45) Korostelev, A.; Trakhanov, S.; Laurberg, M.; Noller, H. F. Crystal Structure of a 70s Ribosome-Trna Complex Reveals Functional Interactions and Rearrangements. *Cell* **2006**, *126*, 1065−1077.
(46) Jin, H.; Kelley, A. C.; Ramakrishnan, V. Crystal Structure of the Hybrid State of Ribosome in Complex with the Guanosine Triphosphatase Release Factor 3. *Proc. Natl. Acad. Sci. U. S. A.* **2011**, *108*, 15798−15803.
(47) Ben-Shem, A.; Jenner, L.; Yusupova, G.; Yusupov, M. Crystal Structure of the Eukaryotic Ribosome. *Science* **2010**, *330*, 1203−1209.
(48) Yan, C.; Wan, R.; Bai, R.; Huang, G.; Shi, Y. Structure of a Yeast Activated Spliceosome at 3.5 a Resolution. *Science* **2016**, *353*, 904−911.
(49) Wan, R.; Yan, C.; Bai, R.; Wang, L.; Huang, M.; Wong, C. C.; Shi, Y. The 3.8 a Structure of the U4/U6.U5 Tri-Snrnp: Insights into Spliceosome Assembly and Catalysis. *Science* **2016**, *351*, 466−475.
(50) Wan, R.; Yan, C.; Bai, R.; Huang, G.; Shi, Y. Structure of a Yeast Catalytic Step I Spliceosome at 3.4 a Resolution. *Science* **2016**, *353*, 895−904.
(51) Golas, M. M.; Sander, B.; Bessonov, S.; Grote, M.; Wolf, E.; Kastner, B.; Stark, H.; Luhrmann, R. 3d Cryo-Em Structure of an Active Step I Spliceosome and Localization of Its Catalytic Core. *Mol. Cell* **2010**, *40*, 927−938.
(52) Galej, W. P.; Wilkinson, M. E.; Fica, S. M.; Oubridge, C.; Newman, A. J.; Nagai, K. Cryo-Em Structure of the Spliceosome Immediately after Branching. *Nature* **2016**, *537*, 197−201.
(53) Butcher, S. E.; Brow, D. A. Towards Understanding the Catalytic Core Structure of the Spliceosome. *Biochem. Soc. Trans.* **2005**, *33*, 447−449.
(54) Azubel, M.; Wolf, S. G.; Sperling, J.; Sperling, R. Three-Dimensional Structure of the Native Spliceosome by Cryo-Electron Microscopy. Mol. *Mol. Cell* **2004**, *15*, 833−839.
(55) Ban, N.; Nissen, P.; Hansen, J.; Moore, P. B.; Steitz, T. A. The Complete Atomic Structure of the Large Ribosomal Subunit at 2.4 Angstrom Resolution. *Science* **2000**, *289*, 905−920.
(56) Wohlgemuth, I.; Beringer, M.; Rodnina, M. V. Rapid Peptide Bond Formation on Isolated 50s Ribosomal Subunits. *EMBO Rep.* **2006**, *7*, 699−703.
(57) Feng, J.; Funk, W. D.; Wang, S. S.; Weinrich, S. L.; Avilion, A. A.; Chiu, C. P.; Adams, R. R.; Chang, E.; Allsopp, R. C.; Yu, J.; et al. The RNA Component of Human Telomerase. *Science* **1995**, *269*, 1236−1241.
(58) Elbashir, S. M.; Harborth, J.; Lendeckel, W.; Yalcin, A.; Weber, K.; Tuschl, T. Duplexes of 21-Nucleotide RNAs Mediate RNA Interference in Cultured Mammalian Cells. *Nature* **2001**, *411*, 494−498.
(59) Hamilton, A. J.; Baulcombe, D. C. A Species of Small Antisense RNA in Posttranscriptional Gene Silencing in Plants. *Science* **1999**, *286*, 950−952.
(60) Fire, A.; Xu, S.; Montgomery, M. K.; Kostas, S. A.; Driver, S. E.; Mello, C. C. Potent and Specific Genetic Interference by Double-Stranded RNA in Caenorhabditis Elegans. *Nature* **1998**, *391*, 806−811.
(61) Lau, N. C.; Lim, L. P.; Weinstein, E. G.; Bartel, D. P. An Abundant Class of Tiny RNAs with Probable Regulatory Roles in Caenorhabditis Elegans. *Science* **2001**, *294*, 858−862.
(62) Lee, R. C.; Ambros, V. An Extensive Class of Small RNAs in Caenorhabditis Elegans. *Science* **2001**, *294*, 862−864.
(63) Reinhart, B. J.; Slack, F. J.; Basson, M.; Pasquinelli, A. E.; Bettinger, J. C.; Rougvie, A. E.; Horvitz, H. R.; Ruvkun, G. The 21-Nucleotide Let-7 RNA Regulates Developmental Timing in Caenorhabditis Elegans. *Nature* **2000**, *403*, 901−906.
(64) Lee, R. C.; Feinbaum, R. L.; Ambros, V. The C. Elegans Heterochronic Gene Lin-4 Encodes Small RNAs with Antisense Complementarity to Lin-14. *Cell* **1993**, *75*, 843−854.
(65) Consortium, E. P. An Integrated Encyclopedia of DNA Elements in the Human Genome. *Nature* **2012**, *489*, 57−74.
(66) van Bakel, H.; Nislow, C.; Blencowe, B. J.; Hughes, T. R. Most "Dark Matter" Transcripts Are Associated with Known Genes. *PLoS Biol.* **2010**, *8*, e1000371.
(67) Guttman, M.; Donaghey, J.; Carey, B. W.; Garber, M.; Grenier, J. K.; Munson, G.; Young, G.; Lucas, A. B.; Ach, R.; Bruhn, L.; et al. Lincrnas Act in the Circuitry Controlling Pluripotency and Differentiation. *Nature* **2011**, *477*, 295−300.
(68) Reuter, J. A.; Spacek, D. V.; Snyder, M. P. High-Throughput Sequencing Technologies. *Mol. Cell* **2015**, *58*, 586−597.
(69) Underwood, J. G.; Uzilov, A. V.; Katzman, S.; Onodera, C. S.; Mainzer, J. E.; Mathews, D. H.; Lowe, T. M.; Salama, S. R.; Haussler, D. Fragseq: Transcriptome-Wide RNA Structure Probing Using High-Throughput Sequencing. *Nat. Methods* **2010**, *7*, 995−1001.
(70) Hsu, P. D.; Lander, E. S.; Zhang, F. Development and Applications of Crispr-Cas9 for Genome Engineering. *Cell* **2014**, *157*, 1262−1278.
(71) Mojica, F. J.; Diez-Villasenor, C.; Garcia-Martinez, J.; Soria, E. Intervening Sequences of Regularly Spaced Prokaryotic Repeats Derive from Foreign Genetic Elements. *J. Mol. Evol.* **2005**, *60*, 174−182.
(72) Jinek, M.; Chylinski, K.; Fonfara, I.; Hauer, M.; Doudna, J. A.; Charpentier, E. A Programmable Dual-RNA-Guided DNA Endonuclease in Adaptive Bacterial Immunity. *Science* **2012**, *337*, 816−821.
(73) Nobelprize.org. In The Official Web Site of the Nobel Prize. https://www.nobelprize.org/: https://www.nobelprize.org/ (accessed November 23, 2017).

DOI: 10.1021/acs.chemrev.7b00519
Chem. Rev. 2018, 118, 4120−4155

(74) Valeur, B.; Berberan-Santos, M. N. A Brief History of Fluorescence and Phosphorescence before the Emergence of Quantum Theory. *J. Chem. Educ.* **2011**, *88*, 731−738.
(75) Stokes, G. G. On the Change of Refrangibility of Light. *Philos. Trans. R. Soc. London* **1852**, *142*, 463−562.
(76) Betzig, E.; Chichester, R. J. Single Molecules Observed by near-Field Scanning Optical Microscopy. *Science* **1993**, *262*, 1422−1425.
(77) Funatsu, T.; Harada, Y.; Tokunaga, M.; Saito, K.; Yanagida, T. Imaging of Single Fluorescent Molecules and Individual Atp Turnovers by Single Myosin Molecules in Aqueous Solution. *Nature* **1995**, *374*, 555−559.
(78) Jablonski, A. Efficiency of Anti-Stokes Fluorescence in Dyes. *Nature* **1933**, *131*, 839−840.
(79) Lakowicz, J. R. *Principles of Fluorescence Spectroscopy*, 3rd ed.; Springer: New York, 2006.
(80) Walter, N. G.; Huang, C. Y.; Manzo, A. J.; Sobhy, M. A. Do-It-Yourself Guide: How to Use the Modern Single-Molecule Toolkit. *Nat. Methods* **2008**, *5*, 475−489.
(81) Walter, N. G.; Bustamante, C. Introduction to Single Molecule Imaging and Mechanics: Seeing and Touching Molecules One at a Time. *Chem. Rev.* **2014**, *114*, 3069−3071.
(82) Cui, B.; Wu, C.; Chen, L.; Ramirez, A.; Bearer, E. L.; Li, W.-P.; Mobley, W. C.; Chu, S. One at a Time, Live Tracking of Ngf Axonal Transport Using Quantum Dots. *Proc. Natl. Acad. Sci. U. S. A.* **2007**, *104*, 13666−13671.
(83) Zhang, Q.; Li, Y.; Tsien, R. W. The Dynamic Control of Kiss-and-Run and Vesicular Reuse Probed with Single Nanoparticles. *Science* **2009**, *323*, 1448−1453.
(84) Dahan, M.; Lévi, S.; Luccardini, C.; Rostaing, P.; Riveau, B.; Triller, A. Diffusion Dynamics of Glycine Receptors Revealed by Single-Quantum Dot Tracking. *Science* **2003**, *302*, 442−445.
(85) Resch-Genger, U.; Grabolle, M.; Cavaliere-Jaricot, S.; Nitschke, R.; Nann, T. Quantum Dots Versus Organic Dyes as Fluorescent Labels. *Nat. Methods* **2008**, *5*, 763.
(86) Webb, D. J.; Brown, C. M. Epi-Fluorescence Microscopy. In *Methods in Molecular Biology*; Humana Press: Totowa, NJ, 2012; Vol. *931*, pp 29−5910.1007/978-1-62703-056-4_2.
(87) Lichtman, J. W.; Conchello, J. A. Fluorescence Microscopy. *Nat. Methods* **2005**, *2*, 910−919.
(88) Weber, M. A.; Stracke, F.; Meixner, A. J. Dynamics of Single Dye Molecules Observed by Confocal Imaging and Spectroscopy. *Cytometry* **1999**, *36*, 217−223.
(89) Segers-Nolten, G. M. J.; Wyman, C.; Wijgers, N.; Vermeulen, W.; Lenferink, A. T. M.; Hoeijmakers, J. H. J.; Greve, J.; Otto, C. Scanning Confocal Fluorescence Microscopy for Single Molecule Analysis of Nucleotide Excision Repair Complexes. *Nucleic Acids Res.* **2002**, *30*, 4720−4727.
(90) Ambrose, E. J. A. Surface Contact Microscope for the Study of Cell Movements. *Nature* **1956**, *178*, 1194−1194.
(91) Fish, K. N. Total Internal Reflection Fluorescence (Tirf) Microscopy. In *Current Protocols in Cytometry*; 2009; Chapter 12, Unit 12.18.10.1002/0471142956.cy1218s50.
(92) Axelrod, D. Total Internal Reflection Fluorescence Microscopy in Cell Biology. *Traffic* **2001**, *2*, 764−774.
(93) Axelrod, D. Cell-Substrate Contacts Illuminated by Total Internal Reflection Fluorescence. *J. Cell Biol.* **1981**, *89*, 141−145.
(94) Sahl, S. J.; Moerner, W. E. Super-Resolution Fluorescence Imaging with Single Molecules. *Curr. Opin. Struct. Biol.* **2013**, *23*, 778−787.
(95) Biteen, J.; Willets, K. A. Introduction: Super-Resolution and Single-Molecule Imaging. *Chem. Rev.* **2017**, *117*, 7241−7243.
(96) Larson, J. D.; Rodgers, M. L.; Hoskins, A. A. Visualizing Cellular Machines with Colocalization Single Molecule Microscopy. *Chem. Soc. Rev.* **2014**, *43*, 1189−1200.
(97) Rinaldi, A. J.; Lund, P. E.; Blanco, M. R.; Walter, N. G. The Shine-Dalgarno Sequence of Riboswitch-Regulated Single Mrnas Shows Ligand-Dependent Accessibility Bursts. *Nat. Commun.* **2016**, *7*, 8976.
(98) Johnson-Buck, A.; Su, X.; Giraldez, M. D.; Zhao, M.; Tewari, M.; Walter, N. G. Kinetic Fingerprinting to Identify and Count Single Nucleic Acids. *Nat. Biotechnol.* **2015**, *33*, 730−732.
(99) Förster, T. Intermolecular Energy Migration and Fluorescence. *Ann. Phys. (Berlin, Ger.)* **1948**, *437*, 55−75.
(100) Joo, C.; Balci, H.; Ishitsuka, Y.; Buranachai, C.; Ha, T. Advances in Single-Molecule Fluorescence Methods for Molecular Biology. *Annu. Rev. Biochem.* **2008**, *77*, 51−76.
(101) Roy, R.; Hohng, S.; Ha, T. A Practical Guide to Single Molecule Fret. Nat. *Nat. Methods* **2008**, *5*, 507−516.
(102) Aramendia, P. F.; Negri, R. M.; Roman, E. S. Temperature Dependence of Fluorescence and Photoisomerization in Symmetric Carbocyanines. Influence of Medium Viscosity and Molecular Structure. *J. Phys. Chem.* **1994**, *98*, 3165−3173.
(103) Sanborn, M. E.; Connolly, B. K.; Gurunathan, K.; Levitus, M. Fluorescence Properties and Photophysics of the Sulfoindocyanine Cy3 Linked Covalently to DNA. *J. Phys. Chem. B* **2007**, *111*, 11064−11074.
(104) Myong, S.; Cui, S.; Cornish, P. V.; Kirchhofer, A.; Gack, M. U.; Jung, J. U.; Hopfner, K. P.; Ha, T. Cytosolic Viral Sensor Rig-I Is a 5′-Triphosphate-Dependent Translocase on Double-Stranded RNA. *Science* **2009**, *323*, 1070−1074.
(105) Myong, S.; Ha, T. Stepwise Translocation of Nucleic Acid Motors. *Curr. Opin. Struct. Biol.* **2010**, *20*, 121−127.
(106) Hwang, H.; Kim, H.; Myong, S. Protein Induced Fluorescence Enhancement as a Single Molecule Assay with Short Distance Sensitivity. *Proc. Natl. Acad. Sci. U. S. A.* **2011**, *108*, 7414−7418.
(107) Sorokina, M.; Koh, H.-R.; Patel, S. S.; Ha, T. Fluorescent Lifetime Trajectories of a Single Fluorophore Reveal Reaction Intermediates During Transcription Initiation. *J. Am. Chem. Soc.* **2009**, *131*, 9630−9631.
(108) Levene, M. J.; Korlach, J.; Turner, S. W.; Foquet, M.; Craighead, H. G.; Webb, W. W. Zero-Mode Waveguides for Single-Molecule Analysis at High Concentrations. *Science* **2003**, *299*, 682−686.
(109) Zhu, P.; Craighead, H. G. Zero-Mode Waveguides for Single-Molecule Analysis. *Annu. Rev. Biophys.* **2012**, *41*, 269−293.
(110) de Torres, J.; Ghenuche, P.; Moparthi, S. B.; Grigoriev, V.; Wenger, J. Fret Enhancement in Aluminum Zero-Mode Waveguides. *ChemPhysChem* **2015**, *16*, 782−788.
(111) Larkin, J.; Foquet, M.; Turner, S. W.; Korlach, J.; Wanunu, M. Reversible Positioning of Single Molecules inside Zero-Mode Waveguides. *Nano Lett.* **2014**, *14*, 6023−6029.
(112) Elson, E. L. Fluorescence Correlation Spectroscopy: Past, Present, Future. *Biophys. J.* **2011**, *101*, 2855−2870.
(113) Tian, Y.; Martinez, M. M.; Pappas, D. Fluorescence Correlation Spectroscopy: A Review of Biochemical and Microfluidic Applications. *Appl. Spectrosc.* **2011**, *65*, 115−124.
(114) Schwille, P.; Meyer-Almes, F. J.; Rigler, R. Dual-Color Fluorescence Cross-Correlation Spectroscopy for Multicomponent Diffusional Analysis in Solution. *Biophys. J.* **1997**, *72*, 1878−1886.
(115) Hwang, L. C.; Gosch, M.; Lasser, T.; Wohland, T. Simultaneous Multicolor Fluorescence Cross-Correlation Spectroscopy to Detect Higher Order Molecular Interactions Using Single Wavelength Laser Excitation. *Biophys. J.* **2006**, *91*, 715−727.
(116) Jung, J.; Ihly, R.; Scott, E.; Yu, M.; Van Orden, A. Probing the Complete Folding Trajectory of a DNA Hairpin Using Dual Beam Fluorescence Fluctuation Spectroscopy. *J. Phys. Chem. B* **2008**, *112*, 127−133.
(117) Dunn, R. C.; Holtom, G. R.; Mets, L.; Xie, X. S. Near-Field Fluorescence Imaging and Fluorescence Lifetime Measurement of Light-Harvesting Complexes in Intact Photosynthetic Membranes. *J. Phys. Chem.* **1994**, *98*, 3094−3098.
(118) Piatkowski, L.; Gellings, E.; van Hulst, N. F. Broadband Single-Molecule Excitation Spectroscopy. *Nat. Commun.* **2016**, *7*, 10411.
(119) Gerhardt, I.; Mai, L.; Lamas-Linares, A.; Kurtsiefer, C. Detection of Single Molecules Illuminated by a Light-Emitting Diode. *Sensors* **2011**, *11*, 905−916.

DOI: 10.1021/acs.chemrev.7b00519
Chem. Rev. 2018, 118, 4120−4155

(120) Piatkowski, L.; Gellings, E.; van Hulst, N. F. Multicolour Single Molecule Emission and Excitation Spectroscopy Reveals Extensive Spectral Shifts. *Faraday Discuss.* **2015**, *184*, 207−220.
(121) Joo, C.; Ha, T. In *Single-Molecule Techniques: A Laboratory Manual*; Selvin, P. R., Ha, T., Eds.; Cold Spring Harbor Laboratory Press: Cold Spring Harbor, N.Y., 2008; Vol. *1*.
(122) Murphy, M. C.; Rasnik, I.; Cheng, W.; Lohman, T. M.; Ha, T. Probing Single-Stranded DNA Conformational Flexibility Using Fluorescence Spectroscopy. *Biophys. J.* **2004**, *86*, 2530−2537.
(123) McKinney, S. A.; Declais, A. C.; Lilley, D. M.; Ha, T. Structural Dynamics of Individual Holliday Junctions. *Nat. Struct. Biol.* **2003**, *10*, 93−97.
(124) Ray, S.; Meyhöfer, E.; Milligan, R. A.; Howard, J. Kinesin Follows the Microtubule's Protofilament Axis. *J. Cell Biol.* **1993**, *121*, 1083−1093.
(125) Ozeki, T.; Verma, V.; Uppalapati, M.; Suzuki, Y.; Nakamura, M.; Catchmark, J. M.; Hancock, W. O. Surface-Bound Casein Modulates the Adsorption and Activity of Kinesin On sio2 Surfaces. *Biophys. J.* **2009**, *96*, 3305−3318.
(126) Woehlke, G.; Ruby, A. K.; Hart, C. L.; Ly, B.; Hom-Booher, N.; Vale, R. D. Microtubule Interaction Site of the Kinesin Motor. *Cell* **1997**, *90*, 207−216.
(127) Lamichhane, R.; Solem, A.; Black, W.; Rueda, D. Single Molecule Fret of Protein-Nucleic Acid and Protein-Protein Complexes: Surface Passivation and Immobilization. *Methods* **2010**, *52*, 192−200.
(128) Selvin, P. R.; Ha, T. *Single-Molecule Techniques: A Laboratory Manual*; Cold Spring Harbor Laboratory Press: Cold Spring Harbor, N.Y., 2008.
(129) Hua, B.; Young Han, K.; Zhou, R.; Kim, H.; Shi, X.; Abeysirigunawardena, S. C.; Jain, A.; Singh, D.; Aggarwal, V.; Woodson, S. A.; et al. An Improved Surface Passivation Method for Single-Molecule Studies. *Nat. Methods* **2014**, *11*, 1233−1236.
(130) Salomon, W. E.; Jolly, S. M.; Moore, M. J.; Zamore, P. D.; Serebrov, V. Single-Molecule Imaging Reveals That Argonaute Reshapes the Binding Properties of Its Nucleic Acid Guides. *Cell* **2015**, *162*, 84−95.
(131) Green, N. M. In *Advances in Protein Chemistry*; Anfinsen, C. B., Edsall, J. T., Richards, F. M., Eds.; Academic Press, 1975; Vol. *29*.
(132) Chaiet, L.; Wolf, F. J. The Properties of Streptavidin, a Biotin-Binding Protein Produced by Streptomycetes. *Arch. Biochem. Biophys.* **1964**, *106*, 1−5.
(133) Lee, G. U.; Kidwell, D. A.; Colton, R. J. Sensing Discrete Streptavidin-Biotin Interactions with Atomic Force Microscopy. *Langmuir* **1994**, *10*, 354−357.
(134) Moy, V.; Florin, E.; Gaub, H. Intermolecular Forces and Energies between Ligands and Receptors. *Science* **1994**, *266*, 257−259.
(135) Aleman, E. A.; Pedini, H. S.; Rueda, D. Covalent-Bond-Based Immobilization Approaches for Single-Molecule Fluorescence. *ChemBioChem* **2009**, *10*, 2862−2866.
(136) Roy, R.; Hohng, S.; Ha, T. A Practical Guide to Single-Molecule Fret. *Nat. Methods* **2008**, *5*, 507−516.
(137) Cisse, I. I.; Kim, H.; Ha, T. A Rule of Seven in Watson-Crick Base-Pairing of Mismatched Sequences. *Nat. Struct. Mol. Biol.* **2012**, *19*, 623−628.
(138) Okumus, B.; Wilson, T. J.; Lilley, D. M. J.; Ha, T. Vesicle Encapsulation Studies Reveal That Single Molecule Ribozyme Heterogeneities Are Intrinsic. *Biophys. J.* **2004**, *87*, 2798−2806.
(139) Jain, A.; Liu, R.; Ramani, B.; Arauz, E.; Ishitsuka, Y.; Ragunathan, K.; Park, J.; Chen, J.; Xiang, Y. K.; Ha, T. Probing Cellular Protein Complexes Using Single-Molecule Pull-Down. *Nature* **2011**, *473*, 484−488.
(140) Ghisaidoobe, A. B. T.; Chung, S. J. Intrinsic Tryptophan Fluorescence in the Detection and Analysis of Proteins: A Focus on Förster Resonance Energy Transfer Techniques. *Int. J. Mol. Sci.* **2014**, *15*, 22518−22538.
(141) Resch-Genger, U.; Grabolle, M.; Cavaliere-Jaricot, S.; Nitschke, R.; Nann, T. Quantum Dots Versus Organic Dyes as Fluorescent Labels. *Nat. Methods* **2008**, *5*, 763−775.
(142) Abelson, J.; Blanco, M.; Ditzler, M. A.; Fuller, F.; Aravamudhan, P.; Wood, M.; Villa, T.; Ryan, D. E.; Pleiss, J. A.; Maeder, C.; et al. Conformational Dynamics of Single Pre-Mrna Molecules During in Vitro Splicing. *Nat. Struct. Mol. Biol.* **2010**, *17*, 504−512.
(143) Krishnan, R.; Blanco, M. R.; Kahlscheuer, M. L.; Abelson, J.; Guthrie, C.; Walter, N. G. Biased Brownian Racheting Leads to Pre-Mrna Remodeling and Capture Prior to First-Step Splicing. *Nat. Struct. Mol. Biol.* **2013**, *20*, 1450−1457.
(144) Blanco, M. R.; Martin, J. S.; Kahlscheuer, M. L.; Krishnan, R.; Abelson, J.; Laederach, A.; Walter, N. G. Single Molecule Cluster Analysis Dissects Splicing Pathway Conformational Dynamics. *Nat. Methods* **2015**, *12*, 1077−1084.
(145) Abelson, J.; Hadjivassiliou, H.; Guthrie, C. Preparation of Fluorescent Pre-Mrna Substrates for an Smfret Study of Pre-Mrna Splicing in Yeast. *Methods Enzymol.* **2010**, *472*, 31−40.
(146) Parks, J. W.; Stone, M. D. Coordinated DNA Dynamics During the Human Telomerase Catalytic Cycle. *Nat. Commun.* **2014**, *5*, 1−10.
(147) Dorywalska, M.; Blanchard, S. C.; Gonzalez, J.; Ruben, L.; Kim, H. D.; Chu, S.; Puglisi, J. D. Site-Specific Labeling of the Ribosome for Single-Molecule Spectroscopy. *Nucleic Acids Res.* **2005**, *33*, 182−189.
(148) Tian, H.; Fürstenberg, A.; Huber, T. Labeling and Single-Molecule Methods to Monitor G Protein-Coupled Receptor Dynamics. *Chem. Rev.* **2017**, *117*, 186−245.
(149) Hoskins, A. A.; Friedman, L. J.; Gallagher, S. S.; Crawford, D. J.; Anderson, E. G.; Wombacher, R.; Ramirez, N.; Cornish, V. W.; Gelles, J.; Moore, M. J. Ordered and Dynamic Assembly of Single Spliceosomes. *Science* **2011**, *331*, 1289−1295.
(150) Hellstrand, E.; Kukora, S.; Shuman, C. F.; Steenbergen, S.; Thulin, E.; Kohli, A.; Krouse, B.; Linse, S.; Åkerfeldt, K. S. Förster Resonance Energy Transfer Studies of Calmodulin Produced by Native Protein Ligation Reveal Inter-Domain Electrostatic Repulsion. *FEBS J.* **2013**, *280*, 2675−2687.
(151) Chakraborty, A.; Wang, D.; Ebright, Y. W.; Korlann, Y.; Kortkhonjia, E.; Kim, T.; Chowdhury, S.; Wigneshweraraj, S.; Irschik, H.; Jansen, R.; et al. Opening and Closing of the Bacterial RNA Polymerase Clamp. *Science* **2012**, *337*, 591−595.
(152) Blanco, M.; Walter, N. G. Analysis of Complex Single-Molecule Fret Time Trajectories. *Methods Enzymol.* **2010**, *472*, 153−178.
(153) Juette, M. F.; Terry, D. S.; Wasserman, M. R.; Altman, R. B.; Zhou, Z.; Zhao, H.; Blanchard, S. C. Single-Molecule Imaging of Non-Equilibrium Molecular Ensembles on the Millisecond Timescale. *Nat. Methods* **2016**, *13*, 341−344.
(154) Schwarz, G. Estimating the Dimension of a Model. *Ann. Statist.* **1978**, *6*, 461−464.
(155) Beausang, J. F.; Goldman, Y. E.; Nelson, P. C. Changepoint Analysis for Single-Molecule Polarized Total Internal Reflection Fluorescence Microscopy Experiments. *Methods in Enzymology*; 2011; Chapter 15, 10.1016/B978-0-12-381270-4.00015-9.
(156) Beausang, J. F.; Shroder, D. Y.; Nelson, P. C.; Goldman, Y. E. Tilting and Wobble of Myosin V by High-Speed Single-Molecule Polarized Fluorescence Microscopy. *Biophys. J.* **2013**, *104*, 1263−1273.
(157) Neuman, K. C.; Abbondanzieri, E. A.; Landick, R.; Gelles, J.; Block, S. M. Ubiquitous Transcriptional Pausing Is Independent of RNA Polymerase Backtracking. *Cell* **2003**, *115*, 437−447.
(158) Wang, M. D.; Schnitzer, M. J.; Yin, H.; Landick, R.; Gelles, J.; Block, S. M. Force and Velocity Measured for Single Molecules of RNA Polymerase. *Science* **1998**, *282*, 902−907.
(159) Harlepp, S.; Marchal, T.; Robert, J.; Léger, J. F.; Xayaphoummine, A.; Isambert, H.; Chatenay, D. Probing Complex RNA Structures by Mechanical Force. *Eur. Phys. J. E: Soft Matter Biol. Phys.* **2003**, *12*, 605−615.
(160) Liphardt, J.; Onoa, B.; Smith, S. B.; Tinoco, I.; Bustamante, C. Reversible Unfolding of Single RNA Molecules by Mechanical Force. *Science* **2001**, *292*, 733−737.
(161) Onoa, B.; Dumont, S.; Liphardt, J.; Smith, S. B.; Tinoco, I.; Bustamante, C. Identifying Kinetic Barriers to Mechanical Unfolding

DOI: 10.1021/acs.chemrev.7b00519
Chem. Rev. 2018, 118, 4120−4155

of the < Em > T. Thermophila</Em> Ribozyme. *Science* **2003**, *299*, 1892−1895.
(162) Zhuang, X. Single-Molecule RNA Science. *Annu. Rev. Biophys. Biomol. Struct.* **2005**, *34*, 399−414.
(163) Camunas-Soler, J.; Ribezzi-Crivellari, M.; Ritort, F. Elastic Properties of Nucleic Acids by Single-Molecule Force Spectroscopy. *Annu. Rev. Biophys.* **2016**, *45*, 65−84.
(164) Capitanio, M.; Pavone, F. S. Interrogating Biology with Force: Single Molecule High-Resolution Measurements with Optical Tweezers. *Biophys. J.* **2013**, *105*, 1293−1303.
(165) Neuman, K. C.; Nagy, A. Single-Molecule Force Spectroscopy: Optical Tweezers, Magnetic Tweezers and Atomic Force Microscopy. *Nat. Methods* **2008**, *5*, 491−505.
(166) Comstock, M. J.; Ha, T.; Chemla, Y. R. Ultrahigh-Resolution Optical Trap with Single-Fluorophore Sensitivity. *Nat. Methods* **2011**, *8*, 335−340.
(167) Hohng, S.; Lee, S.; Lee, J.; Jo, M. H. Maximizing Information Content of Single-Molecule Fret Experiments: Multi-Color Fret and Fret Combined with Force or Torque. *Chem. Soc. Rev.* **2014**, *43*, 1007−1013.
(168) Wallace, M. I.; Molloy, J. E.; Trentham, D. R. Combined Single-Molecule Force and Fluorescence Measurements for Biology. *J. Biol.* **2003**, *2*, 4−4.
(169) Schütz, G. J.; Hinterdorfer, P. Single Molecule Fluorescence and Force Microscopy. *Exp. Gerontol.* **2002**, *37*, 1495−1511.
(170) Duesterberg, V. K.; Fischer-Hwang, I. T.; Perez, C. F.; Hogan, D. W.; Block, S. M. Observation of Long-Range Tertiary Interactions During Ligand Binding by the Tpp Riboswitch Aptamer. *eLife* **2015**, *4*,10.7554/eLife.12362.
(171) Ha, T.; Zhuang, X.; Kim, H. D.; Orr, J. W.; Williamson, J. R.; Chu, S. Ligand-Induced Conformational Changes Observed in Single RNA Molecules. *Proc. Natl. Acad. Sci. U. S. A.* **1999**, *96*, 9077−9082.
(172) Zhuang, X.; Bartley, L. E.; Babcock, H. P.; Russell, R.; Ha, T.; Herschlag, D.; Chu, S. A Single-Molecule Study of RNA Catalysis and Folding. *Science* **2000**, *288*, 2048−2051.
(173) Zhuang, X.; Kim, H.; Pereira, M. J.; Babcock, H. P.; Walter, N. G.; Chu, S. Correlating Structural Dynamics and Function in Single Ribozyme Molecules. *Science* **2002**, *296*, 1473−1476.
(174) Tan, E.; Wilson, T. J.; Nahas, M. K.; Clegg, R. M.; Lilley, D. M.; Ha, T. A Four-Way Junction Accelerates Hairpin Ribozyme Folding Via a Discrete Intermediate. *Proc. Natl. Acad. Sci. U. S. A.* **2003**, *100*, 9308−9313.
(175) Nahas, M. K.; Wilson, T. J.; Hohng, S.; Jarvie, K.; Lilley, D. M.; Ha, T. Observation of Internal Cleavage and Ligation Reactions of a Ribozyme. *Nat. Struct. Mol. Biol.* **2004**, *11*, 1107−1113.
(176) Pljevaljcic, G.; Millar, D. P.; Deniz, A. A. Freely Diffusing Single Hairpin Ribozymes Provide Insights into the Role of Secondary Structure and Partially Folded States in RNA Folding. *Biophys. J.* **2004**, *87*, 457−467.
(177) Xie, Z.; Srividya, N.; Sosnick, T. R.; Pan, T.; Scherer, N. F. Single-Molecule Studies Highlight Conformational Heterogeneity in the Early Folding Steps of a Large Ribozyme. *Proc. Natl. Acad. Sci. U. S. A.* **2004**, *101*, 534−539.
(178) Okumus, B.; Wilson, T. J.; Lilley, D. M.; Ha, T. Vesicle Encapsulation Studies Reveal That Single Molecule Ribozyme Heterogeneities Are Intrinsic. *Biophys. J.* **2004**, *87*, 2798−2806.
(179) Solomatin, S. V.; Greenfeld, M.; Chu, S.; Herschlag, D. Multiple Native States Reveal Persistent Ruggedness of an RNA Folding Landscape. *Nature* **2010**, *463*, 681−684.
(180) Rueda, D.; Bokinsky, G.; Rhodes, M. M.; Rust, M. J.; Zhuang, X.; Walter, N. G. Single-Molecule Enzymology of RNA: Essential Functional Groups Impact Catalysis from a Distance. *Proc. Natl. Acad. Sci. U. S. A.* **2004**, *101*, 10066−10071.
(181) Ditzler, M. A.; Rueda, D.; Mo, J.; Hakansson, K.; Walter, N. G. A Rugged Free Energy Landscape Separates Multiple Functional RNA Folds Throughout Denaturation. *Nucleic Acids Res.* **2008**, *36*, 7088−7099.
(182) Liu, S.; Bokinsky, G.; Walter, N. G.; Zhuang, X. Dissecting the Multistep Reaction Pathway of an RNA Enzyme by Single-Molecule Kinetic "Fingerprinting". *Proc. Natl. Acad. Sci. U. S. A.* **2007**, *104*, 12634−12639.
(183) McDowell, S. E.; Jun, J. M.; Walter, N. G. Long-Range Tertiary Interactions in Single Hammerhead Ribozymes Bias Motional Sampling toward Catalytically Active Conformations. *RNA* **2010**, *16*, 2414−2426.
(184) de Silva, C.; Walter, N. G. Leakage and Slow Allostery Limit Performance of Single Drug-Sensing Aptazyme Molecules Based on the Hammerhead Ribozyme. *RNA* **2008**, *15*, 76−84.
(185) Vusurovic, N.; Altman, R. B.; Terry, D. S.; Micura, R.; Blanchard, S. C. Pseudoknot Formation Seeds the Twister Ribozyme Cleavage Reaction Coordinate. *J. Am. Chem. Soc.* **2017**, *139*, 8186−8193.
(186) Pereira, M. J.; Nikolova, E. N.; Hiley, S. L.; Jaikaran, D.; Collins, R. A.; Walter, N. G. Single Vs Ribozyme Molecules Reveal Dynamic and Hierarchical Folding toward Catalysis. *J. Mol. Biol.* **2008**, *382*, 496−509.
(187) Paudel, B. P.; Rueda, D. Molecular Crowding Accelerates Ribozyme Docking and Catalysis. *J. Am. Chem. Soc.* **2014**, *136*, 16700−16703.
(188) Daher, M.; Widom, J. R.; Tay, W.; Walter, N. G. Soft interactions with model crowders and non-canonical interactions with cellular proteins stabilize RNA folding. *J. Mol. Biol.* **2018**, DOI: 10.1016/j.jmb.2017.10.030.
(189) Haller, A.; Rieder, U.; Aigner, M.; Blanchard, S. C.; Micura, R. Conformational Capture of the Sam-Ii Riboswitch. *Nat. Chem. Biol.* **2011**, *7*, 393−400.
(190) Suddala, K. C.; Rinaldi, A. J.; Feng, J.; Mustoe, A. M.; Eichhorn, C. D.; Liberman, J. A.; Wedekind, J. E.; Al-Hashimi, H. M.; Brooks, C. L., 3rd; Walter, N. G. Single Transcriptional and Translational Preq1 Riboswitches Adopt Similar Pre-Folded Ensembles That Follow Distinct Folding Pathways into the Same Ligand-Bound Structure. *Nucleic Acids Res.* **2013**, *41*, 10462−10475.
(191) Holmstrom, E. D.; Polaski, J. T.; Batey, R. T.; Nesbitt, D. J. Single-Molecule Conformational Dynamics of a Biologically Functional Hydroxocobalamin Riboswitch. *J. Am. Chem. Soc.* **2014**, *136*, 16832−16843.
(192) Suddala, K. C.; Wang, J.; Hou, Q.; Walter, N. G. Mg(2+) Shifts Ligand-Mediated Folding of a Riboswitch from Induced-Fit to Conformational Selection. *J. Am. Chem. Soc.* **2015**, *137*, 14075−14083.
(193) Souliere, M. F.; Altman, R. B.; Schwarz, V.; Haller, A.; Blanchard, S. C.; Micura, R. Tuning a Riboswitch Response through Structural Extension of a Pseudoknot. *Proc. Natl. Acad. Sci. U. S. A.* **2013**, *110*, E3256−E3264.
(194) Fiegland, L. R.; Garst, A. D.; Batey, R. T.; Nesbitt, D. J. Single-Molecule Studies of the Lysine Riboswitch Reveal Effector-Dependent Conformational Dynamics of the Aptamer Domain. *Biochemistry* **2012**, *51*, 9223−9233.
(195) Haller, A.; Altman, R. B.; Souliere, M. F.; Blanchard, S. C.; Micura, R. Folding and Ligand Recognition of the Tpp Riboswitch Aptamer at Single-Molecule Resolution. *Proc. Natl. Acad. Sci. U. S. A.* **2013**, *110*, 4188−4193.
(196) Wood, S.; Ferre-D'Amare, A. R.; Rueda, D. Allosteric Tertiary Interactions Preorganize the C-Di-Gmp Riboswitch and Accelerate Ligand Binding. *ACS Chem. Biol.* **2012**, *7*, 920−927.
(197) Hohng, S.; Wilson, T. J.; Tan, E.; Clegg, R. M.; Lilley, D. M.; Ha, T. Conformational Flexibility of Four-Way Junctions in RNA. *J. Mol. Biol.* **2004**, *336*, 69−79.
(198) Salim, N.; Lamichhane, R.; Zhao, R.; Banerjee, T.; Philip, J.; Rueda, D.; Feig, A. L. Thermodynamic and Kinetic Analysis of an RNA Kissing Interaction and Its Resolution into an Extended Duplex. *Biophys. J.* **2012**, *102*, 1097−1107.
(199) Werner, A.; Konarev, P. V.; Svergun, D. I.; Hahn, U. Characterization of a Fluorophore Binding RNA Aptamer by Fluorescence Correlation Spectroscopy and Small Angle X-Ray Scattering. *Anal. Biochem.* **2009**, *389*, 52−62.
(200) Michelini, F.; Jalihal, A.; Francia, S.; Meers, C.; Neeb, Z. T.; Rossiello, F.; Gioia, U.; Aguado, J.; Luke, B.; Biamonti, G. et al. From

DOI: 10.1021/acs.chemrev.7b00519
Chem. Rev. 2018, 118, 4120−4155

"Cellular" RNA to "Smart" RNA: Multiple Roles of RNA in Genome Stability. *Chem. Rev.* **2018**.
(201) Holmstrom, E. D.; Nesbitt, D. J. Single-Molecule Fluorescence Resonance Energy Transfer Studies of the Human Telomerase RNA Pseudoknot: Temperature-/Urea-Dependent Folding Kinetics and Thermodynamics. *J. Phys. Chem. B* **2014**, *118*, 3853−3863.
(202) Myong, S.; Bruno, M. M.; Pyle, A. M.; Ha, T. Spring-Loaded Mechanism of DNA Unwinding by Hepatitis C Virus Ns3 Helicase. *Science* **2007**, *317*, 513−516.
(203) Lin, C. T.; Tritschler, F.; Lee, K. S.; Gu, M.; Rice, C. M.; Ha, T. Single-Molecule Imaging Reveals the Translocation and DNA Looping Dynamics of Hepatitis C Virus Ns3 Helicase. *Protein Sci.* **2017**, *26*, 1391−1403.
(204) Fairman-Williams, M. E.; Jankowsky, E. Unwinding Initiation by the Viral RNA Helicase Nph-Ii. *J. Mol. Biol.* **2012**, *415*, 819−832.
(205) Shu, D.; Zhang, H.; Jin, J.; Guo, P. Counting of Six Prnas of Phi29 DNA-Packaging Motor with Customized Single-Molecule Dual-View System. *EMBO J.* **2007**, *26*, 527−537.
(206) Pond, S. J.; Ridgeway, W. K.; Robertson, R.; Wang, J.; Millar, D. P. Hiv-1 Rev Protein Assembles on Viral RNA One Molecule at a Time. *Proc. Natl. Acad. Sci. U. S. A.* **2009**, *106*, 1404−1408.
(207) Linden, M. H.; Hartmann, R. K.; Klostermeier, D. The Putative RNAse P Motif in the Dead Box Helicase Hera Is Dispensable for Efficient Interaction with RNA and Helicase Activity. *Nucleic Acids Res.* **2008**, *36*, 5800−5811.
(208) Theissen, B.; Karow, A. R.; Kohler, J.; Gubaev, A.; Klostermeier, D. Cooperative Binding of Atp and RNA Induces a Closed Conformation in a Dead Box RNA Helicase. *Proc. Natl. Acad. Sci. U. S. A.* **2008**, *105*, 548−553.
(209) Ait-Bara, S.; Clerte, C.; Margeat, E. Single-Molecule Fret Characterization of RNA Remodeling Induced by an Antitermination Protein. *Methods Mol. Biol.* **2015**, *1259*, 349−368.
(210) Schuttpelz, M.; Schoning, J. C.; Doose, S.; Neuweiler, H.; Peters, E.; Staiger, D.; Sauer, M. Changes in Conformational Dynamics of Mrna Upon Atgrp7 Binding Studied by Fluorescence Correlation Spectroscopy. *J. Am. Chem. Soc.* **2008**, *130*, 9507−9513.
(211) Cherny, D.; Gooding, C.; Eperon, G. E.; Coelho, M. B.; Bagshaw, C. R.; Smith, C. W.; Eperon, I. C. Stoichiometry of a Regulatory Splicing Complex Revealed by Single-Molecule Analyses. *EMBO J.* **2010**, *29*, 2161−2172.
(212) Pitchiaya, S.; Androsavich, J. R.; Walter, N. G. Intracellular Single Molecule Microscopy Reveals Two Kinetically Distinct Pathways for Microrna Assembly. *EMBO Rep.* **2012**, *13*, 709−715.
(213) Pitchiaya, S.; Heinicke, L. A.; Custer, T. C.; Walter, N. G. Single Molecule Fluorescence Approaches Shed Light on Intracellular RNAs. *Chem. Rev.* **2014**, *114*, 3224−3265.
(214) Pitchiaya, S.; Heinicke, L. A.; Park, J. I.; Cameron, E. L.; Walter, N. G. Resolving Subcellular Mirna Trafficking and Turnover at Single-Molecule Resolution. *Cell Rep.* **2017**, *19*, 630−642.
(215) Hannon, G. J. RNA Interference. *Nature* **2002**, *418*, 244−251.
(216) Ha, M.; Kim, V. N. Regulation of Microrna Biogenesis. *Nat. Rev. Mol. Cell Biol.* **2014**, *15*, 509−524.
(217) Nguyen, T. A.; Jo, M. H.; Choi, Y.-G.; Park, J.; Kwon, S. C.; Hohng, S.; Kim, V. N.; Woo, J.-S. Functional Anatomy of the Human Microprocessor. *Cell* **2015**, *161*, 1374−1387.
(218) Herbert, K. M.; Sarkar, S. K.; Mills, M.; Delgado De la Herran, H. C.; Neuman, K. C.; Steitz, J. A. A. Heterotrimer Model of the Complete Microprocessor Complex Revealed by Single-Molecule Subunit Counting. *RNA* **2016**, *22*, 175−183.
(219) Chandradoss, S. D.; Schirle, N. T.; Szczepaniak, M.; MacRae, I. J.; Joo, C. A Dynamic Search Process Underlies Microrna Targeting. *Cell* **2015**, *162*, 96−107.
(220) Fareh, M.; Yeom, K.-H.; Haagsma, A. C.; Chauhan, S.; Heo, I.; Joo, C. Trbp Ensures Efficient Dicer Processing of Precursor Microrna in RNA-Crowded Environments. *Nat. Commun.* **2016**, *7*, 13694.
(221) Wee, L. M.; Flores-Jasso, F.; Salomon, W. E.; Zamore, P. D. *Cell* **2012**, *151*, 1055−1067.
(222) Wang, H.; La Russa, M.; Qi, L. S. Crispr/Cas9 in Genome Editing and Beyond. *Annu. Rev. Biochem.* **2016**, *85*, 227−264.
(223) Sternberg, S. H.; Redding, S.; Jinek, M.; Greene, E. C.; Doudna, J. A. DNA Interrogation by the Crispr RNA-Guided Endonuclease Cas9. *Nature* **2014**, *507*, 62−67.
(224) Redding, S.; Sternberg, S. H.; Marshall, M.; Gibb, B.; Bhat, P.; Guegler, C. K.; Wiedenheft, B.; Doudna, J. A.; Greene, E. C. Surveillance and Processing of Foreign DNA by the Escherichia Coli Crispr-Cas System. *Cell* **2015**, *163*, 854−865.
(225) Blosser, T. R.; Loeff, L.; Westra, E. R.; Vlot, M.; Künne, T.; Sobota, M.; Dekker, C.; Brouns, S. J. J.; Joo, C. Two Distinct DNA Binding Modes Guide Dual Roles of a Crispr-Cas Protein Complex. *Mol. Cell* **2015**, *58*, 60−70.
(226) Singh, D.; Sternberg, S. H.; Fei, J.; Doudna, J. A.; Ha, T. Real-Time Observation of DNA Recognition and Rejection by the RNA-Guided Endonuclease Cas9. *Nat. Commun.* **2016**, *7*, 12778.
(227) Lim, Y.; Bak, S. Y.; Sung, K.; Jeong, E.; Lee, S. H.; Kim, J.-S.; Bae, S.; Kim, S. K. Structural Roles of Guide RNAs in the Nuclease Activity of Cas9 Endonuclease. *Nat. Commun.* **2016**, *7*, 13350.
(228) Friedman, L. J.; Mumm, J. P.; Gelles, J. RNA Polymerase Approaches Its Promoter without Long-Range Sliding Along DNA. *Proc. Natl. Acad. Sci. U. S. A.* **2013**, *110*, 9740−9745.
(229) Wang, F.; Redding, S.; Finkelstein, I. J.; Gorman, J.; Reichman, D. R.; Greene, E. C. The Promoter-Search Mechanism of Escherichia Coli RNA Polymerase Is Dominated by Three-Dimensional Diffusion. *Nat. Struct. Mol. Biol.* **2012**, *20*, 174−181.
(230) Duchi, D.; Bauer, D. L. V.; Fernandez, L.; Evans, G.; Robb, N.; Hwang, L. C.; Gryte, K.; Tomescu, A.; Zawadzki, P.; Morichaud, Z.; et al. RNA Polymerase Pausing During Initial Transcription. *Mol. Cell* **2016**, *63*, 939−950.
(231) Abbondanzieri, E. A.; Bokinsky, G.; Rausch, J. W.; Zhang, J. X.; Le Grice, S. F. J.; Zhuang, X. Dynamic Binding Orientations Direct Activity of Hiv Reverse Transcriptase. *Nature* **2008**, *453*, 184−189.
(232) Liu, S.; Abbondanzieri, E. A.; Rausch, J. W.; Le Grice, S. F. J.; Zhuang, X. Slide into Action: Dynamic Shuttling of Hiv Reverse Transcriptase on Nucleic Acid Substrates. *Science* **2008**, *322*, 1092−1097.
(233) Kapanidis, A. N.; Margeat, E.; Ho, S. O.; Kortkhonjia, E.; Weiss, S.; Ebright, R. H. Initial Transcription by RNA Polymerase Proceeds through a DNA-Scrunching Mechanism. *Science* **2006**, *314*, 1144−1147.
(234) Winkelman, J. T.; Vvedenskaya, I. O.; Zhang, Y.; Zhang, Y.; Bird, J. G.; Taylor, D. M.; Gourse, R. L.; Ebright, R. H.; Nickels, B. E. Multiplexed Protein-DNA Cross-Linking: Scrunching in Transcription Start Site Selection. *Science* **2016**, *351*, 1090−1093.
(235) Tao, Y. J.; Ye, Q. RNA Virus Replication Complexes. *PLoS Pathog.* **2010**, *6*, e1000943.
(236) Vulliamy, T. J.; Dokal, I. Dyskeratosis Congenita: The Diverse Clinical Presentation of Mutations in the Telomerase Complex. *Biochimie* **2008**, *90*, 122−130.
(237) Alves, D.; Li, H.; Codrington, R.; Orte, A.; Ren, X.; Klenerman, D.; Balasubramanian, S. Single-Molecule Analysis of Human Telomerase Monomer. *Nat. Chem. Biol.* **2008**, *4*, 287−289.
(238) Parks, J. W.; Stone, M. D. Single-Molecule Studies of Telomeres and Telomerase. *Annu. Rev. Biophys.* **2017**, *46*, 357−377.
(239) Hwang, H.; Opresko, P.; Myong, S. Single-Molecule Real-Time Detection of Telomerase Extension Activity. *Sci. Rep.* **2015**, *4*, 1−7.
(240) Wu, R. A.; Dagdas, Y. S.; Yilmaz, S. T.; Yildiz, A.; Collins, K. Single-Molecule Imaging of Telomerase Reverse Transcriptase in Human Telomerase Holoenzyme and Minimal Rnp Complexes. *eLife* **2015**, *4*, e08363.
(241) Berman, A. J.; Akiyama, B. M.; Stone, M. D.; Cech, T. R. The RNA Accordion Model for Template Positioning by Telomerase RNA During Telomeric DNA Synthesis. *Nat. Struct. Mol. Biol.* **2011**, *18*, 1371−1375.
(242) Parks, J. W.; Kappel, K.; Das, R.; Stone, M. D. Single-Molecule Fret-Rosetta Reveals RNA Structural Rearrangements During Human Telomerase Catalysis. *RNA* **2017**, *23*, 175−188.
(243) Lee, Y.; Rio, D. C. Mechanisms and Regulation of Alternative Pre-Mrna Splicing. *Annu. Rev. Biochem.* **2015**, *84*, 291−323.

DOI: 10.1021/acs.chemrev.7b00519
Chem. Rev. 2018, 118, 4120−4155

(244) Semlow, D. R.; Blanco, M. R.; Walter, N. G.; Staley, J. P. Spliceosomal Deah-Box Atpases Remodel Pre-Mrna to Activate Alternative Splice Sites. *Cell* **2016**, *164*, 985−998.
(245) Voith von Voithenberg, L.; Sánchez-Rico, C.; Kang, H.-S.; Madl, T.; Zanier, K.; Barth, A.; Warner, L. R.; Sattler, M.; Lamb, D. C. Recognition of the 3′ Splice Site RNA by the U2af Heterodimer Involves a Dynamic Population Shift. *Proc. Natl. Acad. Sci. U. S. A.* **2016**, *113*, E7169−E7175.
(246) Brody, E.; Abelson, J. The ″Spliceosome″: Yeast Pre-Messenger RNA Associates with a 40s Complex in a Splicing-Dependent Reaction. *Science* **1985**, *228*, 963−967.
(247) Faustino, N. A.; Cooper, T. A. Pre-Mrna Splicing and Human Disease. *Genes Dev.* **2003**, *17*, 419−437.
(248) Moore, M. J.; Query, C. C.; Sharp, P. A. Splicing of Precursors to Mrna by the Spliceosome. *RNA World* **1993**, 1−55.
(249) Staley, J. P.; Guthrie, C. Mechanical Devices of the Spliceosome: Motors, Clocks, Springs, and Things. *Cell* **1998**, *92*, 315−326.
(250) Wahl, M. C.; Will, C. L.; Lührmann, R. The Spliceosome: Design Principles of a Dynamic Rnp Machine. *Cell* **2009**, *136*, 701−718.
(251) Chen, W.; Moore, M. J. The Spliceosome: Disorder and Dynamics Defined. *Curr. Opin. Struct. Biol.* **2014**, *24*, 141−149.
(252) Papasaikas, P.; Valcarcel, J. The Spliceosome: The Ultimate RNA Chaperone and Sculptor. *Trends Biochem. Sci.* **2016**, *41*, 33−45.
(253) Crawford, D. J.; Hoskins, A. A.; Friedman, L. J.; Gelles, J.; Moore, M. J. Visualizing the Splicing of Single Pre-Mrna Molecules in Whole Cell Extract. *RNA* **2007**, *14*, 170−179.
(254) Shcherbakova, I.; Hoskins, A. A.; Friedman, L. J.; Serebrov, V.; Corrêa, I. R.; Xu, M.-Q.; Gelles, J.; Moore, M. J. Alternative Spliceosome Assembly Pathways Revealed by Single-Molecule Fluorescence Microscopy. *Cell Rep.* **2013**, *5*, 151−165.
(255) Hoskins, A. A.; Rodgers, M. L.; Friedman, L. J.; Gelles, J.; Moore, M. J. Single Molecule Analysis Reveals Reversible and Irreversible Steps During Spliceosome Activation. *eLife* **2016**, *5*, e14166.
(256) Cornish, P. V.; Ermolenko, D. N.; Noller, H. F.; Ha, T. Spontaneous Intersubunit Rotation in Single Ribosomes. *Mol. Cell* **2008**, *30*, 578−588.
(257) Crawford, D. J.; Hoskins, A. A.; Friedman, L. J.; Gelles, J.; Moore, M. J. Single-Molecule Colocalization Fret Evidence That Spliceosome Activation Precedes Stable Approach of the 5′ Splice Site and Branch Site. *Proc. Natl. Acad. Sci. U. S. A.* **2013**, *110*, 6783−6788.
(258) Rauhut, R.; Fabrizio, P.; Dybkov, O.; Hartmuth, K.; Pena, V.; Chari, A.; Kumar, V.; Lee, C.-T.; Urlaub, H.; Kastner, B.; et al. Molecular Architecture of the *Saccharomyces Cerevisiae* Activated Spliceosome. *Science* **2016**, *353*, 1399−1405.
(259) Rauhut, R.; Fabrizio, P.; Dybkov, O.; Hartmuth, K.; Pena, V.; Chari, A.; Kumar, V.; Lee, C. T.; Urlaub, H.; Kastner, B.; et al. Molecular Architecture of the Saccharomyces Cerevisiae Activated Spliceosome. *Science* **2016**, *353*, 1399−1405.
(260) Kahlscheuer, M. L.; Widom, J.; Walter, N. G. Single-Molecule Pull-Down Fret to Dissect the Mechanisms of Biomolecular Machines. *Methods in Enzymology*, 1st ed.; p 201510.1016/bs.mie.2015.01.009.
(261) Hilliker, A. K.; Mefford, M. A.; Staley, J. P. U2 Toggles Iteratively between the Stem Iia and Stem Iic Conformations to Promote Pre-Mrna Splicing. *Genes Dev.* **2007**, *21*, 821−834.
(262) Rodgers, M. L.; Tretbar, U. S.; Dehaven, A.; Alwan, A. A.; Luo, G.; Mast, H. M.; Hoskins, A. A. Conformational Dynamics of Stem Ii of the U2 Snrna. *RNA* **2016**, *22*, 225−236.
(263) Rodgers, M. L.; Didychuk, A. L.; Butcher, S. E.; Brow, D. A.; Hoskins, A. A. A Multi-Step Model for Facilitated Unwinding of the Yeast U4/U6 RNA Duplex. *Nucleic Acids Res.* **2016**, *44*, 10912−10928.
(264) Hardin, J. W.; Warnasooriya, C.; Kondo, Y.; Nagai, K.; Rueda, D. Assembly and Dynamics of the U4/U6 Di-Snrnp by Single-Molecule Fret. *Nucleic Acids Res.* **2015**, *43*, 10963−10974.
(265) Guo, Z.; Karunatilaka, K. S.; Rueda, D. Single-Molecule Analysis of Protein-Free U2−U6 Snrnas. *Nat. Struct. Mol. Biol.* **2009**, *16*, 1154−1159.
(266) Sidarovich, A.; Will, C. L.; Anokhina, M. M.; Ceballos, J.; Sievers, S.; Agafonov, D. E.; Samatov, T.; Bao, P.; Kastner, B.; Urlaub, H.; et al. Identification of a Small Molecule Inhibitor That Stalls Splicing at an Early Step of Spliceosome Activation. *eLife* **2017**, *6*, No. e23533.
(267) Karunatilaka, K. S.; Rueda, D. Post-Transcriptional Modifications Modulate Conformational Dynamics in Human U2-U6 Snrna Complex. *RNA* **2014**, *20*, 16−23.
(268) Hoerter, J. A.; Lambert, M. N.; Pereira, M. J.; Walter, N. G. Dynamics Inherent in Helix 27 from Escherichia Coli 16s Ribosomal RNA. *Biochemistry* **2004**, *43*, 14624−14636.
(269) Agrawal, A. A.; Salsi, E.; Chatrikhi, R.; Henderson, S.; Jenkins, J. L.; Green, M. R.; Ermolenko, D. N.; Kielkopf, C. L. An Extended U2af65-RNA-Binding Domain Recognizes the 3&Apos; Splice Site Signal. *Nat. Commun.* **2016**, *7*, 10950.
(270) Hang, J.; Wan, R.; Yan, C.; Shi, Y. Structural Basis of Pre-Mrna Splicing. *Science* **2015**, *349*, 1191−1198.
(271) Yan, C.; Hang, J.; Wan, R.; Huang, M.; Wong, C. C. L.; Shi, Y. Structure of a Yeast Spliceosome at 3.6-Angstrom Resolution. *Science* **2015**, *349*, 1182−1191.
(272) Kurland, C. G. Structure and Function of the Bacterial Ribosome. *Annu. Rev. Biochem.* **1977**, *46*, 173−200.
(273) Schmeing, T. M.; Ramakrishnan, V. What Recent Ribosome Structures Have Revealed About the Mechanism of Translation. *Nature* **2009**, *461*, 1234−1242.
(274) Carter, A. P.; Clemons, W. M.; Brodersen, D. E.; Morgan-Warren, R. J.; Hartsch, T.; Wimberly, B. T.; Ramakrishnan, V. Crystal Structure of an Initiation Factor Bound to the 30≪Em≫S≪/Em≫ Ribosomal Subunit. *Science* **2001**, *291*, 498−501.
(275) de la Cruz, J.; Karbstein, K.; Woolford, J. L. Functions of Ribosomal Proteins in Assembly of Eukaryotic Ribosomes in Vivo. *Annu. Rev. Biochem.* **2015**, *84*, 93−129.
(276) Ramakrishnan, V. Ribosome Structure and the Mechanism of Translation. *Cell* **2002**, *108*, 557−572.
(277) Yusupova, G.; Yusupov, M. Crystal Structure of Eukaryotic Ribosome and Its Complexes with Inhibitors. *Philos. Trans. R. Soc., B* **2017**, *372*, 20160184.
(278) Chen, C.; Stevens, B.; Kaur, J.; Cabral, D.; Liu, H.; Wang, Y.; Zhang, H.; Rosenblum, G.; Smilansky, Z.; Goldman, Y. E.; et al. Single-Molecule Fluorescence Measurements of Ribosomal Translocation Dynamics. *Mol. Cell* **2011**, *42*, 367−377.
(279) Chen, C.; Cui, X.; Beausang, J. F.; Zhang, H.; Farrell, I.; Cooperman, B. S.; Goldman, Y. E. Elongation Factor G Initiates Translocation through a Power Stroke. *Proc. Natl. Acad. Sci. U. S. A.* **2016**, *113*, 7515−7520.
(280) Chen, J.; Coakley, A.; O'Connor, M.; Petrov, A.; O'Leary, S. E.; Atkins, J. F.; Puglisi, J. D. Coupling of Mrna Structure Rearrangement to Ribosome Movement During Bypassing of Non-Coding Regions. *Cell* **2015**, *163*, 1267−1280.
(281) Carter, A. P.; Clemons, W. M.; Brodersen, D. E.; Mogran-Warren, R. J.; Wimberly, B. T.; Ramakrishnan, V. Functional Insights from the Structure Ofthe 30s Ribosomal Subunit and Its Interactions with Antibiotics. *Nature* **2000**, *407*, 340−348.
(282) Matzov, D.; Bashan, A.; Yonath, A. A Bright Future for Antibiotics? *Annu. Rev. Biochem.* **2017**, *86*, 567−583.
(283) Blanchard, S. C.; Gonzalez, R. L.; Kim, H. D.; Chu, S.; Puglisi, J. D. Trna Selection and Kinetic Proofreading in Translation. *Nat. Struct. Mol. Biol.* **2004**, *11*, 1008−1014.
(284) Munro, J. B.; Altman, R. B.; O'Connor, N.; Blanchard, S. C. Identification of Two Distinct Hybrid State Intermediates on the Ribosome. *Mol. Cell* **2007**, *25*, 505−517.
(285) Kim, H. D.; Puglisi, J. D.; Chu, S. Fluctuations of Transfer RNAs between Classical and Hybrid States. *Biophys. J.* **2007**, *93*, 3575−3582.
(286) Fei, J.; Kosuri, P.; MacDougall, D. D.; Gonzalez, R. L. Coupling of Ribosomal L1 Stalk and Trna Dynamics During Translation Elongation. *Mol. Cell* **2008**, *30*, 348−359.

DOI: 10.1021/acs.chemrev.7b00519
Chem. Rev. 2018, 118, 4120−4155

(287) Valle, M.; Zavialov, A.; Sengupta, J.; Rawat, U.; Ehrenberg, M.; Frank, J. Locking and Unlocking of Ribosomal Motions. *Cell* **2003**, *114*, 123−134.
(288) Chen, J.; Petrov, A.; Johansson, M.; Tsai, A.; O'Leary, S. E.; Puglisi, J. D. Dynamic Pathways of −1 Translational Frameshifting. *Nature* **2014**, *512*, 328−332.
(289) Petrov, A.; Grosely, R.; Chen, J.; O'Leary, S. E.; Puglisi, J. D. Multiple Parallel Pathways of Translation Initiation on the Crpv Ires. *Mol. Cell* **2016**, *62*, 92−103.
(290) Widom, J. R.; Dhakal, S.; Heinicke, L. A.; Walter, N. G. Single-Molecule Tools for Enzymology, Structural Biology, Systems Biology and Nanotechnology: An Update. *Arch. Toxicol.* **2014**, *88*, 1965−1985.

NOTE ADDED AFTER ASAP PUBLICATION

This paper was published to the Web on January 24, 2018, with errors in the caption to Figure 5. These were corrected in the version published to the Web on January 31, 2018.

DOI: 10.1021/acs.chemrev.7b00519
Chem. Rev. 2018, 118, 4120−4155